LOW TEMPERATURE PHOTOCATALYTIC OXIDATION OF CARBON MONOXIDE OVER PALLADIUM DOPED TITANIA CATALYSTS

A THESIS SUBMITTED TO
THE GRADUATE SCHOOL OF NATURAL AND APPLIED SCIENCES
OF
MIDDLE EAST TECHNICAL UNIVERSITY

BY

PELİN YETİŞEMİYEN

IN PARTIAL FULFILLMENT OF THE REQUIREMENTS
FOR
THE DEGREE OF MASTER OF SCIENCE
IN
CHEMICAL ENGINEERING

SEPTEMBER 2010

Approval of the thesis:

LOW TEMPERATURE PHOTOCATALYTIC OXIDATION OF CARBON MONOXIDE OVER PALLADIUM DOPED TITANIA CATALYSTS

submitted by **PELİN YETİŞEMİYEN** in partial fulfillment of the requirements for the degree of **Master of Science in Chemical Engineering Department, Middle East Technical University** by,

Prof. Dr. Canan Özgen
Dean, Graduate School of **Natural and Applied Sciences** _____

Prof. Dr. Gürkan Karakaş
Head of Department, **Chemical Engineering** _____

Prof. Dr. Gürkan Karakaş
Supervisor, **Chemical Engineering Dept., METU** _____

Prof. Dr. Ufuk Bakır
Co-Supervisor, **Chemical Engineering Dept., METU** _____

Examining Committee Members:

Prof. Dr. Timur Doğu
Chemical Engineering Dept., METU _____

Prof. Dr. Gürkan Karakaş
Chemical Engineering Dept., METU _____

Prof. Dr. Deniz Üner
Chemical Engineering Dept., METU _____

Prof. Dr. İnci Eroğlu
Chemical Engineering Dept., METU _____

Prof. Dr. Çiğdem Güldür
Chemical Engineering Dept., Gazi University _____

Date: 20.09.2010

I hereby declare that all information in this document has been obtained and presented in accordance with academic rules and ethical conduct. I also declare that, as required by these rules and conduct, I have fully cited and referenced all material and results that are not original to this work.

Name, Last name : Pelin, Yetişemiyen

Signature :

ABSTRACT

LOW TEMPERATURE PHOTOCATALYTIC OXIDATION OF
CARBON MONOXIDE OVER PALLADIUM DOPED TITANIA CATALYSTS

Yetişemiyen, Pelin
M. S., Department of Chemical Engineering
Supervisor: Prof. Dr. Gürkan Karakaş

September 2010, 112 pages

The room temperature photocatalytic oxidation of carbon monoxide in excess air was examined over silica/titania and 0.1%palladium/silica/titania catalysts under UV irradiation. The experiments were conducted in batch re-circulated reactor with the initial 1000 ppm carbon monoxide in air and 0.5 g catalyst charge and the conversion of carbon monoxide to carbon dioxide was followed by FT-IR spectro-photometer. The change in gas composition in dark and under 36 Watts of UV irradiation exposed to a catalyst area of 12.4 centimeter square indicated both adsorption of carbon monoxide and conversion of carbon monoxide to carbon dioxide over the catalyst samples. The effect of catalyst composition (silica/titania) ratio and the presence of palladium oxide were investigated. The catalyst samples were synthesized by sol-gel technique and all samples were hydrothermally treated before calcination in air. The catalyst samples were characterized by XRD and nitrogen adsorption techniques. XRD results indicated that titania is comprised of pure anatase phase and palladium oxide preferantially dispersed over titania. BET surface area of the samples were observed to increase with silica loading and the BJH results showed isotherms of Type V

with H2 hysteresis loops. The highest carbon monoxide adsorption rate constant was achieved with pure silica with the highest surface area. Photocatalytic activity measurements indicated that carbon monoxide in excess air can be successfully oxidized at room temperature over the titania photocatalyts. Higher physisorption was observed over higher silica containing samples and higher oxidation activity was observed with increasing titania/silica ratio. The optimum titania/silica ratio was determined by the titania content and surface area of catalyst. The activity tests were also indicated that the addition of palladium oxide phase synergistically increased the adsorption and oxidation activity of the catalysts.

Keywords: Titania, silica, palladium, photocatalysis, carbon monoxide

ÖZ

PALLADYUM KATKILI TİTANYUM KATALİZÖRLERİ ÜZERİNDE DÜŞÜK SICAKLIKTA KARBON MONOKSİT FOTOKATALİTİK OKSİDASYONU

Yetişemiyen, Pelin
M. S., Kimya Mühendisliği Bölümü
Tez Yöneticisi: Prof. Dr. Gürkan Karakaş

Eylül 2010, 112 Sayfa

Oda sıcaklığında fazladan hava içindeki karbon monoksit fotokatalitik oksidasyonu, UV aydınlatması altında silika/titanyum ve 0.1%palladyum/silika/titanyum katalizörleri üzerinde test edilmiştir. Deneyler 1000 ppm karbon monoksit içeren hava dolaştırmalı ve 0.5 g katalizör yüklü kesikli reaktör içerisinde yapılmıştır ve karbon monoksitin karbon dioksite dönüşümü FT-IR spektrofotometresiyle takip edilmiştir. Karanlıktaki ve 36 Watts aydınlatma altındaki gaz kompozisyonunun değişimi, hem karbon monoksitin adsorpsiyonunu hem de katalizör yüzeyi üzerinde karbon monoksitin karbon dioksite dönüşümünü işaret etmiştir. Katalizör kompozisyon oranının (silika/titanyum) ve palladyum oksit varlığının etkisi araştırılmıştır. Katalizör örnekleri sol-jel tekniği ile sentezlenmiştir ve tüm örnekler hava içinde kalsinasyon yapılmadan önce hidrotermal işlemden geçmiştir. Katalizör örnekleri XRD ve nitrojen adsorpsiyon teknikleri ile

karakterize edilmiştir. XRD sonuçları, titanyumun saf anataz fazını kapsadığını ve palladyum oksitin ayrıcalıklı biçimde titanyum yüzeyi üzerine dağıldığını göstermiştir. Örneklerin BET yüzey alanlarının silika yüklemesiyle arttığı gözlemlenmiştir ve BJH sonuçları Tip V ve H2 histeriz lupu göstermiştir. En yüksek CO adsorpsiyon hız sabiti en yüksek yüzey alanlı saf silika ile sağlanmıştır. Fotokatalitik aktivite ölçümleri, fazladan hava içerisindeki karbon monoksitin oda sıcaklığında titanyum fotokatalizörleri üzerinde başarıyla okside edilebileceğini göstermiştir. Daha yüksek fiziksel adsorpsiyon daha geniş yüzey alanlı silika içeren katalizörler üzerinde gözlemlenirken, daha yüksek oksidasyon aktivitesi artan titanyum/silika oranıyla sağlanmıştır. İdeal titanyum/silika oranı, katalizörün titanyum içeriği ve yüzey alanıyla elde edilmiştir. Aktivite sonuçları ayrıca, karşılıklı etkileşim yaratarak palladyum oksit fazı eklemenin katalizörlerin adsorpsiyonunu ve oksidasyon aktivitesini arttırdığını işaret etmiştir.

Anahtar Kelimeler: Titanyum, silika, palladyum, fotokataliz, karbon monoksit

To My Family

ACKNOWLEDGEMENTS

First and the most, I would like to express my sincere and deep gratitude to my dear supervisor, Prof. Dr. Gürkan Karakaş for his valuable kindness, patience and academic guideness providing me with support and encouragement during the course of this study. I believe that his great knowledge, experience and advices I always appreciate and admire will shed light on my future studies.

I also wish to express my grateful thanks to Prof. Dr. Ufuk Bakır and Prof. Dr. Deniz Üner for their friendly and kind attitude and scientific support.

The help of all the technicians, laboratory and machine shop workers of the Chemical Engineering Department is gratefully acknowledged. The Central Laboratory of the Middle East Technical University is acknowledged for the BET and XRD analysis. I additionally would like to thank Cornel Munteanu and Bilal Bayram for their friendly and patient help during their scientific support for my study. Thanks are due my dear friends; Nur Kandilli, Elif Seda Şayin, Hasan Zerze, Emre Yılmaz and Mert Özkan for their valuable support and friendship.

Last and specially, I would like to express my deep appreciation to my parents who have always supported and encouraged me with their unique love and patience giving me the proud of being their doughter.

TABLE OF CONTENTS

LIST OF TABLES

TABLES

LIST OF FIGURES

FIGURES

LIST OF SYMBOLS AND ABBREVIATIONS

r	Rate of reaction
V_R	Volume of reactor
e^a	Volumetric rate of photon absorption, einstein/m^3.s
θ	Bragg angle, °
β	Line broadening, °
τ	Crystallite size, nm
λ	Wavenumber, Å
A	Absorbance
AcAc	Acetyl Acetone
ASHRAE	American Society of Heating, Refrigerating and Air-Conditioning
BET	Brunauer Emmett Teller
BJH	Barrett-Joyner-Halenda
c_i	Concentration of species *i*
D	Diameter
D_{pore}	Pore diameter
e^-	Electron
EPA	Environmental Protection Agency
E-R	Eley-Rideal
EU	European Union
FT-IR	Fourier Transform Infrared
h	Planck's constant, Joule-seconds
h^+	Hole
η_i	Quantum efficiency of species *i*
K	Equilibrium constant
k	Rate constant
LFL	Lower Flammibility Limit
L-H	Langmuir-Hinshelwood

M	Metal
MCT	Mesoporous Crystalline Titania
MO	Metal Oxide
P_T	Total pressure
Q_i	Specific adsorbed quantity of species *i*
-S	Surface
STP	Standard Temperature and Pressure
t	Time, seconds
TBOT	Titanium n-Butoxide
TEOS	Tetraethy Orthosilicate
UFL	Upper Flammibility Limit
UV	Ultraviolet
υ	Frequency, Hertz
VOC	Volatile Organic Compound
V_{pore}	Pore volume
W_{cat}	Weight of catalyst
wt %	Weight percent
X_A	Conversion of species *i*
XRD	X-Ray Diffraction
y_{i0}	Initial concentration of species *i*
Φ_λ	Quantum Yield

CHAPTER 1

INTRODUCTION AND OBJECTIVE

Oxidation of carbon monoxide is a reaction of general importance for a variety of basic research fields. The conversion of this pollutant gas into carbon dioxide is a crucial step to increase the operational life of CO_2-lasers, purification of fuel cell feed-streams and air cleaning processes.

Firstly, the presence of CO is a problem for CO_2-lasers which are widely used for industrial and medical purposes. The problem that arises during the lasing process of CO_2-lasers is that electrical discharges, used to excite the laser, decompose CO_2 into CO and O_2. The presence of CO and O_2 gases limits the number of pulses achievable. If stoichiometric amounts of CO and O_2 formed during the lasing process can be converted, the lifetime of CO_2-lasers are pro-longed by decreasing CO_2 decomposition to get more achievable pulses [Stark and Harris, 1983; Stark et *al*.,1983].

Next, CO was found to be effective catalyst poison for fuel cells that are energy efficient alternatives to internal combustion engines or fossil fuelled plants by converting chemical energy into electrical energy. The H_2 rich stream which is obtained by reforming the conventional hydrocarbon sources contains CO traces which poison the cell anode electro-catalyst [Stambouli et *al*., 2002; Ruettinger et *al*., 2003] which causes losses in cell efficiency. In order to generate more H_2 and decrease CO level, many techniques have been developed like feeding the reformer effluent to water-gas shift reactors or methanation to eliminate CO but they are found non applicable because of

the requirement to high pressures or releasing greenhouse gases [McCabe et *al*., 1987; Takenaka et *al*., 2004]. Therefore, the selective oxidation of CO in H_2 rich streams (prox) has a special importance for the fuel cell and reforming technologies.

Lastly and the most importantly; CO becomes a threatening and toxic gas indoors causing health impacts on occupants if it is present in air more than 14 ppm (according to EPA and EU standards) [Ao et *al*., 2002; Kim et *al*., 2006; Yu et *al*., 2007]. For getting rid of this air pollutant gas; increasing air exchange rate and using filter-based air purifiers or sorption materials have been followed up. Higher air exchange rate can be attained by mechanical ventilation systems which send the contaminated air out and take fresh air in. However; they are not selective to certain contaminants and causing contact with outdoor particles. Filter-based air purifiers are good at trapping particles but they also increase energy costs. Using activated carbon is also an alternative to adsorb chemicals but it is disadvantageous for not removing larger particles and just changing pollutants from gaseous to solid phase. Therefore; the technique recently developed to get rid of CO indoors, is the oxidation of this gas.

For the above reasons, converting CO into CO_2 has been widely searched and achieved by thermal and catalytic oxidation.

1.1. Thermal Oxidation of Carbon Monoxide

Thermal oxidation is the use of oxygen or air at high temperatures to destroy compounds which is also called as afterburning, fume incineration or thermal combustion. The combustion process comprised of very complex kinetics but the combustion of CO can be depicted shortly as:

$$CO(g) + \tfrac{1}{2} O_2(g) \rightarrow CO_2(g) + \text{heat} \quad (1)$$

In the gas phase oxidation reaction of CO, firstly there must be sufficient concentrations of combustible reactants (CO and O_2) to sustain the combustion process. The lower flammability limit (LFL) and upper flammability limit (UFL) values for CO were reported as 12.2 and 72.5 %, respectively [ASHRAE, 2007] which correspond to several order of magnitude higher concentrations than the toxic levels. In addition to LFL and UFL values, a specific ignition temperature for CO needs to be achieved to burn it with O_2. Ignition temperature for CO was published as 1128°F (608.3°C) [ASHRAE, 2007]. Oxidation of CO is actually a reversible and exothermic reaction that increasing the temperature at its equilibrium state lets CO_2 form CO and O_2 but in order to get higher efficiencies at start-up, higher temperatures are desired for effective collisions of combustion reactants. Moreover, CO combustion is dependant on the correct thermal oxidizer residence time and operating temperature. When these factors are considered, it comes out that as the residence time and temperature increase, CO burning efficiency increases [Zink, 2001].

1.2. Catalytic Oxidation of Carbon Monoxide

Another alternative recently been proposed to oxidize CO in relatively lower temperatures is the catalytic oxidation. Several catalyst formulations involving a noble metal dispersed over a reducible metal oxide, that can also be supported on inert oxides (e.g., titania (TiO_2), zirconia (ZrO_2), silica (SiO_2), etc.), are the most widely investigated formulations for CO catalytic oxidation. In catalytic oxidation, CO is adsorbed over the catalyst surface and gets into reaction with the adsorbed or gaseous O_2. CO has a strong interaction with

noble metal surfaces that its desorption from the surface is the slowest step of the mechanism and the reaction rate is, therefore, controlled by the rate of CO desorption [Berlowitz et *al*., 1988; Tripathi et *al*., 1985].

Noble metal catalysts supported on inert oxides have been tested to see their activity for CO oxidation in lower temperature values compared with thermal oxidation. The studies have generally shown that oxidizing CO over inert oxide catalyst surfaces desires temperatures higher than 250°C while on noble metal supported metal oxide or inert oxide surfaces, a temperature range of 100-200°C is needed [Wierzchowski and Zatorski, 2003; Naknam et *al*., 2007].

As it is understood; since thermal oxidation of CO is a process of combustion requiring temperatures higher than 600°C, it is not applied for CO_2-lasers, fuel cells or air purification demands. Catalytic oxidation of CO, on the other hand, is possible to be achieved at temperatures higher than 150°C that it is mostly used for the purification of automobile exhaust gases. Therefore, a new and promising alternative being possible at low temperatures has recently been introduced to get rid of CO, which is the room temperature photocatalytic oxidation.

In the present study; room temperature photo-oxidation of CO over the Pd doped TiO_2/SiO_2 catalysts was studied for indoor air purification purposes. Photocatalytic activity tests were performed in a re-circulated closed system of a fluidized bed reactor under 36 Watts of irradiation and the CO concentrations were detected by FT-IR. CO conversion with time was observed to search the influence of Pd loading on TiO_2/SiO_2 mixed oxides for converting CO into CO_2 by photo-oxidation.

CHAPTER 2

LITERATURE SURVEY

Common efforts to convert carbon monoxide into carbon dioxide include catalytic oxidation and thermal combustion which require a high temperature range of 150-600°C to overcome the activation energies.

The strong influence of temperature on thermal combustion of CO has been studied by a number of investigators. Niessen studied the oxidation rate of CO at different temperatures and ratios of CO to O_2 and the effect of water vapor. Similar to the other studies, it became clear that at about 650°C the combustion rate of CO increased sharply [Niessen, 2002]. As a result of the high temperature needs of thermal combustion, catalytic oxidation of CO at lower temperatures has become a wide research area and noble metal based catalyst formulations were studied in detail for this aim [Wang et *al*., 2008; Wang et *al*., 2009 ; Ozen et *al*., 2001; Moretti et *al*., 2008; Zhu et *al*., 2007; Sivakumar et *al*., 2009 ; Sheikh et *al*., 2009 ; Chen et *al*., 2008].

The catalysts developed have been achieved to convert CO into CO_2 but the temperature needs for catalytic oxidation have been lowered to only a range of 150-250°C. One of the alternatives for noble metal based catalysts is the CuO-ZnO composite supported on TiO_2. When three oxides were come together and formed CuO/ZnO-TiO_2, CO conversion was achieved only between 165°C-200°C [Moretti et *al*., 2008]. Pd is another noble metal that was proposed as an alternative for doping semiconductors to oxidize CO in lower temperatures. To see the catalytic effect of Pd on CeO_2-TiO_2

compound, the compound alone was firstly tested and CO conversion reached to 50 % at about 300°C. With introducing Pd, the catalyst Pd/CeO_2-TiO_2 exhibited a complete conversion of CO even at ambient temperature [Zhu et *al*., 2007]. To study the activity of Pt supported TiO_2 catalysts, in addition, CO and O_2 containing streams were investigated by Sivakumar [Sivakumar et *al*., 2009]. It was observed that naked TiO_2 did not show any activity for the conversion of CO below 250°C; however, 1 wt % Pt supported catalysts showed the complete conversion of CO in between 100–180°C.

For indoor air cleaning purposes, the concentration of CO in air is very low compared to its upper and lower flammability range and current catalysts requires relatively high temperatures. So there is a great demand for effective removal of CO in indoor air under ambient temperatures. Photocatalytic oxidation uses the energy of photons and with the use of suitable catalyst, considerable amount of energy might be utilized to overcome the activation energy for oxidation.

2.1. Photocatalysis

Photocatalysis is the acceleration of a catalytic reaction by a light source as “photo” means “light”. The aim of photocatalysis is to achieve the activation energy of a reaction by photons instead of by heat or other forms of energy. Photocatalysis can be classified as homogeneous or heterogeneous where homogeneous photocatalysis is mostly implied with organic reactions which are activated by organo metallics, metal ions, etc. Heterogeneous photocatalysis; on the other hand, is the catalytic reaction under a light source where the catalyst is in a different phase from the reactants which provides a surface on which the reaction may take place.

Photocatalysis requires the absorption of photon energy and semiconductors with their light absorption properties were proved to be effective photocatalysts with their suitable band gap.

2.1.1. Semiconductors and Absorption of Light

Semiconductors are commonly defined as the materials which have electrical conductivity between that of conductors (metal) and insulators. Electrical conductivity of a material depends mainly on its energy levels of valence and conduction bands which defines the band gap.

Solid materials are classified by the way the atoms are arranged within the solid so for having regular energy bands, a solid material with crystalline structure is advantageous. If the atoms of a material are placed at a highly ordered structure, that material becomes crystalline while randomly placed atoms make a material amorphous and the position of energy bands disordered. Semiconductors with their atoms crystally arranged have, therefore, collections of energy levels of electrons surrounding each atom and forming energy bands. The major energy bands are “valence band” and “conduction band”. Valence band is defined as the highest range of electron energies where electrons are normally present at absolute zero temperature and conduction band is defined as the range of electron energies, higher than that of the valence band which is present only in conductors or semiconductors. The energy difference between the top of the valence band and the bottom of the conduction band is defined as “band gap” where “Fermi level” is the halfway between the valence and the conduction bands. For semiconductors, band gap is narrow compared with insulators while for conductors, band gap does not exist since the conduction and the valence bands overlap. This explains the electrical conductivity of semiconductors for

which it is easy to jump the electrons from the valence to the conduction band.

In addition to their electrical and conductivity properties, semiconductors are also important with their optical properties. The position of the minimum conduction band and the maximum valence band according to the wavenumber of incoming light determines absorption, transmittance or reflection properties of semiconductors. If the minimum conduction band and the maximum valence band occur at the same wavenumber value of incoming light, the energy band gap is called “direct”; if not, the energy band gap is called “indirect”. Direct band gap semiconductors provide more efficient absorption of light than indirect semiconductors do, which is the transfer of the energy of photons to valence band electrons to be jumped to conduction band. Researchers of photocatalysis, therefore, mostly focus on light absorption features of semiconductors.

Light absorption property of semiconductors depends on band gap position. If a semiconductor has small band gap, then it absorbs low energy photons of medium-to-far infrared region of solar spectrum; if a semiconductor has medium band gap, then it absorbs medium energy photons of near-infrared [Ridley, 1999]. For photocatalysis, UV-range energy of ambient solar spectrum can be utilized. Mainly the catalysts absorbing in the visible region of UV-range (700nm-400nm) are preferable since the UV-visible photons of solar spectrum have enough energy to overcome the high activation energies of photocatalytic reactions [Cao et *al*., 2010; Wang et *al*., 2010; Qiu et *al*., 2008].

2.1.2. Mechanism of Photocatalysis

Upon absorbing UV photons, valence band electrons of the metal oxide (MO) are transfered to conduction band and charge separation takes place leaving positively charged holes behind. Charge separation, like all the chemical reactions, needs a certain activation energy to be overcome by the energy of UV light photons:

$$MO + h\upsilon \rightarrow e^- + h^+ \quad \text{(R.1)}$$

The electron (e^-) and hole (h^+) transport takes place in opposite directions and charges are transferred to the particle surface by diffusion. For the transport of e^- and h^+, charge carrier density and mobility of solid matrix are the important factors. Lower mobility, which is originated form of imperfections and defects, causes the recombination of e^- and h^+.

When e^-/h^+ pairs successfully reach to the outer surface of the metal oxide, they have a potential to react with the adsorbates of ambient molecules, such as H_2O, O_2, CO, VOC's etc., forming free radicals. The adsorption of species can be achieved in both physisorption or chemisorption.

Photocatalytic reactions on metal oxide surfaces, after charge separation and adsorption processes, mainly include redox reactions. Adsorbed O_2 from air and OH^- ions from water vapor over the surface are attracted by the separated e^-/h^+ pairs during several reaction chains on metal oxide surface.

$$O_2 - S + e^- \rightarrow O_2^- - S \quad \text{(oxidation, } e^- \text{ trapping)} \quad \text{(R.2)}$$

$$OH^- \text{ (from } H_2O) - S + h^+ \rightarrow OH\text{-}S \quad \text{(reduction, } h^+ \text{ trapping)} \quad \text{(R.3)}$$

$$OH\text{-}S + OH\text{-}S \rightarrow H_2O_2\text{-}S \quad \text{(R.4)}$$

O_2^--S and OH-S are called as super oxygen and hydroxyl surface free radicals, respectively. They are, afterwards, transfered over the surface to get into photocatalytic reactions.

Both physisorption and chemisorption affect the photocatalytic activity since they determine the type of adsorption. Kato observed that in the adsorption state of N_2O on Si, N_2O was adsorbed onto the surface both by physically and chemically below room temperature so he tried to explain how the photochemistry of N_2O on Si and the features of photo-reactions were affected by the adsorption state [Kato et *al*., 1999]. He concluded that, reaction cross-sections for both physisorbed and chemisorbed N_2O were larger than that of gaseous N_2O. Physisorbed N_2O was mostly photo-dissociated into gaseous N_2 and adsorbed O atoms by Si atoms under UV light illumination before a small fraction of this molecule was desorbed. This was depended on the fact that higher electron transfer probabilities to the adsorbate were seen by physisorption because weak Van der Waals forces were suitable to be substituted by the electrons. On the other hand, not all chemisorbed N_2O was activated by photon irradiation because of the strong bonds formed between the adsorbate and the surface but also it became difficult with chemisorbed N_2O to be desorbed from the surface. Therefore, it can be said that photocatalytic activity depends on the adsorption states of systems with different fractions of chemisorbed and physisorbed adsorbates.
However, it is difficult to keep the electrons and holes separated from each other because of the defects, impurities, disorders or dislocations in the crystal structure of metal oxides. These impurities or dislocations present in the crystal arrangement, make it impossible for e^-/h^+ pairs to follow a continuous route to reach to the surface for an efficient charge transport through the bulk of metal oxide. As a result, at the point where e^-/h^+ pairs are stucked and collected by a dislocation in the bulk or on the surface, they are

combined with each other releasing heat as a side reaction of photocatalysis called as charge recombination [Li et *al*., 2010]:

$e^- + h^+ \rightarrow$ heat (R.5)

Charge separation, charge recombination, formation of free radicals and surface reactions of a photocatalytic system are generally illustrated in Figure 2.1 below:

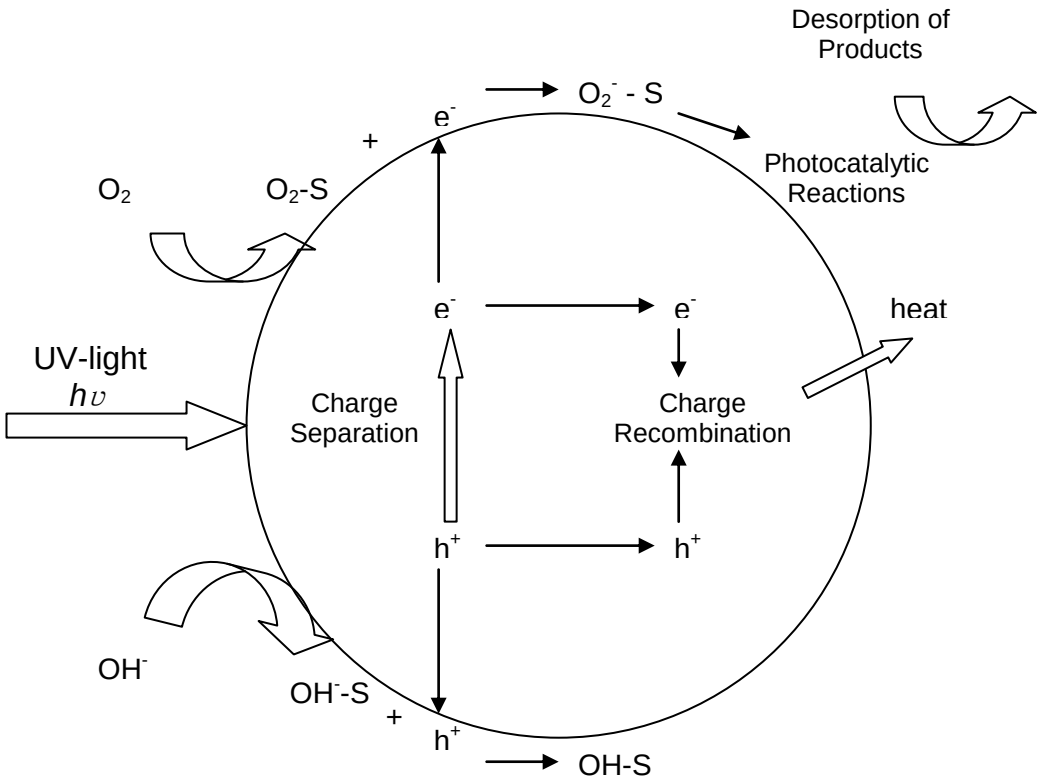

Figure 2.1. Reaction mechanism on a metal oxide photocatalytic system

2.1.3. Quantum Efficiency

The regime of charge separation and charge recombination reactions in the bulk and on the surface of a semiconductor during a photocatalytic reaction determines its quantum efficiency.

Quantum yield (Φ_λ) or quantum efficiency (η) is the activity for the use of photons in a photocatalytic system and defined as the ratio between the observed volumetric molar reaction rate of the process (r) and the volumetric rate of photon absorption by the semiconductor catalyst (e^a):

$$\eta_{catalyst} = \frac{\langle r_A \rangle_{V_R}}{\langle e^a \rangle_{V_R}} \tag{2.1}$$

where A is the reactant and V_R is the volume of the reactor.

The definition of quantum efficiency can also be done in a more simple manner which is:

$$\eta_{catalyst} = \frac{\textit{Number of free radicals generated}}{\textit{Number of photons absorbed}} \tag{2.2}$$

Discrepancies arise in the experimental procedure to evaluate the value of e^a, due to the inherent difficulties derived from the simultaneous absorption and reflection property of semiconductors. Several procedures have been

reported in literature for the applied radiation models [Mondal et *al*., 2010; Ibrahim et *al*., 2003]. One of the used approaches to evaluate the average volumetric rate of photon absorption inside the photo-reactor was reported by Marugan and his research group [Marugan et *al*., 2007]. They studied with SiO_2 supported TiO_2 on cyanide (CN) photocatalytic oxidation for the quantum efficiency determination. In this research study, to calculate the rate of photon absorption, two sequential steps were followed: the evaluation of the inlet radiation flux and the calculation of the average volumetric rate of photon absorption inside the photo-reactor as a function of the catalyst concentration. A radiative transfer equation was applied and the units were $mol_{CN}/m^3.s$ for the rate term and $einstein/m^3.s$ for photon absorption rate term.

2.2. Photocatalytic Oxidation

As mentioned in previous section, large band gap metal oxide semiconductors (e.g. TiO_2, SnO_2, ZnO, WO_3,...) are applied as effective catalysts of photocatalytic reactions. This type of semiconductors are good for being photocatalysts with their additional advantages like having long term stability, non-toxicity, resistance to photo/chemical corrosion and low cost.

They are mainly used in photo-assited degradation or oxidation reactions. To prove that large band gap metal oxide semiconductors, as bare or doped, are good at catalyzing degradation reactions under UV light, scientists mainly focus on the photocatalytic oxidation of methylene blue/orange, formic acid, acetaldehyde, VOC's, formaldehyde, ethanol or phenol in their studies [Jang et *al*., 2010; Xu et *al*., 2010; Jan et *al*., 2010; Akbarzadeh et *al*., 2010; Mu et *al*., 2010; Photong et *al*., 2009; Wang et *al*., 2007; Zou et *al*., 2006].

Furthermore, photocatalytic oxidation by chemisorption of reactants [Dai et *al*., 2009; Vorontsov et *al*., 2005; Lanning et *al*., 1993], kinetic features and reaction pathways [Kachina et *a*l., 2007; Liu et *al*., 2005; Hwang et *al*., 2003; Vorontsov et *al*., 1996], application areas like waste water treatment, organic removal at vapor phase and air purification; and ways of increasing photocatalytic activity [Wu et *al*., 2008; Hung *et al*., 2008; Khan et *al*., 2008; Bosc et *al*., 2006; Hwang et *al*., 2003] are the other studied fields in literature for the purpose of searching photocatalytic oxidation reactions.

Air purification by the photocatalytic oxidation of CO with large band gap metal oxide photocatalysts, has been a developing research area [Zhang et *al*., 2005; Kamegawa et *al*., 2006; Vorontsov et *al*., 1999]. Photocatalytic oxidation of CO, which is called as photo-oxidation, has advantages like being able to occur under a UV-light source at room temperature and atmospheric pressure without a need of heat supply and having low selectivity for the nature of products. This reaction is a heterogeneous type of reaction with a solid catalyst and gas phase reactants (CO and O_2).

2.2.1. Oxidation Kinetics

Similar to lacking studies on many aspects of CO photo-oxidation in literature, detailed information about reaction kinetics and mechanism of this photochemical process is also limited. Photocatalytic oxidation of CO is a gas-phase reaction with slow and fast steps that, in general words, starts with the charge separation and adsorption of reactants onto the surface of solid catalyst then continues with surface reaction followed by the desorption of products.

To oxidize CO on a photocatalyst surface, firstly charge separation and formation of free radicals on the surface are surely needed like all

photocatalytic reactions. Surface reactions, then, desire the adsorption of one or more reactants onto the surface. The mechanism of this step and the rate equations are of great importance for heterogeneous photocatalysis. Mainly two types of reaction mechanisms for the surface reactions of CO photo-oxidation are introduced in literature which are Langmuir-Hinshelwood and Eley-Rideal Mechanisms.

i. Langmuir-Hinshelwood (L-H) Mechanism

Langmuir-Hinshelwood mechanism is a type of reaction kinetics in which both reactants of surface oxidation are adsorbed species. According to this mechanism, when gaseous oxygen and the molecule to be oxidized are adsorbed on photocatalyst surface, they are carried toward each other on the surface and undergo a photo-chemical bimolecular reaction. The products are also adsorbed species which are further desorbed. According to this model, CO photo-oxidation takes place by the reaction of adsorbed CO and super oxygen radicals to form adsorbed CO_2 molecules over the surface:

$$2CO\text{-}S + O_2^-\text{-}S \rightarrow 2CO_2\text{-}S \qquad \text{(R.6)}$$

L-H expression that explains the kinetics of heterogeneous catalytic systems is given by the general equation:

$$r = -\frac{dC}{dt} = \frac{kKC}{1+KC} \qquad (2.3)$$

where *r* is the rate of reaction which is defined as the concentration change of a reactant with respect to time, *k* is the limiting rate constant at maximum coverage and *K* is the equilibrium constant of adsorption.

The limiting step of L-H kinetics is the surface reaction since colliding of two surface reactants is difficult. When two reactants are considered and the term C_S, which is the concentration of active sites, is taken into account; Equation 2.3 takes a more complex form:

$$r = kC_S^{\,2}\,\frac{K_1K_2C_AC_B}{(1+K_1C_A+K_2C_B)^2} \tag{2.4}$$

This L-H rate expression for photo-chemical surface reactions were studied theoretically by many researchers and tried to be simplified to first or less order expressions [Kumar et *al*., 2008]. Most of these researchers approximated L-H rate expression to first order by considering adsorption of both reactants were so low at room temperature ($KC<<1$) that the terms *k* and $K_1C_A+K_2C_B$ were neglected. This assumption reduces Equation 2.4 to:

$$r = C_S^{\,2}K_1K_2C_AC_B \tag{2.5}$$

which is a rate expression of first order with respect to both reactants.

L-H kinetics was shown that it could also be approximated to -1 order by making an assumption that one of the reactants (mostly O_2 in photo-oxidation processes) is the excess reactant ($K_2C_B>>1$), thus neglecting the terms *k* and $1+K_1C_A$ to reduce Equation 2.4 to:

$$r = C_S{}^2 \frac{K_1 C_A}{K_2 C_B} \tag{2.6}$$

which is a rate expression of first order with respect to A and -1 order with respect to B; that is, reactant B inhibits the reaction at all concentrations.

L-H kinetics was observed in many photocatalytic oxidation reactions and studied by researchers on degradation of several species by similar methods, assumptions and results. Although kinetic studies on CO photo-oxidation is limited in literature, for the removal of many model compounds, Langmuir adsorption isotherms were the main issue of the studies since the controlling step of L-H mechanism is the adsorption of reactants in room temperature under UV-light illumination [Zheng et *al*., 2010; Hapeshi et *al*., 2010; Talebian and Nilforoussan, 2006; Valente et *al*., 2006]. By using Langmuir adsorption isotherms; Zheng, Hapeshi, Talebian and Valente tried to observe the adsorption capacity of TiO_2 in the degradation processes of phenylarsonic acid, potassium hydrogenphthalate or methylene blue. In the studies on Langmuir adsorption isotherms; generally, it was assumed that, adsorption sites are unique, there is monolayer adsorption and there is no interaction between the adsorption sites. The equation usually used to model the reaction kinetics, similar to the first order L-H expression, was:

$$Q_{ad} = Q_{sat} \frac{K_{ad} C_{eq}}{1 + K_{ad} C_{eq}} \tag{2.7}$$

where Q_{ad} is the specific adsorbed quantity of the oxidized reactant, Q_{sat} is the maximum adsorption quantity on the catalyst surface, C_{eq} is the initial concentration of the oxidized reactant and K_{ad} is the adsorption constant.

According to the common results of the reaction kinetics studies, L-H degradation rate increases with illumination time and initial concentration of oxidized species depending on the first order kinetics.

Among a number of researchers studying on reaction mechanism of CO photo-oxidation, Zhu made a wide research for the reaction kinetics of low temperature CO photo-oxidation on Pd doped CeO_2-TiO_2 photocatalyst to observe the L-H mechanism [Liang and Zhu, 2009; Zhu et *al*., 2007; Zhu et *al*., 2005]. According to his results, CO was oxidized on Pd doped CeO_2-TiO_2 with a high conversion at ambient temperature under UV light following a L-H type kinetics. At lower temperatures, CO was pre-adsorbed on Pd sites and reacted with super oxygen at the Pd/Ce interface while at higher temperatures, the reaction was carried out between the more weakly adsorbed CO and super oxygen.

Like Zhu, Hwang investigated some results about the kinetics of CO low temperature photocatalytic oxidation on Pt deposited TiO_2 nanoparticles [Hwang et *al*., 2003]. He performed photo-oxidation experiments at ambient temperature and pressure under 200 Watts of UV light following the rate law defined as Equation 2.4. According to the plots he obtained, photocatalytic oxidation rates were linearly proportional to the initial CO concentration and exhibited a Langmurian behaviour for the dependence on O_2 concentration. This linear dependence on CO initial concentration implied that $K_{CO}C_{CO}<<1$ which resulted in the neglection of this term in the denominator.

In their study, Hwang and his research group also found out an alternative observed kinetics which was the Eley-Rideal type mechanism in which super oxygen on the photocatalyst surface reacted with gaseous CO.

ii. *Eley-Rideal (E-R) Mechanism*

Eley-Rideal mechanism differs from Langmuir-Hinshelwood mechanism with the step of photo-chemical reaction. Firstly O_2 molecules are adsorbed over photocatalyst surface then CO molecules react with them directly from their gaseous phase, without being adsorbed. The product is adsorbed CO_2 molecules which are further desorbed.

$$2CO_{(g)} + O_2^-\text{-}S \rightarrow 2CO_2\text{-}S \qquad \text{(R.7)}$$

The limiting step of E-R kinetics, like L-H, is the surface reaction step. Although a number of gaseous CO molecules are surely adsorbed, surface reaction of adsorbed oxygen and gaseous CO is dominant. Therefore, a maximum surface coverage is generally not observed and E-R kinetics is defined with the expression:

$$r = C_S \frac{K_1 K_2 C_A C_B}{1 + K_1 C_A} \qquad (2.8)$$

which is first order with respect to gaseous reactant B and depends on the concentration of adsorbed molecule A. When the concentration of adsorbed reactant A is low ($K_1 C_A << 1$), Equation 2.9 becomes:

$$r = C_S K_1 K_2 C_A C_B \qquad (2.9)$$

which is a first order expression with respect to both reactants.

However, when the concentration of adsorbed reactant A is high (K_1C_A>>1), Equation 2.8 simplifies to:

$$r = C_S K_2 C_B \tag{2.10}$$

where the order is zero with respect to A.

Reduction of several harmful gases by photo-oxidation does not generally follow E-R type kinetics because gaseous reactants are mostly activated by irradiation to be adsorbed on photocatalyst surface and proceed a surface oxidation step, thus there are limited number of literature studies on E-R kinetics. One of them belongs to Wagloehner who proposed that catalytic oxidation of CO on Fe_2O_3 catalyst in excess oxygen followed a route of dissociative adsorption of oxygen molecules getting into reaction with gaseous CO [Wagloehner et *al*., 2008]. In their research study, Wagloehner observed an apparent contradiction between L-H and E-R type kinetics which was explained by him that there was an extremely low coverage of the active Fe sites by CO resulting in the E-R type kinetic model.

2.3. TiO_2 as a Photocatalyst

The most widely studied metal oxide semiconductor for photo-oxidation of molecules is TiO_2 with its superior characteristics. This semiconductor occurs in nature as three different crystal structure; rutile, anatase and brookite phases. The most common and the most stable form is the rutile phase while anatase phase can be converted to rutile phase upon heating.

TiO_2 is used as a photocatalyst in its anatase form under UV light. For low temperature photocatalytic oxidation, anatase has been proved to be superier to rutile phase [Xie et *al*., 2010; Dong et *al*., 2010] because the conduction band location for anatase is more favorable for driving surface redox reactions and very stable surface peroxide groups can be formed at the anatase during photo-oxidation reactions. Furthermore; the band gap energy of anatase phase (3.23 eV) is more suitable for the energy of UV photons than the one of rutile phase (3 eV).

Photocatalytic activity of TiO_2 varies depending on its crystallinity, particle size, specific surface area and other physicochemical properties which can be altered significantly by preparation method. Crystalline structure of TiO_2 depends on its preparation temperature. This semiconductor exists as anatase type crystal at low temperatures while the rutile type crystal is formed at higher temperatures. Generally the phase transformation temperature is between 800 and 1200°C for TiO_2. Zhang examined TiO_2 prepared between 300 and 500°C for NO_x photo-degradation to see the difference between the photocatalytic activities of anatase and mixed phases [Zhang et *al*., 2007]. He reported that, a TiO_2 thin film prepared at about 350°C exhibited as a mixed crystal of 60 % of rutile and 40 % of anatase which showed the highest photocatalytic activity under 375 Watts of UV illumination. Similarly, to observe the dependence of photocatalytic activity on crystal structure of TiO_2, Inagaki prepared additional TiO_2 films above 500°C [Inagaki et *al*., 2006]. At such higher temperatures, TiO_2 phase was transformed from anatase to rutile where the photocatalytic activity decreased to even lower values.

Photocatalytic activity of TiO_2 has been showed to change according to the pretreatment conditions different from temperature. Supphasrirongjaroen and his research group tried to prove that the trapping sites of photo-generated

holes or the surface OH is also an important factor affecting photocatalytic activity of TiO_2 [Supphasrirongjaroen et *al*., 2008]. They prepared samples of TiO_2 by solvothermal method and compared the photocatalytic activities under 500 Watts of UV illumination between TiO_2 samples quenched in different mediums. According to their results, samples quenched in air showed the best photocatalytic activity while the photocatalytic activity of TiO_2 quenched in 30 % H_2O_2 medium is higher than the one in H_2O medium which is the result of enhancing effect of media containing more –OH groups. Amama and Itoh also searched the effect of pretreatment on photocatalytic activity by preparing untreated, pre-illuminated, hydroxylated and pre-chlorinated TiO_2 and testing them under 160 Watts of irradiation [Amama et *al*., 2002]. Quantum efficiency results, which are directly proportional with photocatalytic activity, were in the order of $TiO_2/HCl>TiO_2/P>TiO_2>TiO_2/H_2O$. With these results they explained the surface coverage effect of water, enhancing effect of pre-illumination forming e^-/h^+ pairs and charge separation efficiency of pre-chlorination due to the hole trapping ability of Ti/Cl^- surface.

Increasing photocatalytic activity of TiO_2 has become subject of many other studies focusing on a promising method which is doping TiO_2 with transition metals or metal oxides.

2.3.1. Metal or Metal Oxide Doping on TiO_2

To improve the photocatalytic activity of TiO_2, doping it with transition metals (Pt, Pd, Au, Ag, Cu, Fe, etc.) or metal oxides (SnO_2, ZnO, Cu_2O, etc.) has been applied since the metal/metal oxide serves as a lower energy pathway for gaseous adsorptive species. Depending on its band gap energy, TiO_2 can only absorb UV photons of solar radiation but when it is doped with metals or metal oxides, the absorption range has been proved to enlarge toward visible

light. Improving effect of metal doping is additionally explained with the prevention of charge recombination since the metal dopants on TiO_2 surface trap charge carriers during their migration from the bulk to the surface. The effect of metal ion doping strongly depends on many factors like dopant concentration, distribution of dopants or configuration of doping ions.

i. Spill-Over and Trapping

In the case of photocatalytic systems where a metal species is dispersed upon TiO_2, if the direct adsorption of a gaseous molecule is thermally unfavorable, the metal dopant serves as a lower energy pathway for the gaseous molecule; especially for oxygen. Gaseous oxygen molecules are firstly adsorbed by the metal or metal oxide since this step requires less energy for oxygen compared with the direct adsorption on TiO_2 surface. If electrons on TiO_2 surface are directly trapped by oxygen molecules on the metal dopant, super oxygen ions for surface oxidation are formed here and then transfered on TiO_2 surface. In this case, dopant adsorption becomes to achieve a trapping mechanism. However, it is also possible that oxygen molecules adsorbed by metal ions can follow a second energy pathway and spread over TiO_2 surface from the metal surface and trap electrons here to form super oxygen ions, which is explained as the spill-over mechanism. Spill-over mechanism is mostly seen for hydrogen molecule in catalytic systems [Ilinich et *al*., 2003; Rei et *al*., 2004; Benseradjh et *al*., 2002].

Photocatalytic activity has not been proven yet if it is affected by the dopant adsorption mechanism but the spill-over mechanism was introduced in many research studies to be the dominant mechanism of molecules being adsorbed on doped TiO_2. In his research study, Bowker

introduced the spill-over image of oxygen around Pd particles doped on TiO_2 to photocatalytically oxidize methanol [Bowker et *al*., 2003]. Similarly, Blount and Falconer also observed the spill-over of oxygen from Pt over the TiO_2 surface and formation of super oxygen ions to oxidize toluene under UV light illumination [Blount and Falconer, 2001]. For CO photo-oxidation; on the other hand, among the limited number of studies, Dai and his research group characterized the dopant adsorption mechanism to search for the photo-oxidation of CO on Au/TiO_2 catalyst [Dai et *al*., 2009]. They observed that oxygen was adsorbed firstly on Au particles then spilled over TiO_2 surface to trap electrons.

Spill-over and trapping mechanisms are shown in Figure 2.2:

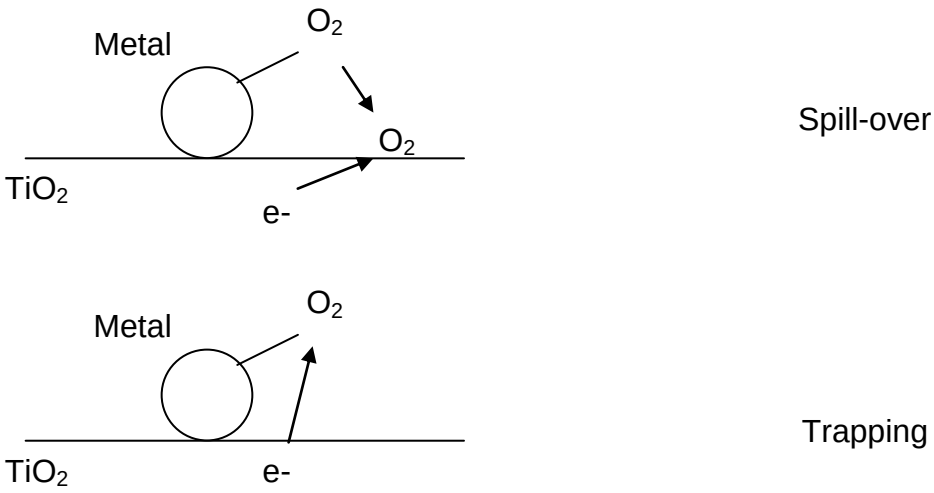

Figure 2.2. Spill-over and trapping on TiO_2 surface

2.3.2. TiO_2 and SiO_2 Based Photocatalysts

There have been many studies on transition metal or metal oxide doping on TiO_2. However, limited number of work on low temperature CO photo-oxidation activity of doped TiO_2 have been reported in literature. Roy reported high photocatalytic activity with creation of redox adsorption sites by Pd^{2+} ion substitution in nano structured TiO_2 [Roy et *al*., 2007]. They prepared catalysts of 1 and 0.5 atom % Pd/TiO_2 and examined their photocatalytic activity in a continuous flow photo reactor under 125 Watts of UV irradiation. The photocatalysts achieved to show 20 % CO conversion at steady state after 200 seconds. Roy also observed that, photocatalytic activity over Pd^{2+} ion substituted TiO_2 was at least 2 orders of magnitude higher than unsubstituted TiO_2 to conclude that Pd^{2+} ions form adsorption sites for CO and O_2 molecules. When loading was increased, it was seen that activity decreased as a result of the broadening of Pd^{2+} band which lowers the photoluminescence.

Effect of doping TiO_2 on photocatalytic oxidation of CO is also studied by Ozen and Uner [Ozen and Uner, 2001]. They firstly investigated the oxygen adsorption isotherms for bare and Pt doped TiO_2. Oxygen adsorption, as mentioned before, is one of the most important steps in photo-oxidation process of CO and it is affected by the pre-treatments sequenced during catalyst preparation. Untreated Pt/TiO_2 photocatalysts showed the highest adsorption capacity due to the oxidative interaction between the catalyst precursor and the adsorbate. However; upon calcination, wetting and drying processes on TiO_2, adsorption decreased by the presence of strongly bounded oxygen on the support surface, increase in bulk density and an accompanying decrease in external surface area. The conversion result of CO (85 % after 5 minutes) under 100 Watts of illumination supported the

proposed role of Pt as a spill-over media for oxygen, thus increasing the rate of reaction.

For photo-catalyzed oxidation of CO, another TiO_2 based photocatalyst, $Au/MnO_x/TiO_2$, was characterized by Kim [Kim et *al*., 2008]. They tried to prove that, metal and metal oxide doped TiO_2 exhibited a shift in the Fermi level to more negative potentials. Such a shift in the Fermi level improved the interfacial charge transfer process. The photocatalytic activity of the catalyst was examined by measuring the CO concentration as a function of irradiation time under UV light illumination of 12 Watts in a batch reactor. The photocatalytic activity heavily depended on the selection of support in the following order: $Au/MnO_x/TiO_2$>Au/TiO_2>Au/MnO_x>MnO_x/TiO_2. The most active catalyst was $Au/MnO_x/TiO_2$ of which the reaction constant was about five times higher than that of Au/TiO_2 and the low photocatalytic activity of MnO_x/TiO_2 explained the crucial role of gold for adsorbing O_2 molecules and increasing the photo-oxidation activity of CO.

Macyk and Kisch studied CO photo-oxidation from the point why it was difficult to photo-catalyze CO oxidation at ambient conditions [Macyk and Kisch, 2007]. After the observations, they explained the reason as the problems seen in the desorption step of the photocatalytic process. They examined TiO_2 supported $RuO_2.xH_2O$ as a catalyst for the thermal and photo-assisted catalytic oxidation of CO and the mechanism of this reaction was investigated in great detail. It was observed that in the case of $30\%RuO_2.xH_2O/TiO_2$, the conversion factor reached to 55 % under visible light illumination (400nm-650nm) which was much higher than the case of SnO_2, Fe_2O_3 and WO_3 supports. Although good adsorption of reactants were seen at room temperature, produced CO_2 was desorbed from the surface only at elevated temperatures (~600 K) resulting in the occupation of the catalyst surface by CO_2 molecules preventing the new adsorption steps.

Silica (SiO_2) is an oxide of silicon and it is well known for having a high specific surface area with high adsorptive capacity. Although bare SiO_2 shows no photocatalytic activity, it takes the role of being a good adsorbent when supported with several metals and metal oxides to increase the number of catalytically active sites on the large surface of this molecule. There are lacking studies in literature on low temperature CO photo-oxidation over metal oxide supported SiO_2, one of which belongs to Kamegawa and his research group [Kamegawa et *al*., 2006]. They took advantage of the high surface area and adsorptive capacity of SiO_2 in CO photo-oxidation on highly dispersed Mo-oxide catalysts supported on SiO_2 (by FT-IR, under UV light, in 293 K) with excess H_2 to develop applicable, cheap, non-metallic and non-polluting catalytic systems to provide pure H_2 to fuel cells. The results showed that the stoichiometric production of CO_2 with degradation of CO was increased with UV light irradiation time and was not affected much by the co-existence of excess H_2. Moreover, after 180 minutes of UV irradiation, CO conversion and selectivity were calculated to be ~100 and 99 %, respectively while the amount of CO stayed constant in 10 minutes of dark test.

Base sites and photo-active sites of fine particles of magnesium oxide (MgO) dispersed on SiO_2 were also studied by Yoshida to examine their photocatalytic activities for low temperature CO oxidation [Yoshida et *al*., 1994]. Some samples including MgO fine particles were prepared and loaded on SiO_2 in different amounts. From the correlation between the population of Mg-O ion pairs and the rate of photo-oxidation, they concluded that catalytically active sites for CO photo-oxidation were Mg-O ion pairs. In their research, a good relationship between the amount of base sites, where CO_2 molecules were chemisorbed, and the rate of CO photo-oxidation was observed thus base sites and photo-active sites were considered to be identical.

CHAPTER 3

EXPERIMENTAL

During the experimental studies, Pd doped TiO_2/SiO_2 photocatalysts were synthesized by “sol-gel method”. The samples were characterized by “X-Ray Diffraction (XRD)” and “BET Technique”. These photocatalysts were then tested for room temperature CO oxidation under UV light illumination in a re-circulated FT-IR and fluidized bed reactor system.

3.1. Photocatalyst Synthesis

3.1.1. Materials

TiO_2/SiO_2 mixed oxides were doped with 0.1 weight % Pd during their sol-gel preparation depending on the recipe introduced by Bayram [Bayram, 2009]. The precursors and chemicals used in the synthesis and their impurities are:

i. *Tetraethy Orthosilicate (TEOS)*: Precursor of SiO_2 (Molecular formula: $C_8H_{20}O_4Si$, 98 %, by Aldrich, CAS number: 78-10-4).
ii. *Titanium (IV) n-Butoxide (TBOT)*: Precursor of TiO_2 (Molecular formula: $C_{16}H_{36}O_4Ti$, 99 %, by Acros Organics, CAS number: 5593-70-4).
iii. *Isopropyl Alcohol (i-PrOH)*: Co-solvent for TEOS and TBOT (Molecular formula: C_3H_8O, by Riedel-de Haen, CAS number: 67-63-0).

iv. *2-4 Pentanedione / Acetylacetone (AcAc)*: In order to decrease the hydrolysis and condensation rates of TBOT (Molecular formula: $C_5H_8O_2$, 99 %, by Acros Organics, CAS number: 123-54-6).
v. *Hydrochloric Acid*: Catalyst for TEOS solution (Molecular formula: HCl, fuming 37 %, by Merck).
vi. *Palladium (II) Acetate ($Pd(OAc)_2$)*: Precursor of Pd ions (Molecular formula: $(CH_3CO_2)_2Pd$, 98 %, by Aldrich, CAS number: 3375-31-3).

3.1.2. Catalyst Synthesis

To obtain Pd doped TiO_2/SiO_2 catalyst samples sol-gel method was utilized. Firstly, SiO_2 was obtained by solving certain volumes of TEOS in i-PrOH and H_2O with HCl catalyst according to the desired SiO_2 percentage in TiO_2. The solution was stirred for half an hour and previously weighed $Pd(OAc)_2$ powder was dropped into TEOS solution at this moment. The new solution was stirred for one hour at 35°C to solve $Pd(OAc)_2$ effectively for the formation of Pd ions. After totally 1.5 hours of stirring, TEOS and $Pd(OAc)_2$ mixture turned into a light brown and dense liquid like a gel. For this mixture, molar ratio of chemicals apart from water were taken as TEOS:i-PrOH:HCl = 1:15:0.001, respectively and water molar amount was chosen as (TEOS+TBOT):H_2O = 1:4 [Bayram, 2009]. During the formation of SiO_2, hydrolysis and condensation steps are followed:

$$Si\text{-}(OR)_4 + n\ H_2O \rightarrow Si\text{-}(OH)_4 + n\ R\text{-}OH \quad \text{(hydrolysis)} \quad (3.1)$$

$$Si\text{-}(OH)_4 \rightarrow SiO_2 + 2\ H_2O \quad \text{(condensation)} \quad (3.2)$$

Secondly, TiO_2 was obtained by solving certain volumes of TBOT in i-PrOH and AcAc. The condensation and hydrolysis rate of TBOT is faster than TEOS [Brinker, 1990]. The aim of using AcAc in this step is to decrease the hydrolysis and condensation rates of TBOT. With the use of AcAc, more crowded radical groups are placed around coordination states of TBOT to cover central Ti atom. Such kind of compounds are named as “chelating agents” that AcAc is the chelating agent of sol-gel process in this study. The solution was stirred for 45 minutes and the molar ratio of chemicals was chosen as TBOT:AcAc:i-PrOH = 1:1:15 [Bayram, 2009]. Upon stirring, the solution turned into a light yellow solution with a temperature increased from room temperature to about 30°C by the effect of adding AcAc.

Lastly, TBOT solution was poured into TEOS solution dropwise to prevent precipitation and the mixture was stirred for 30 minutes after adding some extra water. The sample was then aged in an autoclave at 110°C for 24 hours. It was reported by Liotta that with hydrothermal ageing, the products have a better solid state diffusion [Liotta et *al*., 2009]. The purpose of ageing under high pressure is to ensure that any physical and chemical changes that continue during gelation are completed and new strong chemical bonds are formed, thus this process results in the shrinkage of the sample into a two phase system as bulk and liquid [Brinker, 1990].

After the ageing process, the two phase mixture was dried in an oven at 110°C for 24 hours to get rid of solvents like H_2O and alcohol based components. After drying process, liquid phase of the sample was removed completely and it turned into brown solid pieces which were further broken into powder form. The last step was the calcination of this powder sample in a calcination oven at 500°C for 5 hours during which the amorphous structure was expected to turn into crystalline phase. After this last thermal step, white powder photocatalyst of Pd doped SiO_2/TiO_2 was meshed into

smaller size particles (45 microns) and kept in dark. The photocatalysts synthesized as SiO_2/TiO_2 [Bayram, 2009] and as $Pd/SiO_2/TiO_2$ are listed in Table 3.1 with their codes and weight percentages (See Appendix D for sample sol-gel recipe).

Table 3.1. Photocatalysts with their codes and weight percentages

Photocatalyst Code	**Pd Weight %**	**SiO_2 Weight % in TiO_2**
P-BiB3	0.1	66
P-BiB5	0.1	5
P-BiB10	0.1	10
P-BiB12	0.1	80
P-BiB14	0.1	20
P-BiB16	0.1	100
P-BiB18	0.1	0
P-BiB20	0.1	50
P-BiB22	0.1	35
BiB3	0	66
BiB5	0	5
BiB10	0	10
BiB12	0	80
BiB14	0	20
BiB16	0	100
BiB18	0	0
BiB20	0	50
BiB22	0	35

3.2. Photocatalyst Characterization

3.2.1. X-Ray Diffraction (XRD) Analysis

By using XRD technique; the crystallographic structure and crystallite size (grain size) were obtained. X-rays which are the waves of electromagnetic radiation are sent to the center of crystal structure of the sample and as they are scattered by the atoms of the molecules, the bragg angle theta (θ) between the plane and the X-ray are recorded by the XRD device. When the intensity for each reflection is plotted against the scattering angle (2θ), the relative intensities of the peaks on this graph are observed as the key information from which the structure is determined.

In this study, the characterization of photocatalysts by XRD was carried out by Rigaku Ultimate IV X-Ray Diffractometer. The properties and fixed parameters used during scanning are listed below in Table 3.2.

Table 3.2. Properties and parameters of the XRD device for sample scanning

Parameter	**Value**
X-Ray Tube	CuKα
Voltage	40 kV
Current	40 mA
Filter	Not used
Sampling Width	0.02 deg.
Scan Range	20.00-60.00 deg.
Scan Speed	2.00 deg./min.

3.2.2. Surface Area, Pore Size Distribution and Pore Volume

For the measurement of specific surface area, pore size distribution and pore volume of the catalyst samples, the rule of physical adsorption of gas molecules on a solid surface was applied.

Three researchers named as Stephen Brunauer, Paul Hugh Emmett and Edward Teller published an article about finding the total surface area and specific surface area (total surface area per unit mass) by using Langmuir theory depending on this rule. Langmuir theory is based on the monolayer and multilayer adsorption of gas molecules where it can be applied to each layer. They called this specific surface area measurement technique as “BET Technique” with the initials of their family names. According to the experimental results of BET technique, adsorption isotherms can be plotted as straight lines depending on many BET equations written in terms of equilibrium and saturation pressure, monolayer adsorbed quantity, BET constant and heat of adsorption. The values of the slope and y-intercept of these adsorption isotherms are then used to calculate the total and specific surface area values in addition to the pore properties of solid particles.

For the measurement of specific surface area values of photocatalysts by BET technique, Nitrogen was used as inert gas therefore the adsorption isotherms of Nitrogen obtained at 77 K were used.

To determine the pore size distribution and pore volumes of the photocatalysts, the technique of Barrett-Joyner-Halenda (BJH) (Nitrogen adsorption and desorption branches of the isotherms) was applied. Adsorption isotherms are obtained by admitting a known quantity of Nitrogen to a confined volume containing the adsorbent maintained at constant temperature and constructing the isotherms point-by-point by the admission

to the adsorbent of successive charges of gas with the aid of a volumetric dosing technique and application of the gas laws [Sing et *al*., 1985]. The isotherms were plotted as the adsorbed quantity in cc/g against the relative pressure (P/P_0) on two curves belonging to adsorption and desorption results of the samples. Isotherms give information about the mezoporous (2-50 nm) or microporous (< 2 nm) structures of the photocatalysts. The curves of dV/dlogD against diameter are for the size distribution of the samples.

3.3. Photocatalytic Activity Tests

3.3.1. Experimental Set-Up

For the photocatalytic activity tests of synthesized catalysts, a re-circulated FT-IR and fluidized bed reactor system was built (Figure 3.1). This set-up includes mainly a glass cylinder, a six port valve, a gas pump, a fluidized bed reactor and FT-IR spectro-photometer with its FT-IR cell and data computer. These members are connected by stainless steel, 1/8 inches tubing.

The glass cylinder by Alltech was used as a vessel with known volume of 122 cm^3 for accurate dosing of CO into the system. The volume of cylinder was adjusted by inserting polyamide solid pieces with known volumes into the glass cylinder.

The six port valve of the system was used in two positions which were filling and injection positions. In the filling position, the glass cylinder was filled with CO/He gas mixture from the gas tube while in the injection position, this gas mixture was sent into the closed system of FT-IR and fluidized bed reactor.

The gas is re-circulated through the reactor and FT-IR cell by using diaphragm pump by Parker. This pump increases the pressure of the gas working with 10.0 Volts for the re-circulation. The pump was connected to the exit of six gate valve right before the reactor to create an effective pressure to fluidize the powder catalyst in the reactor.

The tubular fluidized bed type reactor was made by quartz tubing of 4 mm ID and 7 cm long and was pro-truded into irradiation chamber which was illuminated by three of 12 Watts 254 nm UV-C lamps (Philips Model No: TUV PL-S).

Fourier Transform Infrared (FT-IR) spectro-photometer was used to measure the CO and CO_2 gases quantitatively. For this purpose Bruker Equinox 55 FT-IR spectrometer equipped with DEGS detector was used. The FT-IR gas transmission cell used in the experimental set-up has a length of 19.5 cm and a diameter of 6 cm. The two ends of the FT-IR cell were made by CaF_2 windows which are suitable for 150 to 8000 nm.

3.3.2. Calibration

The system was firstly calibrated in order to determine the corresponding absorbance peaks of certain compositions. By using polyamide solid pieces, the glass cylinder was fixed to a known volume and it was filled from a gas tube of 1 % CO in He in the filling position of six gate valve while room air was being passed by the gas pump through the empty reactor and FT-IR cell. Room air in the system with zero CO concentration was scanned by FT-IR spectro-photometer to be taken as the reference line of the absorbance spectrum. Afterwards, the six gate valve was turned to injection position and the collected CO/He mixture was injected into the system and circulated for

10 minutes before being scanned by FT-IR to record the CO absorbance peaks against wavenumber. This was done for a number of different volumes of gas mixture by washing the system with air in between.

The recorded volumes of CO/He gas mixture were converted into CO/Air composition values (See Appendix A.1 for sample calculation). Absorbance peaks of each concentration against a certain wavenumber range was recorded by the OPUS software which was named as calibration curves. CO wavenumber range was 2025-2225 cm^{-1} while for CO_2 it is 2250-2400 cm^{-1}. CO concentration *versus* absorbance graph was drawn in Excel using the calibration curves to obtain a third order equation to calculate the CO changing concentration for each sample during the photocatalytic activity tests (See Appendix B for the calibration curves and finding the calibration equation).

3.3.3. Carbon Monoxide Photo-Oxidation Tests

The larger part of home made quartz reactor was filled with 0.5 g of photocatalyst powder sample fixed with reactor wool. CO concentration of 1000 ppm in air was chosen as the initial gas concentration to start the oxidation reactions, therefore the glass cylinder was filled with 66 cm^3 of CO/He mixture from the gas tube. During filling, room dry air was passed through the reactor system and the background spectrum where time was set to zero was plotted by FT-IR spectro-photometer. When filling of glass cylinder was completed, the closed system of reactor and FT-IR cell was injected with 1 % CO in He gas mixture from glass tube to obtain 1000 ppm CO in air.

The CO/Air mixture was firstly re-circulated for 10 minutes to obtain a homogeneous mixture and the initial CO concentration was plotted as a peak by FT-IR where the time was set to t=1. The re-circulation was further extended to 360 minutes in the dark as the blank test (Phase I) in order to ensure any possibility of non photocatalytic reaction under room temperature by recording FT-IR spectrum every 15 minutes.

The second part of the experiment (Phase II) was started when three UV-C lamps were switched on at t=360 to start 36 Watts of illumination and the test was continued until CO concentration was observed to reach to zero. Absorbance data were taken in every 15 minutes to follow the change in gas composition as a result of photocatalytic reaction. Absorbance peaks of CO and CO_2 in the wavenumber range of 2025-2400 cm^{-1} were recorded by the OPUS® software on the absorbance spectrum. CO absorbance peaks (at 2098.172 cm^{-1}) for each time interval of 15 minutes were then converted into concentration values by using the third order equation of calibration curve and with these concentration values, graphs of CO percent conversion *versus* time were plotted.

CHAPTER 4

RESULTS AND DISCUSSION

4.1. Photocatalyst Characterization

The synthesized catalyst samples tested for CO photocatalytic oxidation were characterized by XRD analysis and BET technique.

4.1.1. XRD Analysis

XRD patterns of SiO_2/TiO_2 samples were studied previously and it was reported that all SiO_2/TiO_2 samples contain amorphous silica and anatase TiO_2 phases [Bayram, 2009].

The seven characteristic peaks of anatase and rutile TiO_2 with 2-Theta values and crystal surfaces are investigated in Table 4.1 below [JADE software database]:

Table 4.1. Characteristic peaks of anatase and rutile TiO_2

Crystal Structure	#	I (fix)	I (var)	h k l	2-Theta
Anatase TiO_2	1	100	100	1 0 1	25.3
	2	10	14	1 0 3	36.9
	3	20	29	0 0 4	37.8
	4	10	15	1 1 2	38.6
	5	35	65	2 0 0	48.1
	6	20	41	1 0 5	53.9
	7	20	42	2 1 1	55.1
Rutile TiO_2	1	100	86	1 1 0	27.5
	2	50	56	1 0 1	36.1
	3	8	9	2 0 0	39.2
	4	25	32	1 1 1	41.2
	5	10	13	2 1 0	44.1
	6	60	100	2 1 1	54.3
	7	20	34	2 2 0	56.6

After the precursors of TiO_2, SiO_2 and Pd were mixed and dried following the sol-gel route with hydrothermal treatment, which was explained in detail in Section 3.1, powder samples were calcined at 500°C in air for 5 hours. Crystal structure of Pd doped mixed oxides were also investigated by XRD and the results are presented in Figure 4.1. As it can be seen clearly from this figure that, for all photocatalyst samples except 0.1 % Pd doped SiO_2, the major diffraction peaks occur at 2θ values around 25, 38, 48 and 55 indicating 101, 112, 200 and 211 planes of anatase structure, respectively. These results are in good agreement with the previous work [Bayram 2009]. The amorphous silica background was observed for 0.1%Pd/100%SiO_2 sample and the presence of PdO phase was evidenced for 0.1%Pd/80%SiO_2/20%TiO_2 and 0.1%Pd/66%SiO_2/34%TiO_2 samples at 2θ value of 34, which is coherent with its characteristic value [Zhang et *al*., 2002].

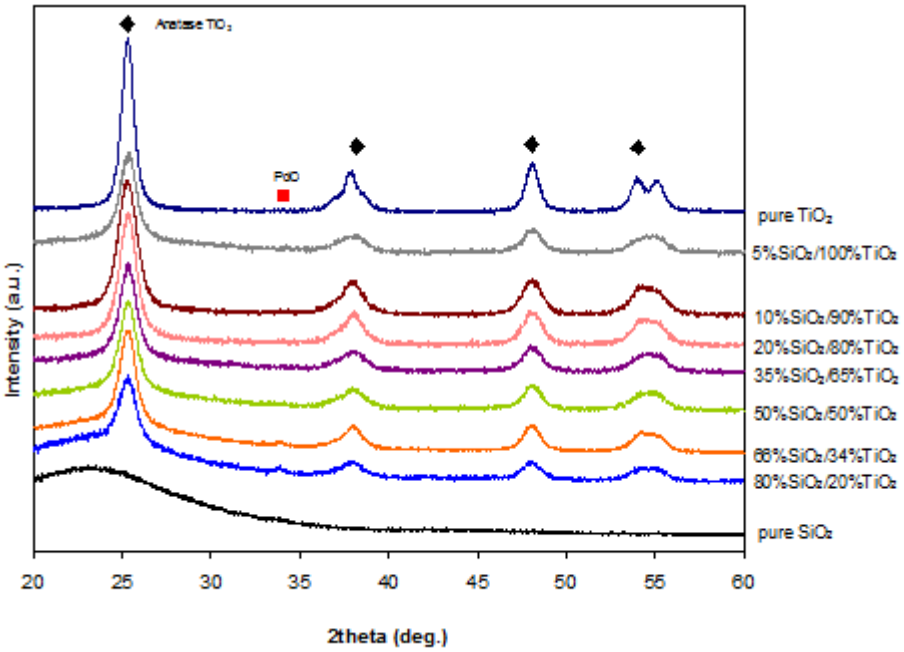

Figure 4.1. X-Ray diffraction results for 0.1 % Pd doped SiO_2/TiO_2 samples and the effect of SiO_2/TiO_2 ratio

When the XRD results are analyzed carefully, the PdO peak becomes smaller with decreasing SiO_2 content and disappears completely with the sample including 50 % SiO_2. This might be attributed to the better dispersion of PdO over the TiO_2 phase than the SiO_2 surface. This result is consistent with literature from the point that PdO shows a better dispersion over TiO_2 surface than on SiO_2 which is related to the rather strong PdO-TiO_2 interaction [Venezia et *al*., 2009]. There might be another explanation for this phenomena that PdO structure can be converted into metallic Pd over TiO_2 surface but a new peak for Pd around 40 degrees [Zhang et *al*., 2002] would be expected in that case which is not observed in the present results. To conclude, it can be interpreted that Pd loading on SiO_2/TiO_2 samples did not

alter the crystal structure of TiO_2 and Pd is preferentially dispersed over the TiO_2 crsytallites in PdO form.

To see the effect of TiO_2 dispersion over SiO_2, the crystallite size of TiO_2 particles were determined by using Scherrer's equation (see Appendix A.2 for sample calculation of crystallite size). Crystallite size of TiO_2 particles are summarized in Table 4.2. The results reveal that particles are well dispersed over SiO_2 and larger TiO_2 crystallites are formed over the surface in the presence of SiO_2. The pure TiO_2 crystallite size is around 10 nm and about the half of that size was obtained in silica matrix. Similar results were already published in literature [Devi et *al*., 2010; Jung et *al*., 2002]. The amorphous structure of SiO_2 does not permit further analysis on SiO_2 crsytallites.

Table 4.2. Crystallite sizes of TiO_2

Pd wt %	**SiO_2 wt %**	**TiO_2 wt %**	**Crystallite Size (nm)**
0.1	0	100	10
0.1	5	95	6.8
0.1	10	90	6.3
0.1	20	80	7.0
0.1	35	65	6.9
0.1	50	50	6.3
0.1	66	34	6.3
0.1	80	20	4.8

In the study of Kim and his research group, the crystallite size effect on the absorption band of TiO_2 was searched and they pointed out that when crystallite size increases, the absorption band shifts toward the larger wavelength region therefore the band gap energy of TiO_2 decreases [Kim et *al*., 2007]. As a result, for the samples with TiO_2 rich compositions (0, 5, 20

and 35 % SiO_2 in TiO_2), larger crystallite size TiO_2 may lead higher band gap which shifts the absorption edge to UV range. Thus better photocatalytic activity should be expected with higher SiO_2/TiO_2 ratio with smaller crystallite size.

4.1.2. BET Surface Area and BJH Pore Size Distribution and Pore Volume

Nitrogen adsorption technique was used to explore the textural properties of the catalyst samples. The surface area and pore size distribution of the samples were determined by BET and BJH methods. More details can be found in Section 3.2.2. The BET results of SiO_2/TiO_2 mixed oxides indicated that surface area of the samples are decreasing with TiO_2 loading. Moreover, the increase of TiO_2 loading up to 34 % steps up pore size and pore volume while further increase of TiO_2 loading yields samples with smaller pore size. Therefore, optimum TiO_2 content for surface area, pore size and pore volume values was accepted as 34 % for SiO_2/TiO_2 catalyst samples [Bayram, 2009].

Surface area values changing with different SiO_2/TiO_2 [Bayram, 2009] and $Pd/SiO_2/TiO_2$ compositions are introduced in Table 4.3.

Table 4.3. BET results for synthesized samples

Pd wt %	SiO_2 wt %	TiO_2 wt %	Surface Area (m^2/g)
0	0	100	9.69
0	10	90	251
0	20	80	308
0	35	65	416
0	50	50	479
0	66	34	643
0	80	20	675
0	100	0	536
0.1	0	100	96
0.1	5	95	231
0.1	10	90	265
0.1	20	80	345
0.1	35	65	355
0.1	50	50	427
0.1	66	34	664
0.1	80	20	674
0.1	100	0	752

The smallest surface area for Pd doped samples is belong to 0.1 % Pd doped TiO_2 (96 m^2/g) and the highest area was achieved with the synthesis of 0.1 % Pd doped SiO_2 (752 m^2/g). Introducing Pd to each sample of SiO_2/TiO_2 mixed oxides is observed to increase their BET surface area. For instance, surface area of bare TiO_2 and bare SiO_2, synthesized by the same method, was reported as 9.7 m^2/g and 536 m^2/g which were increased drastically by only 0.1 % Pd loading. The addition of SiO_2 snynergistically increases the surface area of $Pd/SiO_2/TiO_2$ samples like the case in SiO_2/TiO_2 catalysts. Only 5 % addition of SiO_2 to TiO_2 increases the surface area of Pd doped TiO_2 to 231 m^2/g. These results are in good agreement with crystallite size measurement.

In order to observe the pore size distribution of the samples, N_2 adsorption isotherms of the samples were analyzed by BJH method. The N_2 adsorption isotherms of 0.1%Pd/100%TiO_2, 0.1%Pd/100%SiO_2 and 0.1%Pd/50%SiO_2/ 50%TiO_2 are presented in Figure 4.2, 4.3 and 4.4. (N_2 adsorption isotherms of the other photocatalyst samples are presented in Appendix E.1).

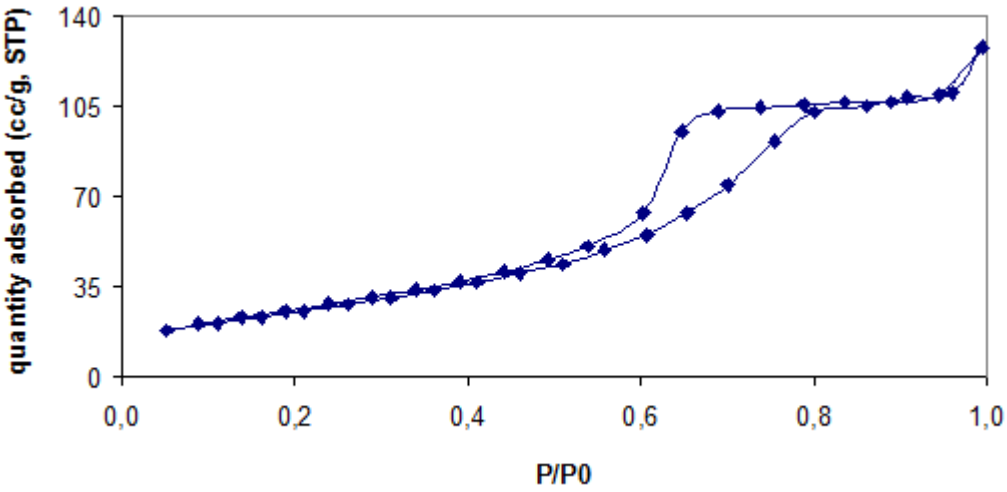

Figure 4.2. Nitrogen adsorption/desorption isotherms of 0.1%Pd/100%TiO_2 sample

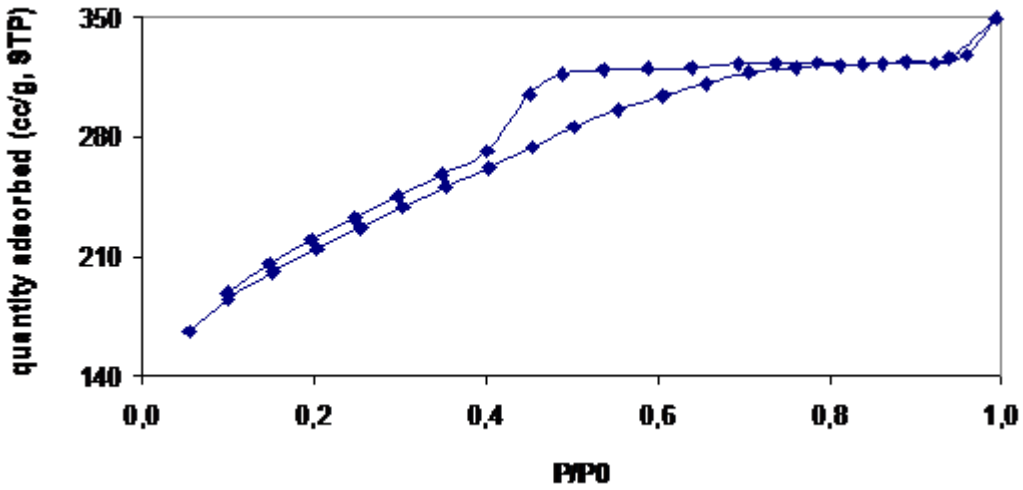

Figure 4.3. Nitrogen adsorption/desorption isotherms of 0.1%Pd/100%SiO_2 sample

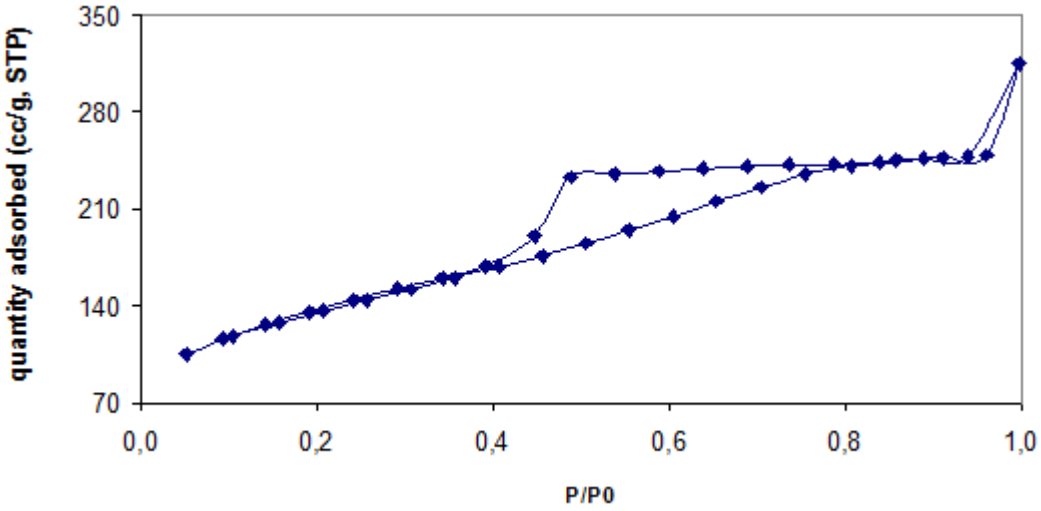

Figure 4.4. Nitrogen adsorption/desorption isotherms of 0.1%Pd/50%SiO_2/50%TiO_2

The pore size distributions were obtained as dV/dlogD against pore diameter in logarithmic scale and the average pore size values were evaluated. Figures from 4.5 to 4.7 illustrate the pore size distributions of the samples 0.1%Pd/100%TiO_2, 0.1%Pd/100%SiO_2 and 0.1%Pd/50%SiO_2/50%TiO_2 and, pore diameters and pore volumes are given in Table 4.4 for all samples (See Appendix E.2 for the pore size distributions of other samples).

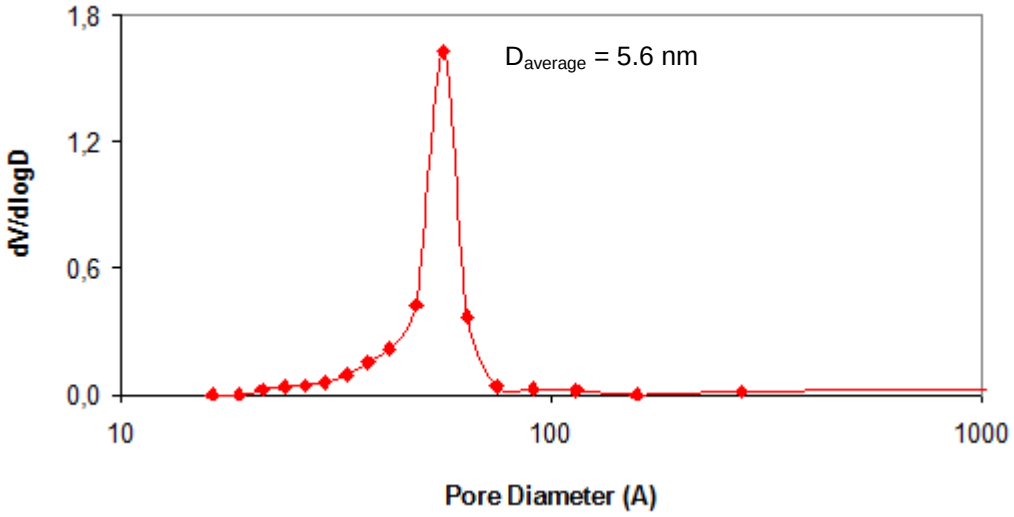

Figure 4.5. Pore size distribution for (0.1%Pd/100%TiO_2) sample

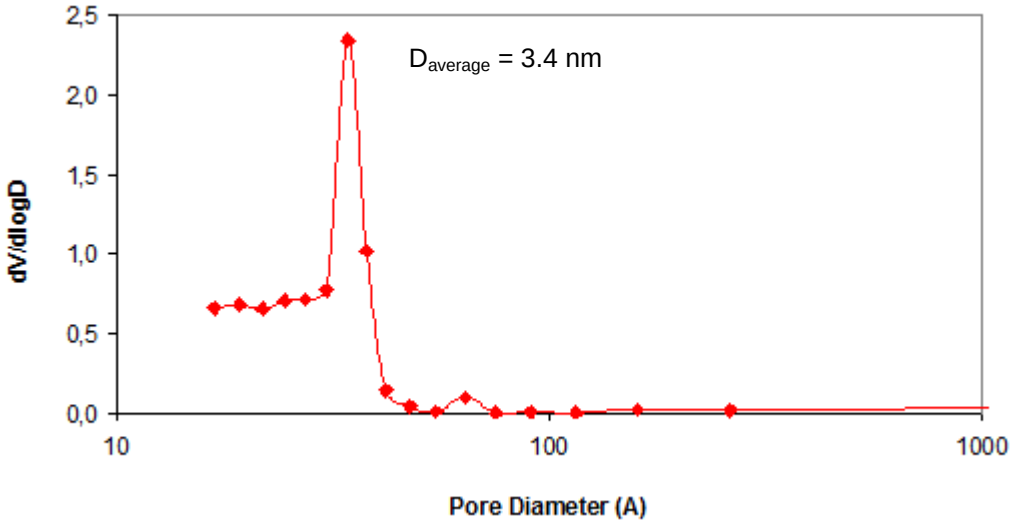

Figure 4.6. Pore size distribution for
(0.1%Pd/100%SiO_2) sample

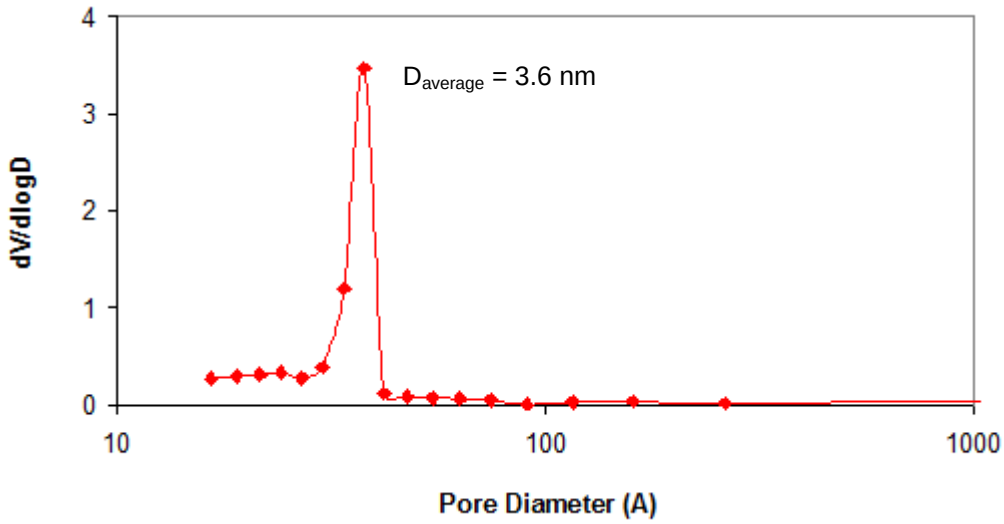

Figure 4.7. Pore size distribution for
0.1%Pd/50%SiO_2/50%TiO_2 sample

Table 4.4. Average pore diameters and pore volumes

Pd wt %	SiO_2 wt %	TiO_2 wt %	D_{pore} (nm)	V_{pore} (cc/g)
0	0	100	4.8	0.17
0	10	90	7.9	0.45
0	20	80	8	0.6
0	35	65	4.3	0.45
0	50	50	4.6	0.45
0	66	34	8.4	1.01
0	80	20	3.3	0.44
0	100	0	1.5	0.26
0.1	0	100	5.6	0.22
0.1	5	95	3.3	0.14
0.1	10	90	6.5	0.52
0.1	20	80	6.5	0.57
0.1	35	65	3.4	0.22
0.1	50	50	3.6	0.35
0.1	66	34	6.6	0.78
0.1	80	20	7.9	0.78
0.1	100	0	3.4	0.43

N_2 adsorption isotherms indicate that Nitrogen adsorption volumes for the samples including 5, 35, 50 and 100 % SiO_2 in TiO_2 with 0.1 % Pd are relatively smaller and possible in lower pressures in addition to the narrower hysteresis shape of the samples with 5 and 35 % SiO_2. This is characteristic of the presence of micropores in the structures of these samples [Braconnier et *al*., 2009]. Microporous structure is created by SiO_2 and the most effective micropores to adsorb Nitrogen at low pressures was achieved with the sample including 100 % SiO_2 while the weakest adsorption was observed over the micropores of 0.1%Pd/5%SiO_2/95%TiO_2 sample.

0.1 % Pd doped TiO_2 has the medium size mesopore diameter compared with the other samples. When the pore diameters increase toward meso scale values, the adsorption isotherms shift to larger volumes and higher relative pressures, which can be observed for the samples of 0.1 % Pd doped 10, 20, 66 and 80 % SiO_2 in TiO_2. This indicates that introduction of SiO_2 creates a partial stabilization of the porosity and mostly increases the adsorption capacity. Mesopores of the catalyst with 80 % SiO_2 is the most effective one to adsorb Nitrogen at higher pressures while the one with 10 % SiO_2 does not have so strong mesopores to adsorb Nitrogen.

The samples 10%SiO_2/90%TiO_2, 20%SiO_2/80%TiO_2 and 35%SiO_2/65%TiO_2 have pore diameters 7.9, 8 and 4.3 nm, respectively [Bayram, 2009] which were decreased to 6.5, 6.5 and 3.4 nm with Pd addition. According to Table 4.4, there is a direct relation between the pore diameter and the pore volume of the Pd doped samples which introduces similar pore shapes with different sizes for the synthesized catalysts. All isotherms can be classified as Type V and H2 hysteresis loops are observed between the adsorption and the desorption curves which indicate the weak interaction between the N_2 and the sample surface and the presence of ink-bottle-type pore structures with a narrow entrance and a large cavity [Sing et *al*., 1984; Kim et *al*., 2007].

4.2. Photocatalytic Activities

Photocatalytic activity tests were performed by using the re-circulated closed system of fluidized bed reactor coupled with FT-IR cell. The details of the system, the methodology for quantitative measurement of CO and CO_2 by using FT-IR spectrometer and the photocatalytic activity tests were explained in detail in Sections 3.3.1-3.3.3.

0.5 g of each photocatalyst sample was placed in reactor which was flushed with fresh air prior to experiment. The proper volume of CO gas which corresponds to 1000 ppm CO in air was dosed into the reaction system and the gas was started to re-circulate by turning on the diaphragm pump. The mixing period of CO with air in the reaction system was performed and FT-IR spectrometer stability was assured by performing initial stage of experiments in dark. Thus the perfect mixing, adsorption of CO over catalyst surface and stable FT-IR spectra were obtained during the dark initial period of the experiments. During the re-circulation of CO gas, the IR bands for CO and CO_2 against a wavenumber range of 2050-2400 cm^{-1} was followed by FT-IR with the help of OPUS® software. In Figure 4.8, the time course of FT-IR gas phase spectra over 0.1%Pd/20%SiO_2/80%TiO_2 catalyst in initial dark period is presented as example. As it is shown in the figure, there is no significant change in CO concentration (2025-2225 cm^{-1}) which indicates the homogeneous mixing of CO and air taking place in the first 15 minutes of the experiment. Also the comparison of CO absorbance with calibration work performed without catalyst allowed us to observe any adsorption of CO over the catalyst surface. As it is seen from the spectra, no change was observed on the CO peak intensities (2025-2225 cm^{-1}) except some small changes in CO_2 absorption bands (2250-2400 cm^{-1}). The CO_2 bands are very difficult to quantify by using FT-IR spectroscopy because of the sensitivity of CO_2 gas to ambient conditions as well as human activity in laboratory.

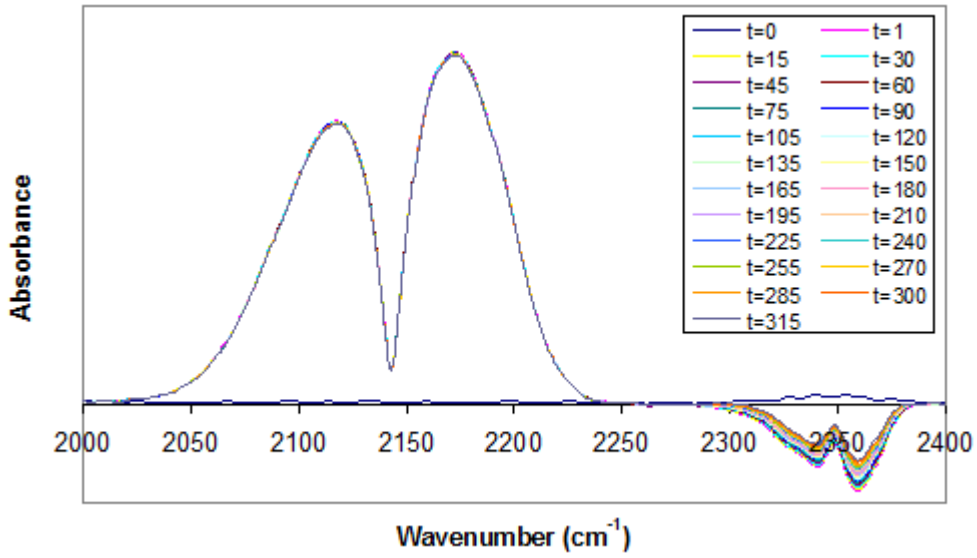

Figure 4.8. Time course FT-IR spectra of gas phase over 0.1%Pd/20%SiO_2/80%TiO_2 catalyst under room temperature initially charged with 1000 ppm CO in air in dark with 15 minutes of time intervals (time<360).

After the steady conditions assessed by FT-IR spectrum, the second phase of the experiments were started by turning on the light source in irradiation chamber. In Figure 4.9 the time course FT-IR spectra of gas phase during the second phase is presented. As it is seen from the figure, the CO absorption intensity diminished with respect to time and evolution of CO_2 evidenced the CO photo-oxidation (See Appendix C for the photocatalytic activity test absorbance peaks of the other samples).

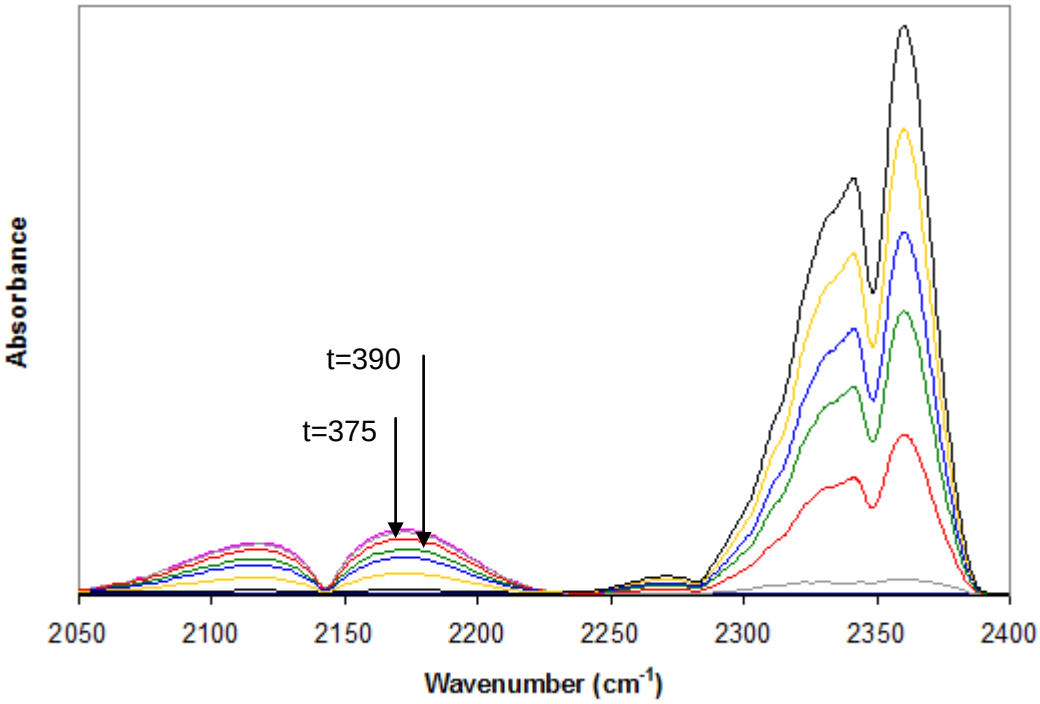

Figure 4.9. Time course FTIR spectra of gas phase over 0.1%Pd/20%SiO_2/80%TiO_2 catalyst under room temperature initially charged with 1000 ppm CO in air under 36 Watts of 254 nm irradiation with 15 minutes of time intervals (time≥360).

The CO and CO_2 concentrations obtained by quantitative analysis of FT-IR absorbance was converted to fractional conversion values for CO and CO_2 by utilizing calibration equation as detailed in Appendix B:

$$C_{CO} = (2*10^{7})A^{3} + (2*10^{6})A^{2} + (1715.1)A$$

The change of 1000 ppm CO in air with respect to time over 0.1%Pd/20%SiO_2/80%TiO_2 catalyst under room temperature is given in Figure 4.10 as per cent conversion with respect to time.

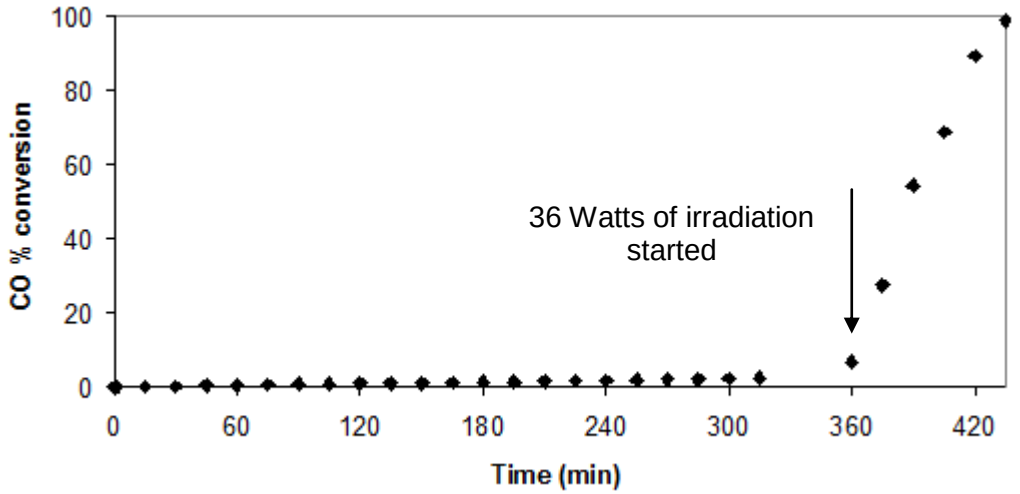

Figure 4.10. Conversion of 1000 ppm CO over 0.1%Pd/20%SiO_2/80%TiO_2 catalyst at room temperature.

As it is illustrated for 0.1%Pd/20%SiO_2/80%TiO_2 catalyst, the photocatalytic activity of all catalyst samples were tested in dark and under irradiation by performing Phase I and Phase II of experiments. The experimental results of photocatalytic oxidation of CO over SiO_2/TiO_2 and their palladium doped counterparts are shown in Figure 4.11 and Figure 4.12 including bare SiO_2 and bare TiO_2 respectively (the conversion results at the end of the 10 hours of activity test show a change of ±1 for each catalyst sample according to the repeat tests).

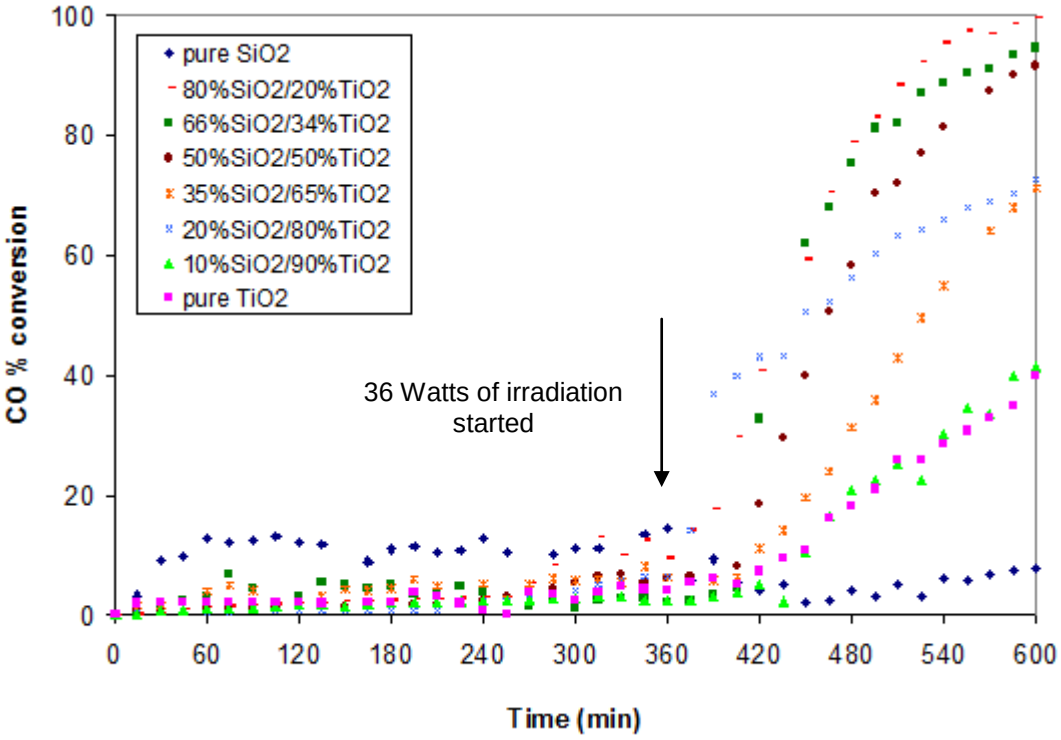

Figure 4.11. The effect of SiO_2/TiO_2 ratio of the catalyst on the photocatalytic oxidation of 1000 ppm CO in air

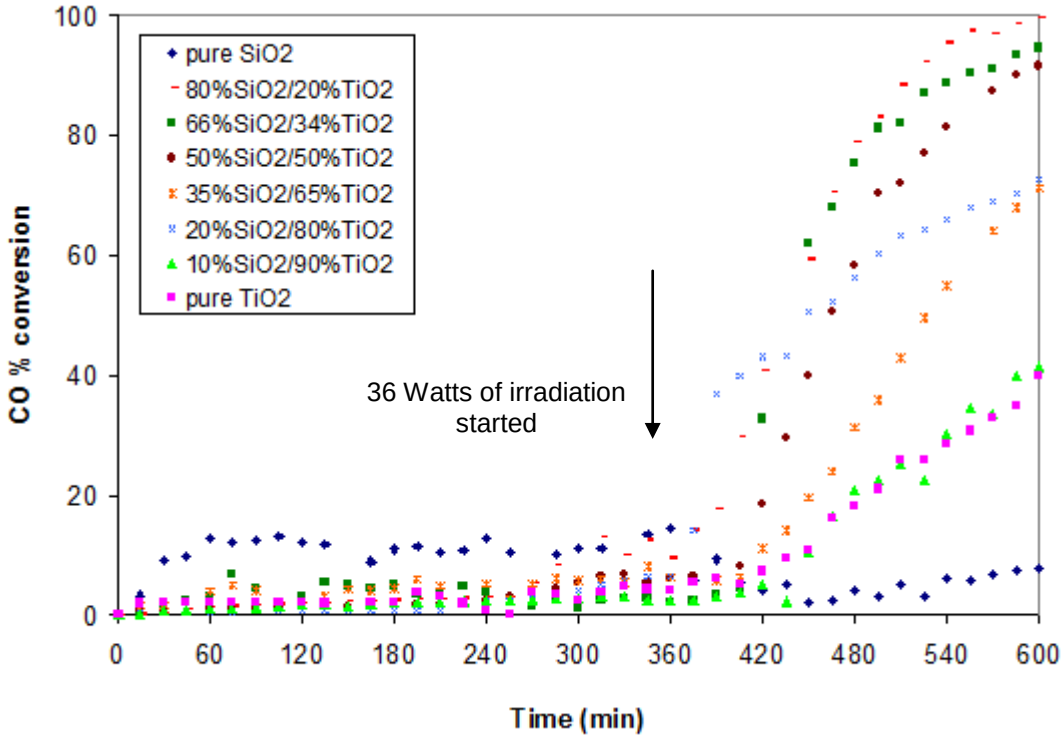

Figure 4.12. The effect of 0.1 % Pd loading
on the photocatalytic oxidation of 1000 ppm CO in air.

As it is seen from the results, slight decrease in CO concentration in dark can be explained by CO adsorption over the catalyst under room temperature. The CO adsorption is more pronounced in Pd doped samples and large surface area samples such as pure silica. Considerable amount of CO adsorption was observed over the pure silica and desorption was observed after the light on at 360 minutes as a result of slight increase in temperature of irradiation cabinet. The reactor temperature rise was measured as 4°C as a result of heat dissipation of UV lights. The adsorption of CO over Pd and PdO has been studied and reported in literature extensively [Bondzie et *al*., 2000; Kan et *al*., 2008; Osorio et *al*., 2007]. There might be a limited conversion to

CO_2 even at room temperature as it was reported by Mirkelamoglu for Pd catalysts [Mirkelamoglu, 2006; Mirkelamoglu and Karakas, 2006]. However due to the low stability and sensitivity of CO_2 absorption bands, limited thermal oxidation activity over Pd/SiO_2 could not quantified by CO_2 concentration change.

For both Pd doped and undoped catalyst samples, considerable oxidation activity was observed for all samples except pure SiO_2 and Pd/SiO_2 where limited adsorption and thermal oxidation were monitored. All TiO_2 containing samples performed photocatalytic CO oxidation. Since CO photocatalytic oxidation is an exothermic reaction, there is the probability of a local heat release which can change the reactor temperature. The gas mixture in the system has a volume of 66 cm^3 and for 1000 ppm CO, the volume becomes:

$(66cm^3)(1000cm^3/10^6cm^3) = 0.066\ cm^3$

Moles of CO = $(0.066cm^3)(1mol/22.4lt)(1lt/1000cm^3) = 2.9x10^{-6}$ mole

Since the heat of reaction for CO oxidation is -282.99 kJ/mole, the heat released during the 4 hours of photocatalytic oxidation is:

$(2.9x10^{-6}mole)(282.99\ kJ/mole) = 8.2x10^{-4}$ kJ/4hr = $2.1x10^{-4}$ kJ/hr which is a low and can be neglected value for the temperature change of the reactor.

Kinetics of CO photo-oxidation was analyzed by using CO conversion data for 1000 ppm initial CO concentration in air. The presence of excess oxygen enabled the kinetic analysis for pseudo second, first and half order with respect to the CO concentration. The photocatalytic conversion data was fit to the second, first and half order kinetic expressions and the best fit was

obtained by half order with respect to the CO concentration. On the other hand, the adsorption rates over the catalyst samples during the Phase I of the experiments were also analyzed by pseudo first order kinetics under the experimental conditions applied (See Appendix A.3 for the derivation of the rate expressions and calculation of the rate constant values). The half order rate expression for CO photo-oxidation is:

$$r_{Aphoto} = -k_{photo}.C_A^{0.5} \qquad \text{(P.1)}$$

where r_{Aphoto} is the rate of CO degradation, k_{photo} is the photocatalytic oxidation rate constant and C_A is the CO concentration. Equation P.1 was turned into:

$$\sqrt{1-X_A} = k''t \qquad \text{(P.2)}$$

and;

$$k'' = k_{photo}\frac{1}{2}\sqrt{\frac{VP_T y_{A_0}}{W_{cat}RT}} \qquad \text{(P.3)}$$

where X_A is the CO conversion, P_T is the total pressure (1 atm), y_{A_0} is the initial concentration of CO in air (1000 ppm = 0.001 mol/mol), R is the gas constant (0.08206 atm.L/mol/K), T is the reaction temperature (293.15 K), t is time in minutes, V is the volume of the gas mixture in the system (66 cm^3=0.066 L) and W_{cat} is the weight of catalyst as 0.5 g.

Similarly, the rate expression for CO adsorption derived from the first order kinetics,

$$r_{A\,ads} = -k_{ads}.C_A \qquad \text{(P.4)}$$

was:

$$\ln(1 - X_A) = k''t \qquad \text{(P.5)}$$

and;

$$k'' = k_{ads}\frac{VP_T y_{A_0}}{W_{cat}RT} \qquad \text{(P.6)}$$

In literature, the kinetics of CO oxidation has been studied widely and first order kinetics were reported for Pt/TiO_2 catalysts [Li et *al*., 2006; Hwang et *al*., 2003; Zhang et *al*., 2005] while first or second order kinetics were reported for TiO_2/SiO_2 [Zhao and Yang, 2003] for thermal oxidation. The adsorption rate constants and photocatalytic oxidation rate constants in the units $s^{-1}g_{cat}^{-1}$ evaluated for the Phase I (dark period) and Phase II (under irradiation) over the SiO_2/TiO_2 and $Pd/SiO_2/TiO_2$ catalyst samples are presented in Table 4.5.

Table 4.5. k_{ads} and k_{photo} values for the synthesized samples

Pd wt %	SiO_2 wt %	TiO_2 wt %	k_{ads} ($s^{-1}g_{cat}^{-1}$)	k_{photo} ($s^{-1}g_{cat}^{-1}$)
0	0	100	0.0017	0.014
0	10	90	0.0016	0.014
0	20	80	0.0015	0.026
0	35	65	0.0015	0.027
0	50	50	0.0012	0.054
0	66	34	0.0012	0.046
0	80	20	0.0015	0.063
0	100	0	0.0044	0.031
0.1	0	100	0.0057	0.25
0.1	5	95	0.0028	0.09
0.1	10	90	0.0028	0.23
0.1	20	80	0.0029	0.15
0.1	35	65	0.0028	0.12
0.1	50	50	0.0029	0.07
0.1	66	34	0.0062	0.1
0.1	80	20	0.0071	0.08
0.1	100	0	0.0114	0.03

4.2.1. CO Adsorption Activities

Adsorption activities of the samples are compared in Figure 4.13 and 4.14. For SiO_2/TiO_2 samples, adsorption activity is related to surface area. This can be directly observed from Figure 4.13 that higher surface area promotes CO adsorption over the catalyst surface. The highest adsorption was achieved by pure SiO_2 with its highest surface area.

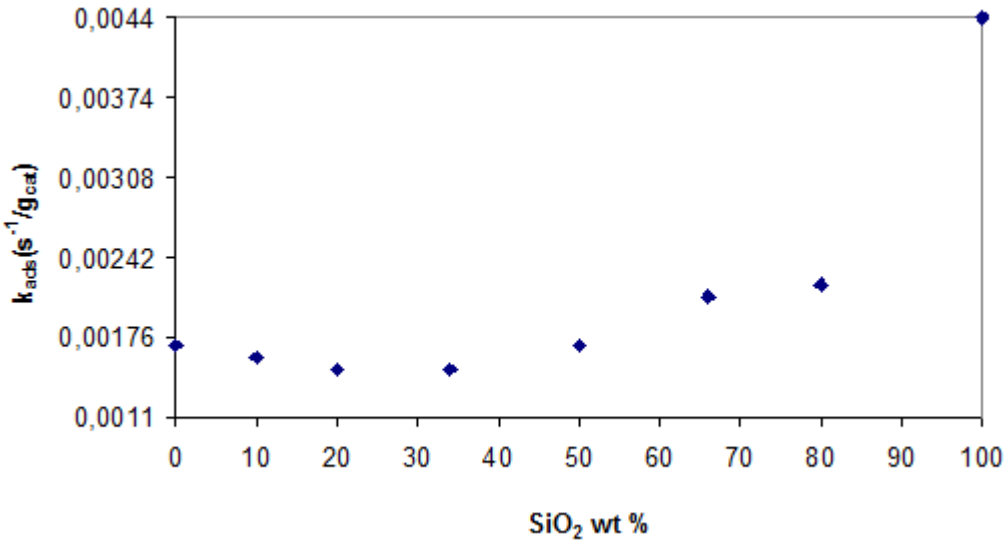

Figure 4.13. The effect of SiO_2 loading
on CO adsorption rates over SiO_2/TiO_2 samples

When Figure 4.14 is taken into consideration, it can be clearly seen that the adsorption capacities of undoped samples were increased effectively by 0.1 % Pd addition. While the adsorption rate constants of pure TiO_2, pure SiO_2 and 50%SiO_2/50%TiO_2 samples were 0.0017, 0.0044 and 0.0012 $s^{-1}g_{cat}^{-1}$ respectively, these values were trippled by Pd doping. The highest adsorption activities are seen in the samples including 66, 80 and 100 % SiO_2 in TiO_2 with 0.1 % Pd. The highest CO adsorption capacity of these samples can be explained by the presence of PdO particles on their surfaces while for the sample 0.1%Pd/100%SiO_2, the CO adsorption is additionally supported by the high surface area characteristic.

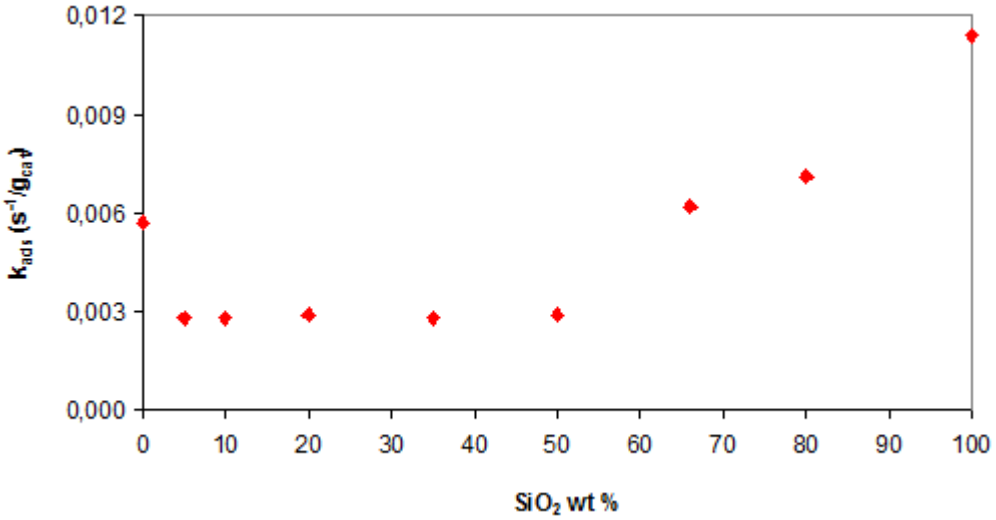

Figure 4.14. The effect of Pd loading
on CO adsorption rates over $Pd/SiO_2/TiO_2$ samples

It is possible that PdO particles on Pd doped catalyst samples with 66, 80 and 100 % SiO_2 were reduced by CO in addition to surface adsorption during the dark period. To test this probability, 0.1%Pd/100%SiO_2 sample was re-circulated with 1000 ppm CO in air for 6 hours in dark and post reaction sample of the catalyst was sealed and later analyzed by XRD which is presented in Figure 4.15.

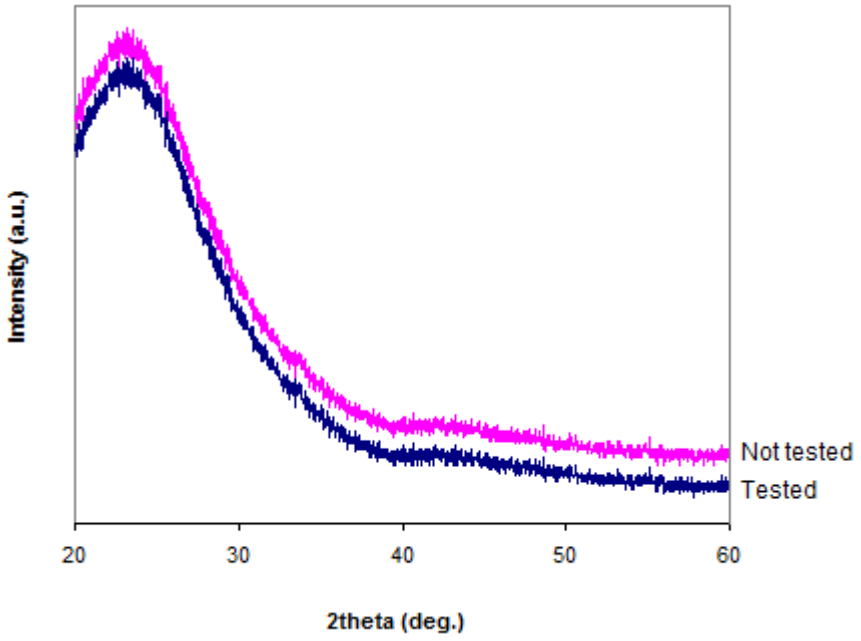

Figure 4.15. Comparison of PdO peak between the tested and not tested 0.1%Pd/100%SiO_2 catalyst sample

The PdO peak showed a slightly lower peak than the one without being tested. This brings about that only portion of PdO was reduced by CO or the weak bonds between PdO and the SiO_2 surface caused PdO to be broken down over the surface and the oxygen atom released by this dissociation was catched by the adsorbed oxygen atoms and desorbed as O_2 gas [Kochubey et *al*., 1996; Bondzie et *al*., 2000]. The smallest crystallite sizes (4.8 and 6.17 nm) and the highest surface areas (664, 674 and 752 m^2/g) of the samples with 66, 80 and 100 % SiO_2, can also explain their higher adsorption capacity by the presence of stronger bonds between CO and SiO_2 surface which limit the CO desorption [Pavlova et *al*., 1996].

For the bare TiO_2 and the samples with 5, 10, 20, 35 and 50 % SiO_2 concentrations, on the other hand, lower CO adsorption rates are observed. When the surface area of these samples are considered it is clear that the adsorption is favored with larger surface area and PdO phase does not disperse well on low surface area samples. Like in the study of Chou and Vannice, the adsorption is not favored over larger Pd particles [Chou and Vannice, 2004]. The higher CO adsorption rate of 0.1%Pd/100%TiO_2 and the decreasing order of adsorption, therefore, may be depended on the decreasing size of Pd particles.

4.2.2. CO Photo-Oxidation Activities

In Figure 4.16 the photocatalytic activities of SiO_2/TiO_2 samples are compared. It is clearly seen from the figure that no activity was observed for pure SiO_2 as it is expected while the highest photocatalytic activity was achieved with 80%SiO_2/20%TiO_2 sample. Photocatalytic activity results indicate two counter effects of surface area and TiO_2 loading. The TiO_2 loading causes a decrease in surface area and thus the adsorption rate of CO while the higher ratio of SiO_2/TiO_2 leads higher reaction rates per unit mass of photocatalyst.

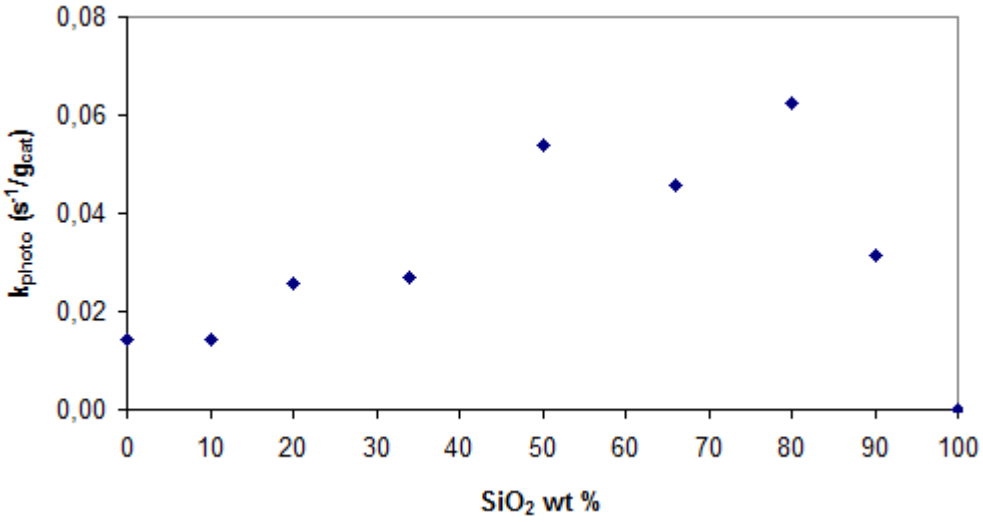

Figure 4.16. The effect of SiO_2/TiO_2 ratio
on the photocatalytic oxidation rates over SiO_2/TiO_2 samples

Figure 4.17 illustrates the CO photo-oxidation rate constants of the Pd loaded SiO_2/TiO_2 catalyst samples under 36 Watts of irradiation. By introducing Pd, photocatalytic oxidation rate constants were increased drastically for each catalyst sample and $Pd/SiO_2/TiO_2$ samples were observed to show an increasing photocatalytic activity with increasing TiO_2 concentration and come to a maximum for the sample 0.1%Pd/100%TiO_2. The XRD results already indicated the effect of TiO_2 loading on the PdO dispersion. The activity and adsorption rate of the larger PdO clusters over lower TiO_2 containing catalysts, with 66 and 80 % SiO_2 concentrations, are lower than the better dispersed PdO particles over lower surface area samples. The agglomerated PdO particles over lower TiO_2 loading, might act as charge recombination centers which results with lower photocatalytic efficiency. Smaller PdO crystallites scavenge free electrons and promote the oxidation activity [Yang et *al*., 2002; Luo et *al*., 2006].

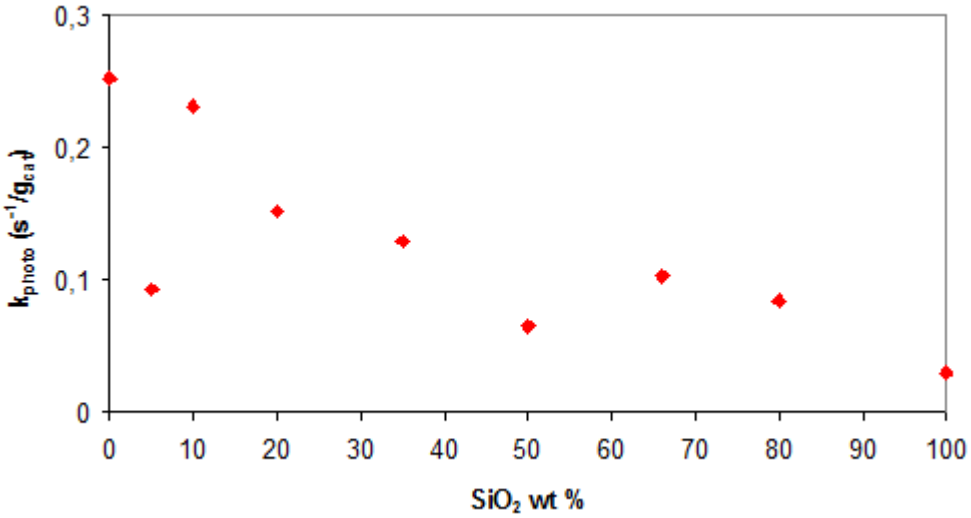

Figure 4.17. The effect of Pd loading
on the photocatalytic oxidation rates over $Pd/SiO_2/TiO_2$ samples

0.1%Pd/100%SiO_2 catalyst sample performed no photocatalytic activity and the small rate constant (0.03 $s^{-1}g_{cat}^{-1}$) it showed was depended on the thermal oxidation of CO caused by the 4°C of temperature increase in the reactor cabinet by the 36 Watts of irradiation.

The smallest photocatalytic oxidation rate constant was observed with the sample 0.1%Pd/50%SiO_2/50%TiO_2 (0.07 $s^{-1}g_{cat}^{-1}$). In spite of its well dispersed surface PdO particles, the CO photocatalytic oxidation over the sample with 50 % SiO_2 concentration was not activated effectively depending on the lowest CO adsorption capacity of this catalyst. In addition, the relatively smaller photo-oxidation rate constant of the Pd doped sample with 5 % SiO_2 concentration (0.09 $s^{-1}g_{cat}^{-1}$) was explained as the mostly microporous structure it showed depending on the XRD results compared with the higher photocatalytic activities of the catalysts with mesoporous

structures. This result is in accordance with the studies in literature on the improvement effect of mesopore structures on the photocatalytic oxidation activities [Zhu et *al*., 2009; Chan et *al*., 2009; Yuan et *al*., 2008].

The highest photocatalytic activities for the SiO_2/TiO_2 mixed oxides were observed for the ones with the highest CO adsorption capacities while the highest activities for Pd doped samples were obtained by the catalysts showing the lowest CO adsorption rates. Therefore, for SiO_2/TiO_2 samples Eley-Rideal type mechanism and for their Pd doped equivalents, Langmuir-Hinshelwood type kinetics can be suggested as effective mechanism for CO photo-oxidation.

CHAPTER 5

CONCLUSIONS

Photocatalytic oxidation of CO over different compositions of SiO_2/TiO_2 catalyst samples and their 0.1 wt % Pd doped counterparts were studied at room temperature.

XRD patterns of SiO_2/TiO_2 samples revealed that the samples comprised of amorphous SiO_2, anatase TiO_2 and PdO phases. The preferential dispersion of PdO crystallites over TiO_2 was observed. XRD peak width analysis indicated the formation of smaller anatase crystallites in the presence of SiO_2. On the other hand, the surface area of catalyst samples increased drastically with the addition of SiO_2 and PdO.

Photocatalytic activity tests were conducted by using the re-circulated closed system of fluidized bed reactor coupled with FT-IR cell under excess O_2 in dark and UV irradiation separately. CO adsorption rate constants were calculated by assuming the pseudo first order rate equation with respect to the CO concentration. The photocatalytic conversion data were analyzed and successful fit was obtained for half order with respect to the CO concentration. Limited CO adsorption was observed over SiO_2/TiO_2 samples in dark and the maximum adsorption rate constant (k_{ads}) was determined as 0.0044 $s^{-1}g_{cat}^{-1}$ for pure SiO_2 which has the highest surface area. For PdO loaded SiO_2/TiO_2 samples, the CO adsorption was favored by the presence of PdO and adsorption rate constants were obtained as 0.0062 and 0.0071 s^{-}

$^{1}g_{cat}^{-1}$ for 0.1% PdO loaded 66%SiO_2/34%TiO_2 and 80%SiO_2/ 20%TiO_2 respectively.

Photo-oxidation rate constants (k_{photo}) of SiO_2/TiO_2 catalysts indicated that the TiO_2 is the photocatalytically active phase where pure SiO_2 does not have any oxidation activity under the experimental conditions. The highest photo-oxidation activity was observed over 80%SiO_2/20%TiO_2 sample with the rate constant of 0.063 $s^{-1}g_{cat}^{-1}$. For SiO_2/TiO_2 mixed oxides, it is cleared that TiO_2 loading caused a decrease in surface area thus the CO adsorption rate but increasing SiO_2/TiO_2 ratio improved the photo-oxidation activities. On the other hand, 0.1 % Pd doping synergistically increased the photocatalytic oxidation activity of all TiO_2 containing catalyst samples. Lower photo-oxidation activities were observed for the samples containing less TiO_2 amount and larger surface PdO clusters than the ones with higher TiO_2 concentrations and better dispersed PdO particles. The photocatalytic oxidation rate constants, therefore generally decreased with increasing SiO_2 concentration and showed a maximum for 0.1%Pd/100%TiO_2 sample (0.25 $s^{-1}g_{cat}^{-1}$). Lowest photocatalytic activity was observed over 0.1%Pd/50%SiO_2/ 50%TiO_2 sample (0.07 $s^{-1}g_{cat}^{-1}$).

As a result, it can be said that pure TiO_2 showed a photocatalytic oxidation activity and adding SiO_2 to increase the surface area of the photocatalyst caused a decrease in oxidizing CO under 36 Watts of irradiation. On the other hand, Pd loading both to pure TiO_2 and SiO_2/TiO_2 mixed oxides improved the photocatalytic activity that SiO_2 addition was concluded to be disadvantageous and Pd doping was found to be advantageous to obtain effective catalysts for the room temperature photocatalytic oxidation of CO.

REFERENCES

Ahiska R., Guler E., *Thermoelectric characterization of n-type (Bi_2Te_3)Se_3 semiconductors in a temperature range 11-373 K,* Journal of Science, 18(3), pp. 481-487, (2005).

Akbarzadeh R., Umbarkar S., Sonawane R., Takle S., Dongare M., *Vanadia–titania thin films for photocatalytic degradation of formaldehyde in sunlight*, Applied Catalysis A: General, 374(1-2), pp.103-109, (2010).

Amama P., Itoh K., Murabayashi M., *Gas-phase photocatalytic degradation of trichloroethylene on pretreated TiO_2*, Applied Catalysis B: Environmental, 37(4), pp. 321-330, (2002).

Ao C. H., Lee S. C., Yu J. C., *Photocatalyst TiO_2 Supported on Glass Fiber for Indoor Air Purification*: *Effect of NO on the Photodegradation of CO and NO_2*, Journal of Photochemistry and Photobiology A: Chemistry, 156 (1-3), pp. 171-177, (2003).

Araya P., Gracia F., Cortes J., Wolf E. E., *FTIR study of the reduction reaction of NO by CO over Rh/SiO_2 catalysts with different crystallite size*, Journal of Applied Catalysis B: Environmental, 38 (2), pp. 77-90, (2002).

Argazzi R., Bignozzi C., *Light-Induced Charge Separation across Ru(II)-Modified Nanocrystalline TiO_2 Interfaces with Phenothiazine Donors*, Journal of Physical Chemistry B, 101 (14), pp. 2591-2597, (1997).

Bayram B., *Photocatalytic Activity of Titania-Silica Mixed Oxides Prepared With Co-Hydrolization*, MSc Thesis, METU, Ankara, (2009).

Benseradjh F., Sadi F., Chater M., *Hydrogen spillover studies on diluted Rh/Al_2O_3 catalyst*, Journal of Applied Catalysis A: General, 228(1-2), pp. 135-144, (2002).

Berlowitz P. J., Peden C. H. F., Goodman D. W., *Kinetics of CO Oxidation on Single Crystal Pd, Pt and Ir*, Journal of Physical Chemistry, 92, pp. 5210-5221, (1988).

Blount M., Falconer J., *Characterization of Adsorbed Species on TiO2 after Photocatalytic Oxidation of Toluene,* Journal of Catalysis, 200 (1), pp. 21-33, (2001).

Bondzie V. A., Kleban P. H., Dwyer D. J., *Kinetics of PdO formation and CO reduction on Pd(110),* Journal of Surface Science, 465 (3), pp. 266-276, (2000).

Bosc F., Ayral A., Keller N., Keller V., *Room Temperature Visible Light Oxidation of CO by High Surface Area Rutile TiO_2-Supported Metal Photocatalyst*, Applied Catalysis B: Environmental, 69 (3-4), pp. 133–137, (2006).

Bowker M., James D., Stone P., Bennett R., Perkins N., Millard L., Greaves J., Dickinson A., *Catalysis at the metal-support interface: exemplified by the photocatalytic reforming of methanol on Pd/TiO_2*, Journal of Catalysis, 217 (2), pp. 427-433, (2003).

Braconnier B., Paez C., Lambert S., Alie C., Henrist C., Poelman D., Pirard J., Cloots R., Heinrichs B., *Ag- and SiO_2-doped porous TiO_2 with enhanced thermal stability*, Journal of Microporous and Mesoporous Materials, 122, pp. 247-254, (2009).

Calatayud M., Markovits A., Minot C., *Restoring the band gap of metal oxide surfaces by redox adsorption*, Journal of Molecular Structure: THEOCHEM, 709(1-3), pp. 87-96, (2009).

Cao G., Li Y., Zhang Q., Wang H., *Synthesis and characterization of $La_2O_3/TiO_{2-x}F_x$ and the visible light photocatalytic oxidation of 4-chlorophenol*, Journal of Hazardous Materials, 178 (1-3), pp. 440-449, (2010).

Chen C. S., You J. H., Lin J. H., Chen Y. Y., *Effect of Highly Dispersed Active Sites of Cu/TiO_2 Catalyst on CO Oxidation,* Journal of Catalysis Communications, 9 (14), pp. 2381-2385, (2008).

Chan C., Chang C., Hsu W., Wang S., Lin J., *Photocatalytic activities of Pd-loaded mesoporous TiO_2 thin films*, Journal of Chemical Engineering, 152 (2-3), pp. 492-497, (2009).

Chou P., Vannice M. A., *Calorimetric heat of adsorption measurements on palladium : III. Influence of crystallite size and support on O_2 adsorption*, Journal of Catalysis, 105 (2), pp.342-351, (2004).

Chou P., Vannice M. A., *Calorimetric heat of adsorption measurements on palladium : III. Influence of crystallite size and support on CO adsorption*, Journal of Catalysis, 104 (1), pp. 17-30, (2004).

Cun W., Jincai Z., Xinming W., Bixian M., Guoying S., Pingan P., Jiamo F., *Preparation, characterization and photocatalytic activity of nano-sized ZnO/SnO_2 coupled photocatalysts*, Applied Catalysis B: Environmental, 39 (3), pp. 269-279, (2002).

Dai W., Chen X., Zheng X., Zhengxin D., Wang X., Liu P., Fu X., *Photocatalytic Oxidation of CO on TiO_2: Chemisorption of O_2, CO and H_2,* Journal of ChemPhysChem, 10 (2), pp. 411-419, (2009).

Dai W., Chen X., Zheng X., Wang X., Liu P., Fu X., Yang H., *The promoted effect of UV irradiation on preferential oxidation of CO in an H_2-rich stream over Au/TiO_2*, Journal of Power Sources, 188 (2), pp. 507-514, (2009).

Devi L. G., Murthy B. N., Kumar S. G., *Photocatalytic activity of TiO_2 doped with Zn^{2+} and V^{5+} transition metal ions: Influence of crystallite size and dopant electronic configuration on photocatalytic activity*, Journal of Materials Science and Engineering, 166 (1), pp. 1-6, (2010).

Dong D., Li P., Zahou Q., Zhang Y., Jia C., Li P., *Investigation on the photocatalytic degradation of pyrene on soil surfaces using nanometer anatase TiO_2 under UV irradiation*, Journal of Hazardous Materials, 174 (1-3), pp. 859-863, (2010).

Ersoz T. I., *Application of Semiconductor Films Over Glass/Ceramic Surfaces and Their Low Temperature Photocatalytic Activity,* MSc Thesis, METU, Ankara, (2009).

Garbato L., Rucci A., *Ionicity dependence of lattice thermal conductivity in tetrahedral semiconductors*, Journal of Chemical Physics Letters, 61(3), pp. 542-544, (2001).

Gardner S. D., Hoflund G. B., Schryer D. R., Schryer J., Upchurch B. T., Kielin E. J., *Catalytic Behaviour of Noble Metal/Reducible Oxide Materials for Low-Temperature Carbon Monoxide Oxidation. 1. Comparison of Catalyst Performance,*Journal of Langmuir, 7 (10), pp. 2135-2139, (1991).

Gurlo A., *Interplay between O_2 and SnO_2: Oxygen Ionosorption and Spectroscopic Evidence for Adsorbed Oxygen,* Journal of Physical and Theoretical Chemistry, 42 (3), pp. 812-816, (2006).

Hapeshi E., Achilleos A., Vasquez M.I., Michael C., Xekoukoulotakis N.P., Mantzavinos D., Kassinos D., *Drugs degrading photocatalytically: Kinetics and mechanisms of ofloxacin and atenolol removal on titania suspensions,* Journal of Water Research, 44 (6), pp. 1737-1746, (2010).

Howard J. B., Williams G. C., Fine D. H., *Kinetics of Carbon Monoxide Oxidation in Postflame Gases*, Symposium (International) on Combustion, 14 (1), pp. 975-986, (1973).

Hsiunga T. L., Wanga H. P., Wang H. C., *XANES Studies of Photocatalytic Active Species in Nano TiO_2-SiO_2,* Journal of Radiation Physics and Chemistry, 75 (11), pp. 2042-2045, (2006).

Hwang S., Lee M. C., Choi W., *Highly Enhanced Photocatalytic Oxidation of CO on Titania Deposited with Pt Nanoparticles: Kinetics and Mechanism,* Journal of Applied Catalysis B: Environmental, 46 (1), pp. 49-63, (2003).

Hung W., Chen Y. C., Chu H., Tseng T. K., *Synthesis and Characterization of TiO_2 and Fe/TiO_2 Nanoparticles and Their Performance for Photocatalytic Degradation of 1,2-Dichloroethane,* Journal of Applied Surface Science, 255 (5), pp. 2205-2213, (2008).

Ibrahim H., Lasa H., *Photo-catalytic degradation of air borne pollutants apparent quantum efficiencies in a novel photo-CREC-air reactor*, Journal of Chemical Engineering Science, 58 (3-6), pp. 943-948, (2003).

Ilinich O., Gribov E., Simonov P., *Water denitrification over catalytic membranes: hydrogen spillover and catalytic activity of macroporous membranes loaded with Pd and Cu*, Journal of Catalysis Today, 82 (1-4), pp. 49-56, (2003).

Inagaki M., Nonaka R., Tryba B., Morawski A., *Dependence of photocatalytic activity of anatase powders on their crystallinity*, Journal of Chemosphere, 64 (3), pp. 437-445, (2006).

Jang Y.H., Kochuveedu S.T., Cha M., Jang Y.J., Lee J.Y., Kim J., Ryu D.Y., Kim D.H., *Synthesis and photocatalytic properties of hierarchical metal nanoparticles/ZnO thin films hetero nanostructures assisted by diblock copolymer inverse micellar nanotemplates*, Journal of Colloid and Interface Science, 345 (1), pp.125-130, (2010).

Jung K., Park S., Ihm S., *Linear relationship between the crystallite size and the photoactivity of non-porous titania ranging from nanometer to micrometer size*, Journal of Applied Catalysis A: General, 224 (1-2), pp. 229-237, (2002).

Kachina A., Preis S., Lluellas G. C., Kallas J*., Gas-Phase and Aqueous Photocatalytic Oxidation of Methylamine: The Reaction Pathways*, International Journal of Photoenergy, Article ID 32524, pp. 1-6, (2007).

Kamegawa T., Takeuchi R., Matsuoka M., Anpo M., *Photocatalytic oxidation of CO with various oxidants by Mo oxide species highly dispersed on SiO_2 at 293 K*, Journal of Catalysis Today, 111(3-4), pp. 248-253, (2006).

Kan H.H., Shumbera R.B., weaver J.F., *Adsorption and abstraction of oxygen atoms on Pd (1 1 1): Characterization of the precursor to PdO formation*, Journal of Surface Science, 602(7), pp. 1337-1346, (2008).

Kato H., Lee J., Sawabe K., Matsumoto Y., *Photochemistry of N_2O on Si(100): surface photo-oxidation*, Journal of Surface Science, 445 (2-3), pp. 209-223, (1999).

Khan R., Kim T. J., *Preparation and Application of Visible Light Responsive Ni Doped and SnO_2 Coupled TiO_2 Nanocomposite Photocatalysts,* Journal of Hazardous Materials, 163 (2-3), pp. 1179-1184, (2009).

Kim D.S., Han S.J., Kwak S.Y., *Synthesis and photocatalytic activity of mesoporous TiO_2 with the surface area, crystallite size and pore size,* Journal of Colloid and Interface Science, 316 (1), pp. 85-91, (2007).

Kim J.H., Han M.K., Lee S.M., Hwang D.K., Shul Y.G., *Characterization of Au/MnOx/TiO_2 for Photocatalytic Oxidation of Carbon Monoxide*, Journal of Top Catal, 47 (3-4), pp. 109-115, (2008).

Kim J. H., Seo G., Cho D., Choi B., Kim J. B., Park H. J., Kim M. W., Song S. J., Kim G. J., Kato S., *Development of Air Purification Device Through Application of Thin-Film Photocatalyst,* Journal of Catalysis Today, 111 (3-4), pp. 271-274, (2006).

Kochubey D. I., Pavlova S. N., Novgorodov B. N., Kryukova G. N., Sadykov V. A., *The influence of support on the low-temperature activity of Pd in the reaction CO oxidation,* Journal of Catalysis, 161, pp. 500-506, (1996).

Kozlova E., Korobkina T., Vorontsov A., Parmon V., *Enhancement of the O_2 or H_2 photoproduction rate in a Ce^{3+}/Ce^{4+}–TiO_2 system by the TiO_2 surface and structure modification*, Journal of Applied Catalysis A: General, 367 (1-2), pp. 130-137, (2009).

Kumar K.V., Porkodi K., Rocha F., *Langmuir Hinshelwood kinetics: A theoretical study*, Journal of Catalysis Communications, 9 (1), pp. 82-84, (2008).

Li Q., Wang K., Zhang S., Zhang M., Yang J., Jin Z., *Effect of photocatalytic activity of CO oxidation on Pt/TiO_2 by strong interaction between Pt and TiO_2 under oxidizing atmosphere,* Journal of Molecular Catalysis A: Chemical, 258 (1-2), pp. 83-88, (2006).

Li R., Liu J., Cai N., Zhang M., Wang P., *Synchronously Reduced Surface States, Charge Recombination, and Light Absorption Length for High-Performance Organic Dye-Sensitized Solar Cells*, Journal of Physical Chemistry, 114 (13), pp. 4461-4464, (2010).

Liang F., Zhu H., Qin Z., Wang G., Wang J*., Effects of CO_2 on the stability of Pd/CeO_2–TiO_2 catalyst for low-temperature CO oxidation,* Journal of Catalysis Communications, 10 (5), pp. 737-740, (2009).

Liotta L. F., Gruttadauria M., Di Carlo G., Perrini G., Librando V., *Heterogeneous catalytic degradation of phenolic substrates: Catalysts activity*, Journal of Hazardous Materials, 162 (2-3), pp. 588-606, (2009).

Liu B., Cheng X., He J., *Zn^{2+}-La^{3+} Co-Doped TiO_2 Photocatalyst for the Purification of Air*, Journal of Bioinformatics and Biomedical Engineering of Beijing, 20 (11-13), pp. 1-4, (2009).

Liu H., Lian Z., Ye X., Shangguan W., *Kinetic Analysis of Photocatalytic Oxidation of Gas-Phase Formaldehyde over Titanium Dioxide*, Journal of Chemosphere, 60(5), pp. 630-635, (2005).

Luo M.F., Pu Z.Y., He M., Jin J., Jin L.Y., *Characterization of $PdO/Ce_{0.8}Y_{0.2}O_{1.9}$ catalysts for carbon monoxide and methane oxidation,* Journal of Molecular Catalysis A: Chemical, 260(1-2), pp. 152-156, (2006).

Lanning, John A. and Anderson, Larry G.; in *Proc. of 1993 Annual Meeting of Air & Waste Management Assoc*.; Denver, Colorado; June, 1993; No. 93-WA71.03

Macyk W., Kisch H., *Photoassited Catalytic Oxidation of Carbon Monoxide at Room Temperature*, Journal of Monatshefte für Chemie 138, pp. 935–940 (2007).

Marugan J., Grieken R., Cassano A., Alfano O., *Quantum efficiency of cyanide photo-oxidation with TiO_2/SiO_2 catalysts: Multivariate analysis by experimental design*, Journal of Catalysis Today, 129 (1-2), pp. 143-151, (2007).

McCabe R. W., Mitchell P.J., *Exhaust-Catalyst Development for Methanol Fuelled Vehicles: 2. Synergism Between Palladium and Silver in Methanol and Carbon Monoxide Oxidation Over an Alumina-Supported Palladium-Silver Catalyst,* Journal of Catalysis, 103 (2), pp. 419-425, (1987).

Mikhaylov R., Lisachenko,A., Shelimov B., Kazansky V., Alberto G., Coluccia S., *FTIR and TPD Analysis of Surface Species on a TiO_2 Photocatalyst Exposed to NO, CO and NO-CO Mixtures: Effect of UV-Vis Light Irradiation,* Journal of Physical Chemistry, 113 (47), 20381-20387, (2009).

Mondal A., Basu R., Das S., Nandy P., *Increased quantum efficiency in hybrid photoelectrochemical cell consisting of thionine and zinc oxide nanoparticles,* Journal of Photochemistry and Photobiology, 211 (2-3), pp. 143-146, (2010).

Moretti E., Storaro L., Talon A., Patrono P., Pinzari F., Montanari T., Ramis G., Lenarda M., *Preferential CO Oxidation (CO-PROX) over CuO-ZnO/TiO_2 Catalysts,* Journal of Applied Catalysis A: General, 344 (1-2), pp. 165-174, (2008).

Mu R., Xu Z., Li L., Shao Y., Wan H., Zheng S., *On the photocatalytic properties of elongated TiO_2 nanoparticles for phenol degradation and Cr(VI) reduction*, Journal of Hazardous Materials, 176 (1-3), pp.495-502, (2010).

Naknam P., Luengnaruemitchai A., Wongkasemjit S., Osuwan S., *Preferential catalytic oxidation of carbon monoxide in pesence of hydrogen over bimetallic AuPt supported on zeolite catalysts,* Journal of Power Sources, 165 (1), pp. 353-358, (2007).

Nayak J., Sahu S. N., Kasuya J., Nozaki S., *CdS–ZnO composite nanorods: Synthesis, characterization and application for photocatalytic degradation of 3,4-dihydroxy benzoic acid*, Journal of Applied Surface Science, 254(22), pp. 7215-7218, (2008).

Nguyen L. T. K., Aydemir U., Baitinger M., Bauer E., Borrman H., Burkhardt U., Custers J., Haghighirad A., Höfler R., Luther K. D., Ritter F., Assmus W., Grin Y., Pashen S., *Atomic ordering and thermoelectric properties of the n-type clathrate* $Ba_8Ni_{3.5}Ge_{42.1-0.4}$, Journal of Dalton Transactions, 2010 (39), pp. 1071-1077, (2009).

Niessen W. R., *Combustion and Incineration Processes: Applications in Environmental Engineering, 3rd edition*, Marcel Dekker Inc., New York, (2002).

Osorio G.P., Castillon F., Simakov A., Tiznado H., Zaera F., Fuentes S., *Effect of ceria-zirconia ratio on the interaction of CO with* PdO/Al_2O_3-$(Ce_x$-$Zr_{1-x})O_2$ *catalysts prepared by sol-gel method*, Journal of Applied Catalysis B: Environmetal, 69(3-4), pp.219-225, (2007).

Ozen I., Uner D., *Heterogeneous Photo and Thermal Catalytic Oxidation of CO: Effects of Metal Deposition,* Journal of Studies in Surface Science and Catalysis, 133, pp. 445-451, (2001).

Pan L., Qin X. Y., Liu M., *Effects of Se doping on thermoelectric properties of* Zn_4Sb_3 *at low-temperatures,* Journal of Materials Physics, 12 (2), pp. 257-261, (2010).

Photong S., Boonamnuayvitaya V., *Preparation and characterization of amine-functionalized* SiO_2/TiO_2 *films for formaldehyde degradation*, Journal of Applied Surface Science, 255(23), pp.9311-9315, (2009).

Qiu R., Zhang D., Mo Y., Song L., Brewer E., Huang X., Xiong Y., *Photocatalytic activity of polymer-modified ZnO under visible light irradiation*, Journal of Hazardous Materials, 156 (1-3), pp. 80-85, (2008).

Rahman F., Loughlin K., Al-Saleh M., Saeed M., Tukur N., Hossain M., Karim K., Mamedov A., *Kinetics and mechanism of partial oxidation of ethane to ethylene and acetic acid over MoV type catalysts*, Journal of Applied Catalysis: A General, 375 (1), pp. 17-25, (2010).

Reddya K. M., Manorama S. V., Reddy A. R., *Bandgap Studies on Anatase Titanium Dioxide Nanoparticles,* Journal of Materials Chemistry and Physics, 78 (1), pp. 239-245, (2002).

Rei B., Yeh G., Pan C., *Catalysis-spillover-membrane-2: The rate enhancement of methanol steam reforming reaction in a membrane catalytic reactor*, Journal of Catalysis Today, 97(2-3), pp. 167-172, (2004).

Ridley B. K., *Large Band Gap Semiconductors,* Journal of Physics, 23, pp. 577-582, (1999).

Ruettinger W., Illinich O., Farrauto R. J., *A New Generation of Water Gas Shift Catalysts for Fuel Cell Applications,* Journal of Power Sources, 118 (1-2), pp. 61-65, (2003).

Sano T., Negishi N., Kutsuna S., Takeuchi K., *Photocatalytic Mineralization of Vinyl Chloride on TiO_2,* Journal of Molecular Catalysis A: Chemical, 168 (1-2), pp. 233-240, (2001).

Sano T., Negishi N., Sakai E., Matsuzawa S., *Contributions of photocatalytic/catalytic activities of TiO_2 and γ-Al_2O_3 in nonthermal plasma on oxidation of acetaldehyde and CO*, Journal of Molecular Catalysis A: Chemical, 245(1-2), pp. 235-241, (2006).

Sasirekha N., Basha S., Shanthi K., *Photocatalytic performance of Ru doped anatase mounted on silica for reduction of carbon dioxide*, Journal of Applied Catalysis B: Environmental, 62 (1-2), pp. 169-180, (2009).

Schuler A., Votsmeier M., Kiwic P., Gieshoff J., Hauptmann W., Drochner A., Vogel H., *NH_3-SCR on Fe zeolite catalysts – From model setup to NH_3 dosing*, Journal of Chemical Engineering, 154 (1-3), pp. 333-340, (2009).

Sheikh S. M., Harraz F. A., Abdel-Halim K. S., *Catalytic Performance of Nanostructured Iron Oxides Synthesized by Thermal Decomposition Technique,* Journal of Alloys and Compounds, 487 (1-2), pp. 716-723, (2009).

Shen Q., Inoguchi M., Toyoda T., *The influence of chemical post-etching and UV irradiation on the optical absorption and thermal diffusivity of porous silicon studied by photoacoustic technique*, Journal of Thin Solid Films, 499 (1-2), pp. 161-167, (2006).

Sing K.S.W., Everett D.H., Haul R.A.W., Moscou L., Pierotti R.A., Rouquerol J., Siemieniewska T., *Reporting Physisorption Data for Gas/Solid Systems With Special Reference to the Determination of Surface Area and Porosity*, Jornal of Pure and Applied Chemistry, 57 (4), pp. 603-619, (1985).

Sivakumar M., Towata A., Yasui K., Tuziuti T., Kozuka T., Tsujimoto M., Zhong Z., Iida Y., *Fabrication of Nanosized Pt on Rutile TiO_2 Using a Standing Wave Sonochemical Reactor (SWSR) – Observation of an Enhanced Catalytic Oxidation of CO,* Journal of Ultrason Chemistry, 17 (1), pp. 213-218, (2009).

Spitzer D. P., *Lattice thermal conductivity of semiconductors: A chemical bond approach,* Journal of Physics and Chemistry of Solids, 31 (1), pp. 19-40, (2002).

Stambouli A. B., Traversa E., *Fuel Cells, an Alternative to Standard Sources of Energy,* Journal of Renewable and Sustainable Energy Reviews, 6 (3), pp. 297-306, (2002).

Stark D. S., Harris M. R., *Platinum-Catalysed Recombination of CO and O_2 in Sealed $CO_{2\ TEA}$ Lasers,* Journal of Physics E: Scientific Instruments, 11 (4), pp. 316-319, (1978).

Stark D. S., Crocker A., Steward G. J., *A Sealed 100-Hz $CO_{2\ TEA}$ Laser Using CO_2 Concentrations and Ambient-Temperature Catalysts,* Journal of Physics, E: Scientific Instruments, 16 (2), pp. 158-161, (1983).

Supphasrirongjaroen P., Praserthdam P., Panpranot J., Ranong D., Mekasuwandumrong O., *Effect of quenching medium on photocatalytic activity of nano-TiO_2 prepared by solvothermal method*, Journal of Chemical Engineering Journal, 138 (1-3), pp. 622-627, (2008).

Talebian N., Nilforoussan M.R., *Comparative study of the structural, optical and photocatalytic properties of semiconductor metal oxides toward degradation of methylene blue,* Journal of Thin Solid Films, 518 (8), pp. 2210-2215, (2010).

Tripathi A. K., Gupta N. M., *Pretreatment Effect on the Catalyst Activity and on the Enthalpy Changes during Exposure of Pd/SnO_2 and Pd Metal to CO, O_2 and CO+O_2,* Journal of Catalysis, 153 (2), pp. 208-217, (1995).

Takenaka S., Shimizu T., Otsuka K., *Complete Removal of CO in Hydrogen Rich Gas Stream Through Methanation Over Supported Metal Catalysts,* International Journal of Hydrogen Energy, 29 (10), pp. 1065-1073, (2004).

Valente J.P.S., Padilha P.M., Florentino A.O., *Studies on the adsorption and kinetics of photodegradation of a model compound for heterogeneous photocatalysis onto TiO_2*, Journal of Chemosphere, 64 (7), pp. 1128-1133, (2006).

Venezia A. M., Carlo G. Di, Pantaleo G., Liotta L. F., Melaet G., Kruse N., *Oxidation of CH_4 over Pd supported on TiO_2-doped SiO_2: Effect of Ti(IV) loading and influence of SO_2,* Journal of Applied Catalysis B: Environmental, 88 (3-4), pp. 430-437, (2009).

Verma A. S., Sarkar B. K., Jindal V. K., *Inherent properties of binary tetrahedral semiconductors,* Journal of Physica B: Condensed Matter, 405 (7), pp. 1737-1739, (2009).

Vorontsov A. V., Kozlov D. V., Smirniotis P. G., Parmon V. N., *TiO_2 Photocatalytic Oxidation: II. Gas Phase Processes,* Journal of Kinetics and Catalysis, 46 (3), pp. 422-436, (2004).

Vorontsov A. V., Savinov E. V., Kurkin E. N., Torbova O. D., Parmon V. N., *Kinetic Features of the Steady State Photocatalytic CO Oxidation by Air on TiO_2,* Journal of Reaction Kinetics and Catalysis Letters, 62 (1), pp. 83-88, (1996).

Wagloehner S., Reichert D., Leon-Sorzano D., Balle P., Geiger B., Kureti S., *Kinetic modeling of the oxidation of CO on Fe_2O_3 catalyst in excess of O_2,* Journal of Catalysis, 260 (2), pp. 305-314, (2008).

Wang D., Ma Z., Dai S., Diu J., Nie Z., Engelhard M. H., Huo Q., Wang C., Kou R., *Low Temperature Synthesis of Tunable Mesoporous Crystalline Transition Metal Oxides and Applications as Au Catalyst Supports,* Journal of Phys. Chem. C, 112 (35), pp. 13499-13509, (2008).

Wang H. F., Gong X. Q., Guo Y. L., Lu G., Hu P*., Structure and Catalytic Activity of Gold in Low-Temperature CO Oxidation*, Journal of Phys. Chem. C., 113 (15), pp. 6124-6131, (2009).

Wang J., Uma S., Klabunde K.J., *Visible and UV light photocatalytic activities of transition metal oxide/silica aerogels*, Journal of Microporous and Mesoporous Materials, 75(1-2), (2004), pp.143-147.

Wang X., He Z., Zhong S., Xiao X., *Photocatalytic Synthesis of Hydrocarbon Oxygenates from C_2H_6 and CO_2 over Pd-MoO_3/SiO_2 Catalyst*, Journal of Natural Gas Chemistry, 16(2), (2007), pp.173-178.

Wang Y., Feng C., Zhang M., Yang J., Zhang Z., *Enhanced photocatalytic activity of N-doped TiO_2 in relation to single-electron-trapped oxygen vacancy and doped nitrogen*, Journal of Applied Catalysis B: Environmental, In Press Accepted Manuscript, Available online 21 July 2010.

Wang Z., Huang B., Dai Y., Qui X., Zhang X., Wang P., Liu H., Yu J., *Highly Photocatalytic ZnO/In_2O_3 Heteronanostructures Synthesized by a Coprecipitation Method*, Journal of Phys. Chem. C., 113 (11), pp. 4613-4617, (2009).

Weerachawanasak P., Mekasuwandumrong O., Arai M., Fujita S, Praserthdam P, Panpranot J., *Effect of strong metal–support interaction on*

the catalytic performance of Pd/TiO_2 in the liquid-phase semihydrogenation of phenylacetylene, Journal of Catalysis, 262 (2), pp. 199-205, (2009).

Wierzchowski P. T., Zatorski L. W., *Kinetics of Catalytic Oxidation of Carbon Monoxide and Methane Combustion Over Alumina Supported Ga_2O_3, SnO_2, or V_2O_5*, Journal of Applied Catalysis B: Environmental, 44 (1), pp. 53-65, (2003).

Wodiunig S., Patsis V., Comninellis C., *Electrochemical promotion of RuO-catalysts for the gas phase combustion of C_2H_4*, Journal of Solid State Ionics, Volumes 136-137, pp. 813-817, (2000).

Wu G., Chen T., Su W., Zhou G., Zong X., Lei Z., Li C., *H_2 Production with Ultra Low CO Selectivity via Photocatalytic Reforming of Methanol on Au/TiO_2 Catalyst,* International Journal of Hydrogen Energy 33 (4), pp. 1243-1251, (2008).

Xie M., Jing L., Zhou J., Lin J., Fu H*., Synthesis of nanocrystalline anatase TiO_2 by one-pot two-phase separated hydrolysis-solvothermal processes and its high activity for photocatalytic degradation of rhodamine B*, Journal of Hazardous Materials, 176 (1-3), pp. 139-145, (2010).

Xing N., Wang X., Zhang A., Liu Z., Guo X., *Eley-Rideal mode of formamide species formation in selective catalytic reduction of NO_x by C_2H_2 over ferrierite based catalysts,* Journal of Catalysis Communications, 9 (11-12), pp. 2117-2120, (2008).

Xu C., Cao L., Su G., Liu W., Yu Y., Qu X., *Preparation of ZnO/Cu_2O compound photocatalyst and application in treating organic dyes*, Journal of Hazardous Materials, 176(1-3), pp.807-813, (2010).

Yan T., Long J., Shi X., Wang D., Li Z., Wang X., *Efficient Photocatalytic Degradation of Volatile Organic Compounds by Porous Indium Hydroxide Nanocrystals*, Journal of Environmental Science Technology, 44 (4), pp.1380-1385, (2010).

Yang L., Shi C., He X., Cai J., *Catalytic combustion of methane over PdO supported on Mg-modified alumina*, Journal of Applied Catalysis B: Environmental, 38 (2), pp. 117-125, (2002).

Yoshida H., Tanaka T., Nakatsuka K., Funabiki T., Yoshida S., *Base Sites of Magnesium Oxide Dispersed on Silica as Active Sites for CO Photooxidation*, Journal of Studies in Surface Science and Catalysis, 90, pp.473-478, (1994).

Yu H., Zhang K., Rossi C., *Theoretical Study on Photocatalytic Oxidation of VOCs Using Nano-TiO_2 Photocatalyst,* Journal of Photochemistry and Photobiology A: Chemistry, 188 (1), pp. 65-73, (2007).

Yuan S., Sheng K., Zhang J., Yamashita H., He D., *Synthesis of thermally stable mesoporous TiO_2 and investigation of its photocatalytic activity,* Journal of Mesoporous and Microporous Materials, 110 (2-3), pp. 501-507, (2008).

Zhang K., Jing D., Chen Q., Guo L., *Influence of Sr-doping on the photocatalytic activities of CdS–ZnS solid solution photocatalysts*, Journal of Hydrogen Energy, 35 (5), pp. 2048-2057, (2009).

Zhang M., An T., Hu X., Wang C., Sheng G., Fu J., *Preparation and photocatalytic properties of a nanometer ZnO–SnO_2 coupled oxide,* Applied Catalysis A: General, 260 (2), pp. 215-222, (2004).

Zhang M., Jin S., Zhang J., Zhang Z., Dang H., *Effect of calcination and reduction treatment on the photocatalytic activity of CO oxidation on Pt/TiO_2*, Journal of Molecular Catalysis A: Chemical, 225 (1), pp. 59-63, (2005).

Zhang W., Zhang T., Yin W., Cao G., *Relationship Between Photocatalytic Activity and Structure of TiO_2 Thin Film*, Journal of Chemical Physics, 20(1), (2007).

Zhao J., Jang X., *Photocatalytic oxidation for indoor air purification: a literature review*, Journal of Building and Environment, 38 (5), pp. 645-654, (2003).

Zheng S., Cai Y., O'Shea K., *TiO_2 photocatalytic degradation of phenylarsonic acid*, Journal of Photochemistry and Photobiology A: Chemistry, 210 (1), pp. 61–68, (2010).

Zhu H., Qin Z., Shan W., Shen W., Wang J., *CO Oxidation at Low Temperature Over Pd Supported on CeO_2-TiO_2 Composite Oxide*, Journal of Catalysis Today, 126 (3-4), pp. 382-386, (2007).

Zhu H., Qin Z., Shan W., Shen W., Wang J., *Low-temperature oxidation of CO over Pd/CeO_2–TiO_2 catalysts with different pretreatments*, Journal of Catalysis, 233 (1), pp. 41-50, (2005).

Zhu S., Zhang D., Zhang X., Zhang L., Ma X., Zhang Y., Cai M., *Sonochemical incorporation of nanosized TiO_2 inside mesoporous silica with high photocatalytic performance*, Journal of Microporous and Mesoporous Materials, 126 (1-2), pp. 20-25, (2009).

Zink J., *Hazardous Waste Disposal by Thermal Oxidation,* Catalogue of John Zink Company, (2001).

Zou L., Luo Y., Hooper M., Hu E., *Removal of VOCs by photocatalysis process using adsorption enhanced TiO_2–SiO_2 catalyst*, Journal of Chemical Engineering and Processing, 45 (11), pp.959-964, (2006).

APPENDIX A

SAMPLE CALCULATIONS

A.1. Calculation of CO/He Gas Mixture Volume for the Test System

Gas tube: 1 % CO in He = 10000 ppm CO in He

If 1000 ppm CO in air is chosen for the test system, glass cylinder filled with CO/He mixture is needed to be fixed to the true volume. This volume is calculated by considering the dilution of 10000 ppm CO in He gas mixture by 10 times with room air re-circulating through the closed system.

System Volume = $(551\ cm^3)_{FTIR\ Cell}+(3.6\ cm^3)_{Reactor}+(35.5\ cm^3)_{Pipes} = 590\ cm^3$

To dilute the gas mixture by 10 times: $590/9 = 66\ cm^3$ of volume must be fixed in the glass tube for CO/He mixture.

Other arbitrary volumes of CO/He mixture and their corresponding CO/Air compositions are included in Table A.1.

Table A.1. CO/He volumes and their calculated CO concentrations in air

CO/He Volume (cm^3)	CO in Air (ppm)
122.2	1850
99	1500
82.5	1250
66	1000
49.5	750
33	500
19.5	295
15	225

A.2. Calculation of Crystallite Size

Crystallite size was calculated using the method developed by Scherrer which is defined as:

$$\tau = \frac{K\lambda}{\beta \cos\theta} \tag{A.1}$$

where τ is the crystallite size in nanometers, K is the shape factor which is equal to 0.9, λ is the X-ray wavelength which is typically 1.54 Å (0.154 nm), β is the line broadening at half the maximum diffraction peak in radians which is determined by graphical measurement and θ is the bragg angle of the maximum peak in degrees.

For "0.1%Pd/80%SiO_2/20%TiO_2" sample:

β = 1.06° = 1.06° * 2 * $\frac{\pi}{360°}$ = 0.0185 rad

θ = 25.3°

$$\tau = \frac{(0.9)(0.154)}{(0.0185)(\cos 25.3)} = 7.602 \text{ nm}$$

A.3. Rate Expression Derivation and Calculation of *k* Values

Low temperature photo-oxidation of CO was assumed as half order according to CO concentration. Therefore the rate expression became:

$$r_{A\,photo} = -k_{photo} C_A^{0.5}$$

where $r_{A\,photo}$ is the rate of CO degradation, k_{photo} is the photo-oxidation rate constant and C_A is the CO concentration. When this equation was rearranged, it came out that:

$$\frac{dX_A}{dt} = -k_{photo}\left(\frac{P_T y_A}{RT}\right)^{0.5}$$

$$\frac{dX_A}{dt} = -k_{photo}\sqrt{\frac{P_T y_{A_0}}{RT}}\cdot\sqrt{1-X_A}$$

$$\int \frac{dX_A}{\sqrt{1-X_A}} = -k_{photo}\sqrt{\frac{P_T y_{A_0}}{RT}}\int dt$$

$$-2\sqrt{1-X_A} = -k_{photo}\sqrt{\frac{P_T y_{A_0}}{RT}}t$$

where X_A is the CO conversion, P_T is the total pressure (1 atm), y_{A_0} is the initial concentration of CO in air (1000 ppm = 0.001 mol/mol), R is the gas constant (0.08206 atm.L/mol/K), T is the reaction temperature (293.15 K) and t is time in minutes. To get the true units for k_{photo} ($min^{-1}g_{cat}^{-1}$), the rate expression should be added new terms like V (volume of the gas mixture in the system, 66 cm^3=0.066 L) and W_{cat} (weight of catalyst as 0.5 g previously mentioned):

$$\sqrt{1-X_A} = k_{photo}\frac{1}{2}\sqrt{\frac{VP_T y_{A_0}}{W_{cat}RT}}t \qquad \text{(A.2)}$$

Equation A.2 is the general rate expression of low temperature photocatalytic oxidation of CO over SiO_2/TiO_2 and $Pd/SiO_2/TiO_2$ photocatalyst samples.

To calculate k_{photo} for each sample, a graphical solution was followed. For this, Equation A.2 was firstly rearranged as:

$$\sqrt{1-X_A} = k''t$$

where;

$$k'' = k_{photo}\frac{1}{2}\sqrt{\frac{VP_T y_{A_0}}{W_{cat}RT}} \qquad \text{(A.3)}$$

$\sqrt{1-X_A}$ is directly proportional with t and the plot of $\sqrt{1-X_A}$ *versus* t for the photocatalytic activity data of Phase II can be drawn to find the slope (k'').

Below, the rate expression graph of P-BiB14 (0.1%Pd/20%SiO_2/80%TiO_2) for Phase II can be seen as example.

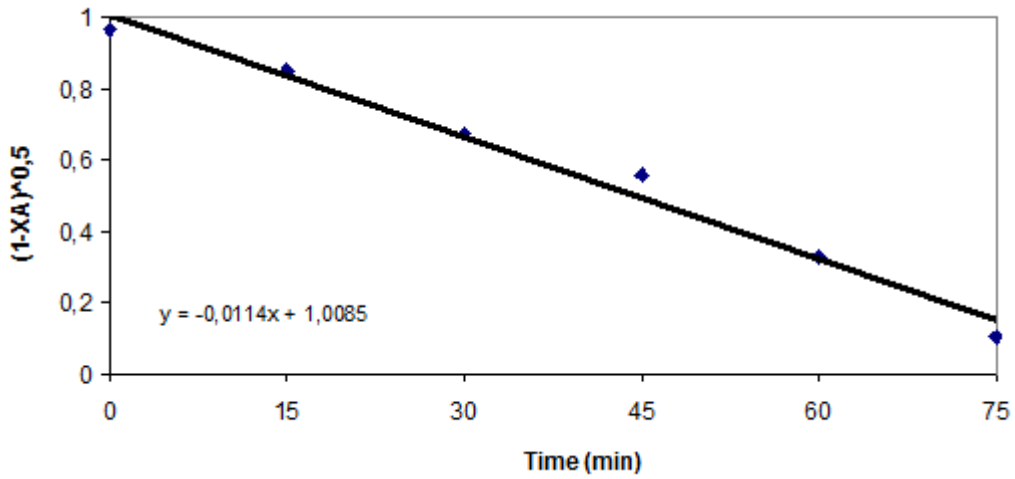

Figure A.1. Rate expression plot and slope of P-BiB14 under illumination

In order to find CO adsorption rate constants, the adsorption was assumed as pseudo first order with respect to CO concentration and the adsorption rate equation was come out as:

$$r_{A\,ads} = -k_{ads} C_A$$

where $r_{A\,ads}$ is the rate of CO adsorption and k_{ads} is the adsorption rate constant. When this equation was rearranged, it came out that:

$$\frac{dX_A}{dt} = -k_{ads}\left(\frac{P_T y_A}{RT}\right)$$

$$\frac{dX_A}{dt} = -k_{ads} y_{A_0}(1 - X_A).\frac{P_T}{RT}$$

$$\int \frac{dX_A}{1 - X_A} = -k_{ads} y_{A_0} \frac{P_T}{RT} \int dt$$

$$\ln(1 - X_A) = k_{ads} y_{A_0} \frac{P_T}{RT} t$$

When the terms V and W_{cat} were added, the last equation was turned into:

$$\ln(1 - X_A) = k_{ads} \frac{V P_T y_{A_0}}{W_{cat} RT} t \qquad \text{(A.4)}$$

Equation A.4 is the general rate expression of CO adsorption over SiO_2/TiO_2 and $Pd/SiO_2/TiO_2$ photocatalyst samples.

To calculate k_{ads} for each sample, Equation A.4 was rearranged as:

$$\ln(1 - X_A) = k'' t$$

where;

$$k'' = k_{ads} \frac{V P_T y_{A_0}}{W_{cat} RT} \qquad \text{(A.5)}$$

$\ln(1-X_A)$ is directly proportional with t and the plot of $\ln(1-X_A)$ *versus* t for the adsorption activity data of Phase I can be drawn to find the slope (k''). Below, the rate expression graph of P-BiB14 (0.1%Pd/20%SiO_2/80%TiO_2) for Phase I (the dark test) can be seen as example.

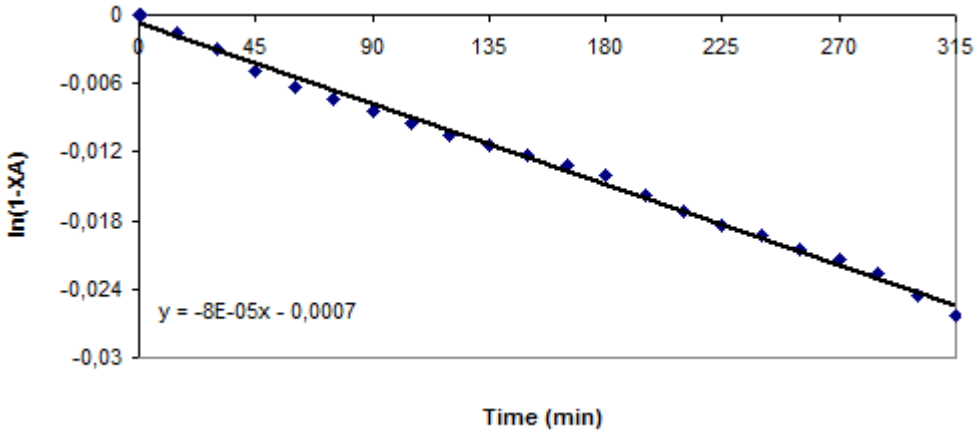

Figure A.2. Adsorption activity plot and slope of P-BiB14 in the dark

When both slopes of under illumination and in dark plots (0.0114 and 0.00008 min^{-1}, respectively) are substituted into equation A.3 and A.5 as k'', rate constants can be obtained as k_{photo} = 0.152 and k_{ads} = 0.0029 $s^{-1}g_{cat}^{-1}$.

APPENDIX B

CALIBRATION OF THE TEST SYSTEM

For each concentration of CO in air, data were taken by FTIR to plot the absorbance peaks of each concentration in a wavenumber range of 2000-2250 cm^{-1}. These calibration curves are as seen in Figure B.1.

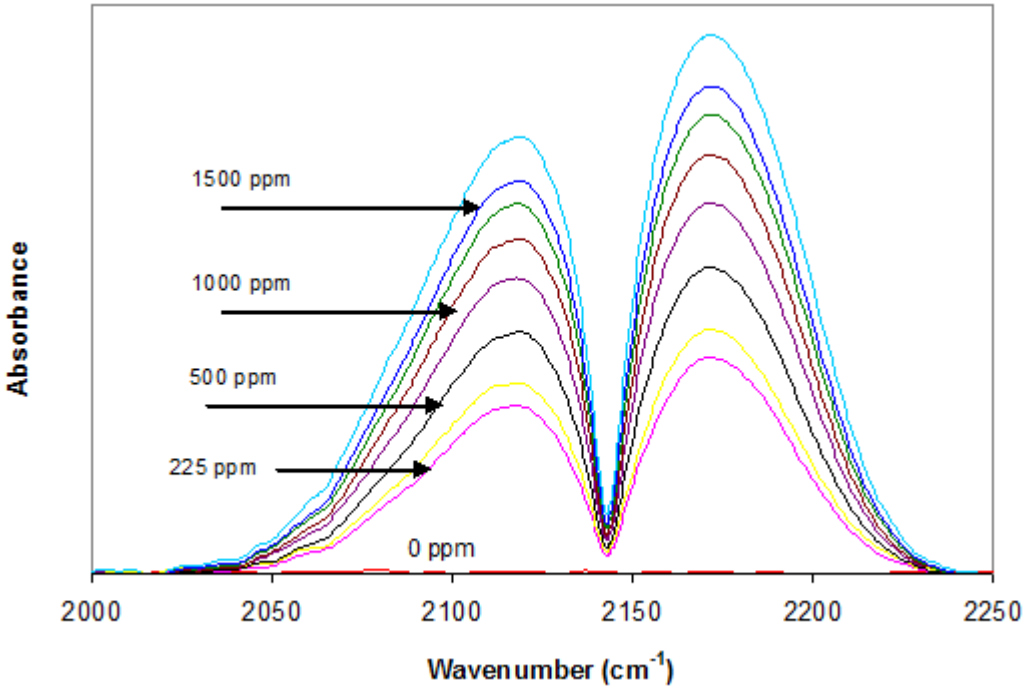

Figure B.1. Calibration curves for CO obtained by FTIR during the dark re-circulation of several concentrations of CO in air

To get the calibration third order equation, CO concentration was plotted against absorbance at the wavenumber point of 2098.172 cm^{-1}. On the vertical line of 2098.172 cm^{-1}, CO concentration *versus* absorbance is plotted as Figure B.2.

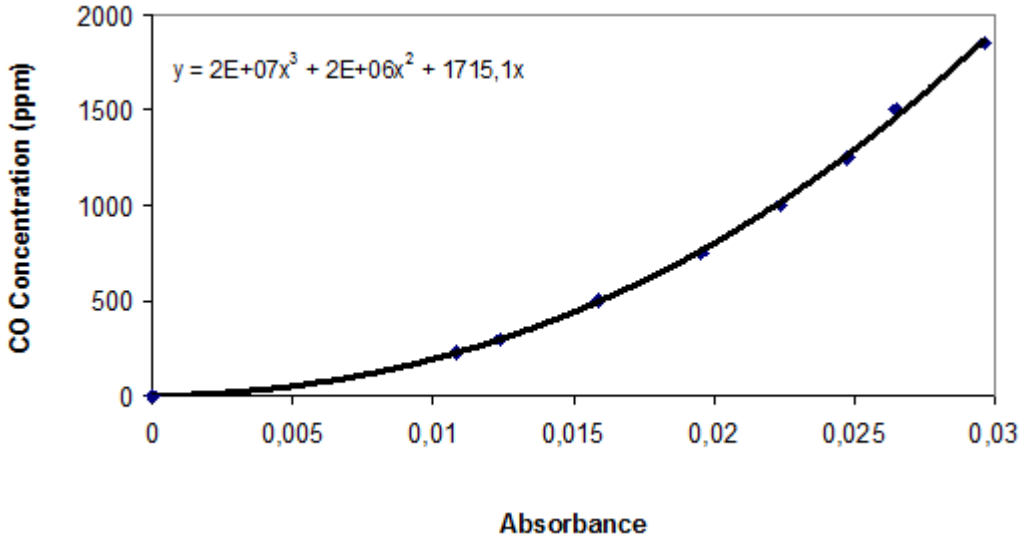

Figure B.2. CO concentration values in air and their corresponding absorbance values on the wavenumber point of 2098.172 cm^{-1}

The third order equation of the curve passing through the data above is:

$$C_{CO} = (2*10^{7})A^{3} + (2*10^{6})A^{2} + (1715.1)A \qquad \text{(EB.1)}$$

where C_{CO} is CO concentration in air in ppm and A is absorbance.

APPENDIX C

ABSORBANCE PEAKS DURING PHOTOCATALYTIC ACTIVITY TESTS

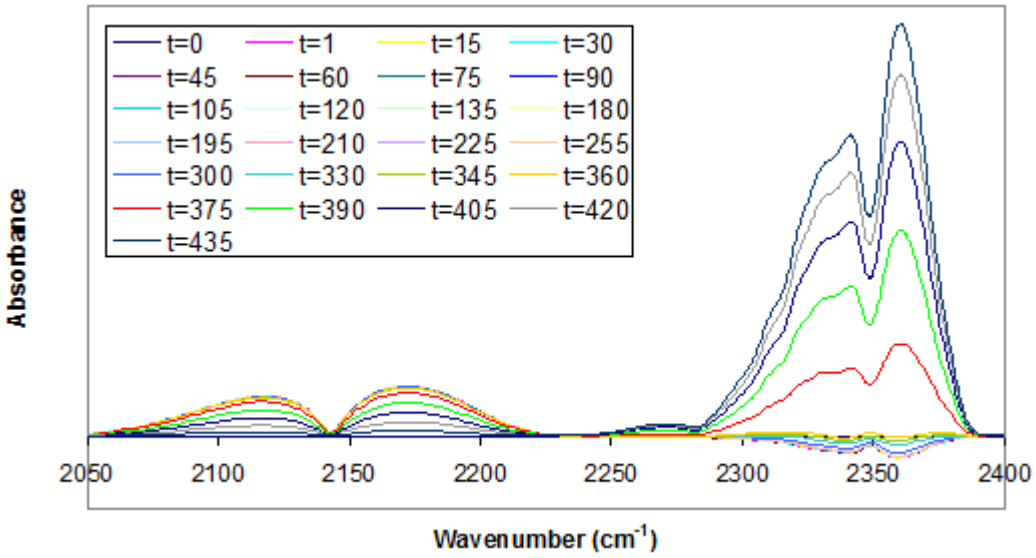

Figure C.1. Absorbance peaks for P-BiB3 (0.1%Pd/66%SiO_2/34%TiO_2) both in dark and under illumination with 15 minutes of time intervals

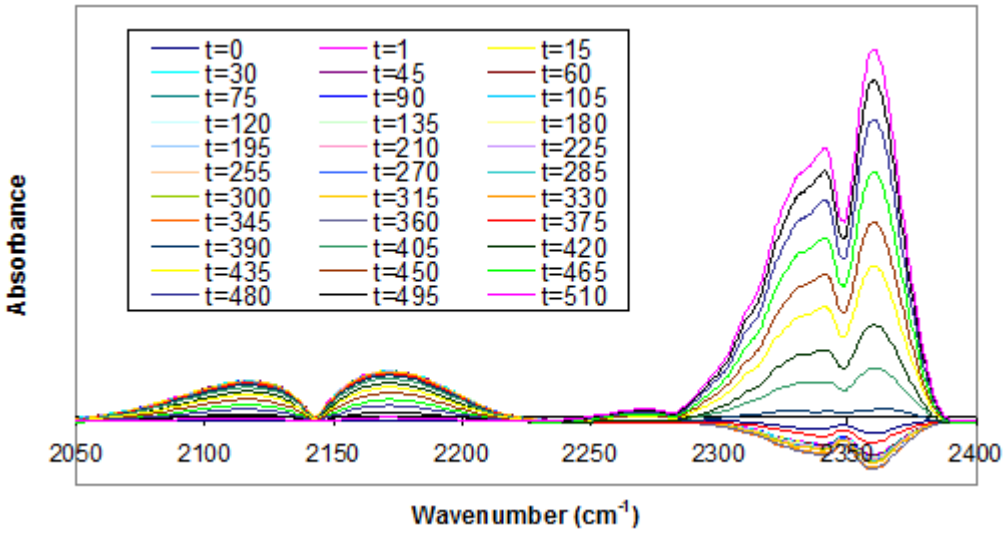

Figure C.2. Absorbance peaks for P-BiB5 (0.1%Pd/5%SiO_2/95%TiO_2) both in dark and under illumination with 15 minutes of time intervals

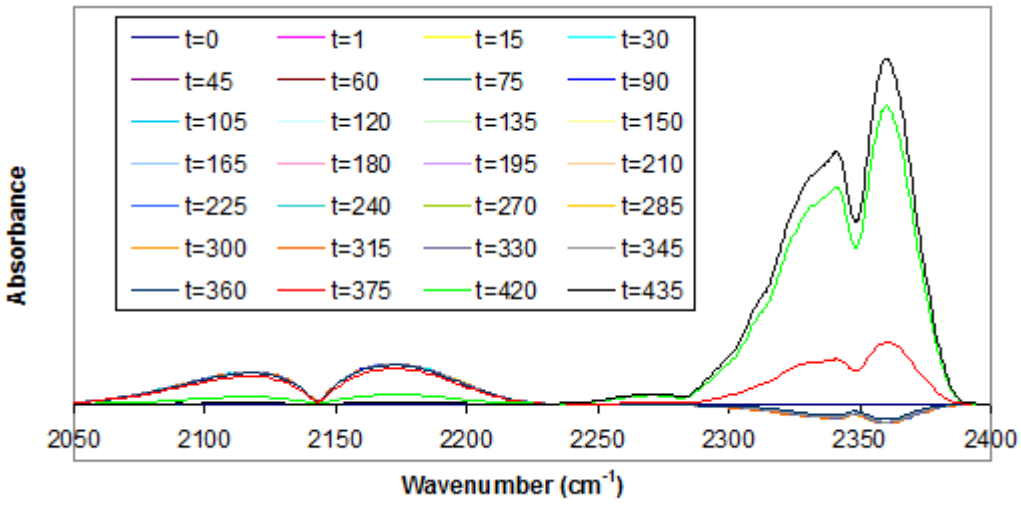

Figure C.3. Absorbance peaks for P-BiB10 (0.1%Pd/10%SiO_2/90%TiO_2) both in dark and under illumination with 15 minutes of time intervals

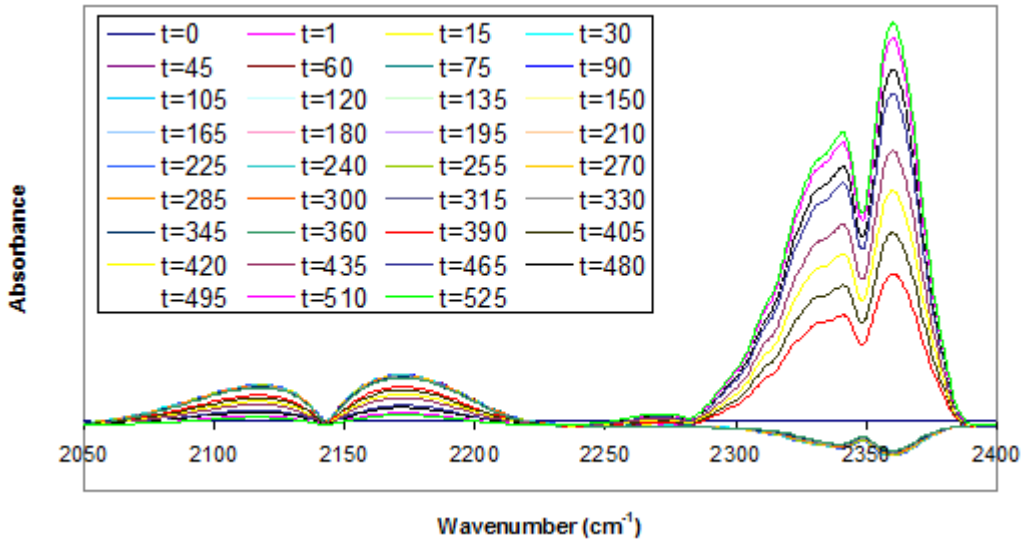

Figure C.4. Absorbance peaks for P-BiB12 (0.1%Pd/80%SiO_2/20%TiO_2) both in dark and under illumination with 15 minutes of time intervals

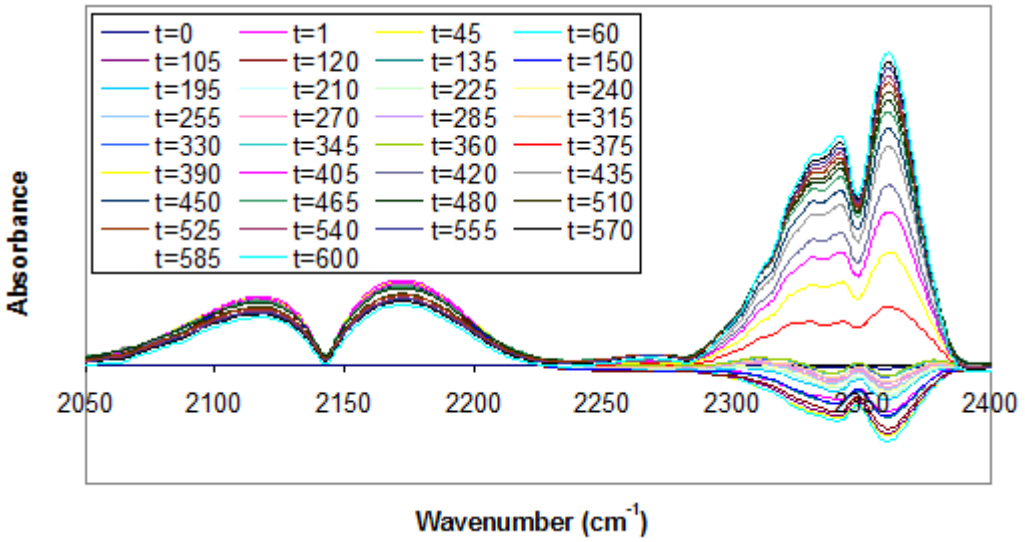

Figue C.5. Absorbance peaks for P-BiB16 (0.1%Pd/100%SiO_2) both in dark and under illumination with 15 minutes of time intervals

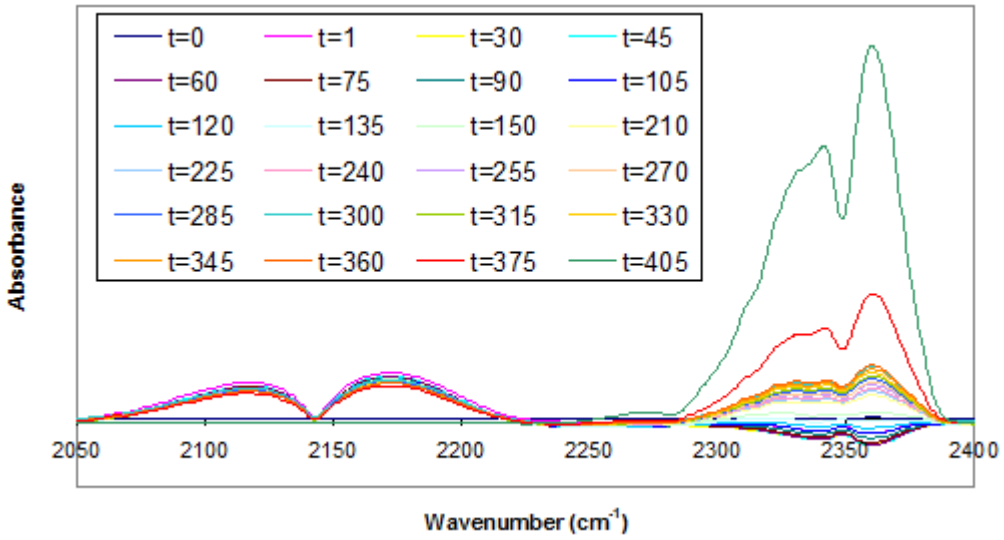

Figure C.6. Absorbance peaks for P-BiB18 (0.1%Pd/100%TiO_2) both in dark and under illumination with 15 minutes of time intervals

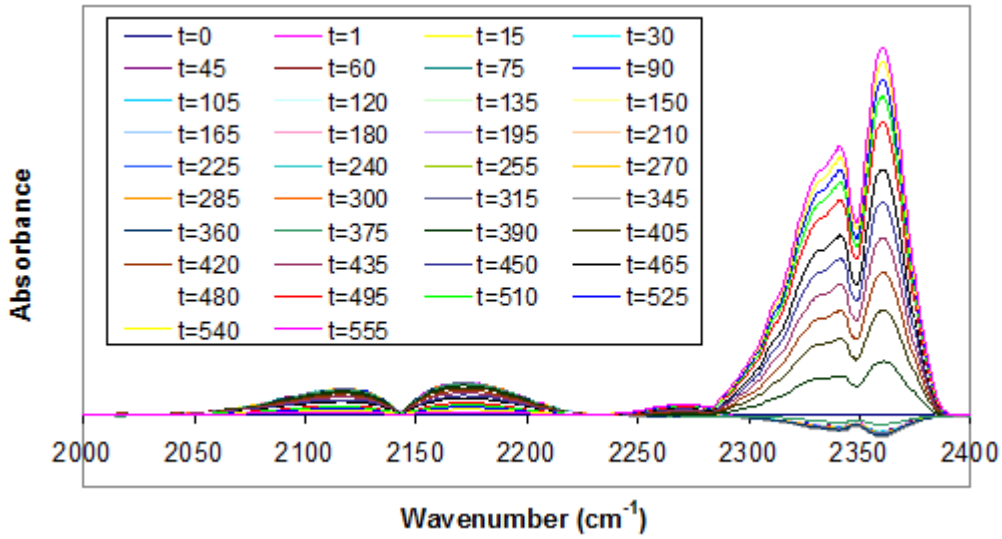

Figure C.7. Absorbance peaks for P-BiB20 (0.1%Pd/50%SiO_2/50%TiO_2) both in dark and under illumination with 15 minutes of time intervals

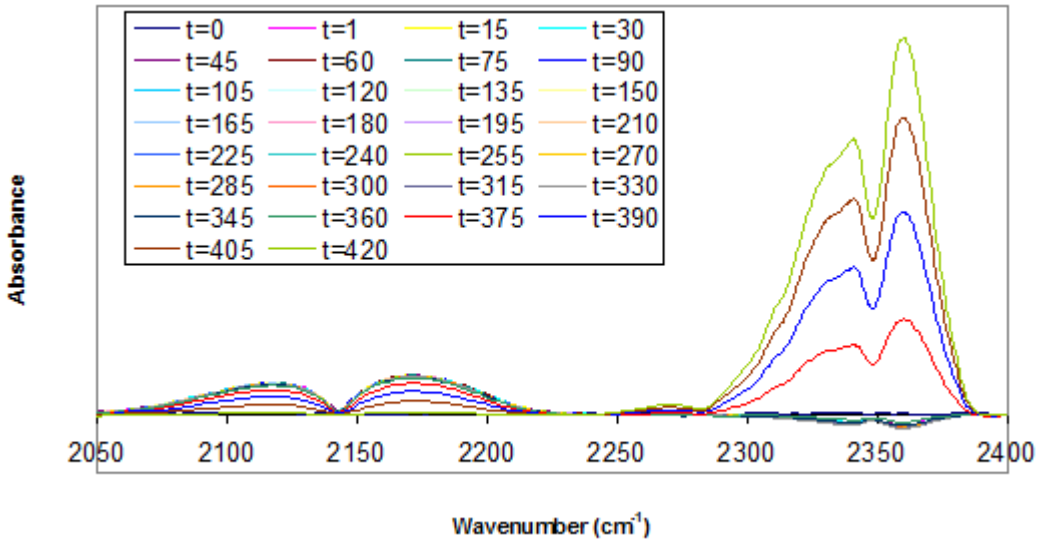

Figure C.8. Absorbance peaks for P-BiB22 (0.1%Pd/35%SiO_2/65%TiO_2) both in dark and under illumination with 15 minutes of time intervals

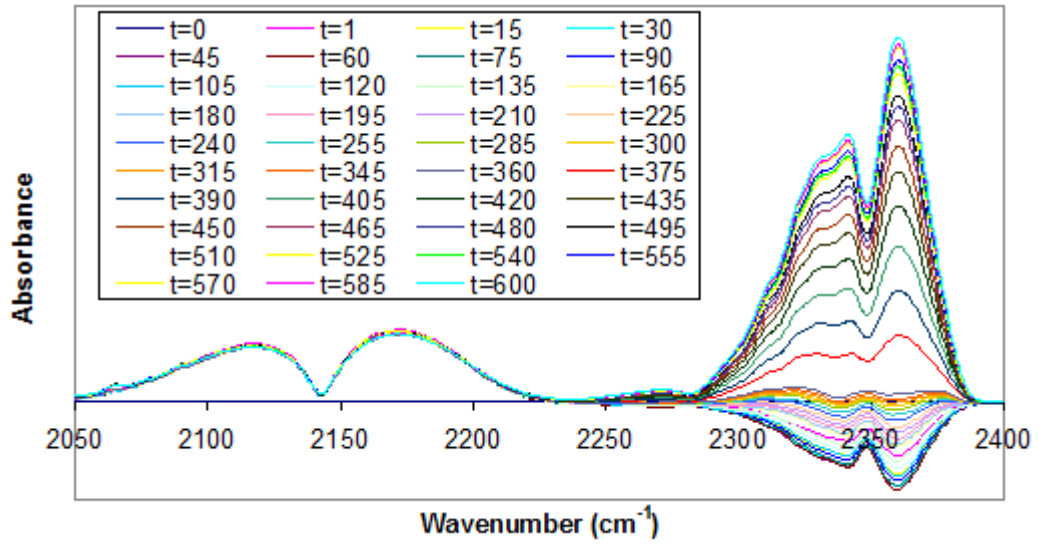

Figure C.9. Absorbance peaks for BiB16 (pure SiO_2) both in dark and under illumination with 15 minutes of time intervals

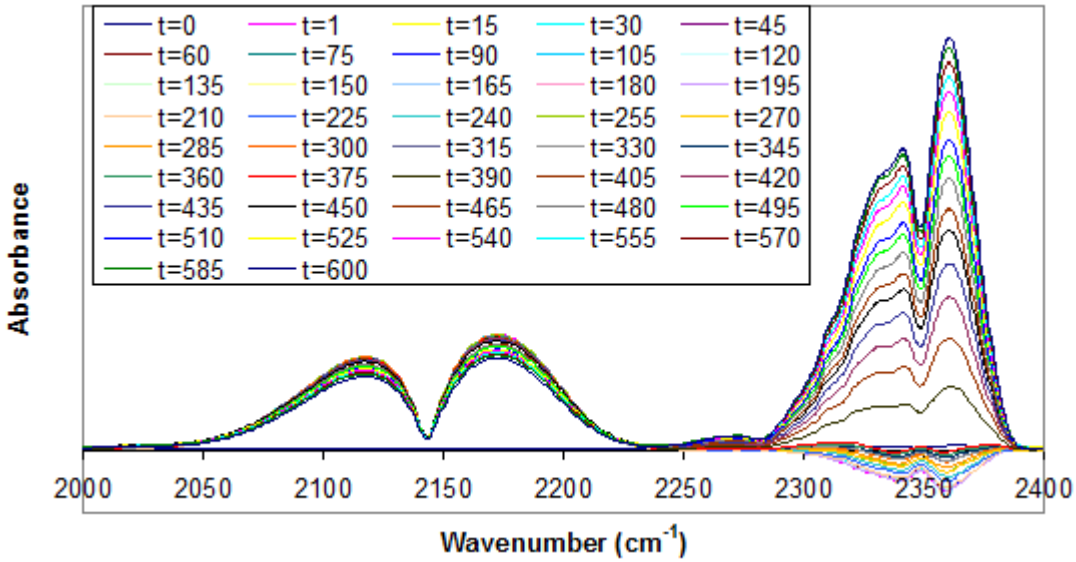

Figure C.10. Absorbance peaks for BiB18 (pure TiO_2)
both in dark and under illumination with 15 minutes of time intervals

APPENDIX D

SAMPLE RECIPE FOR SOL-GEL

The sol-gel procedure of 5 grams of P-BiB12 (0.1%Pd/80%SiO_2/20%TiO_2) is explained below as a sample recipe:

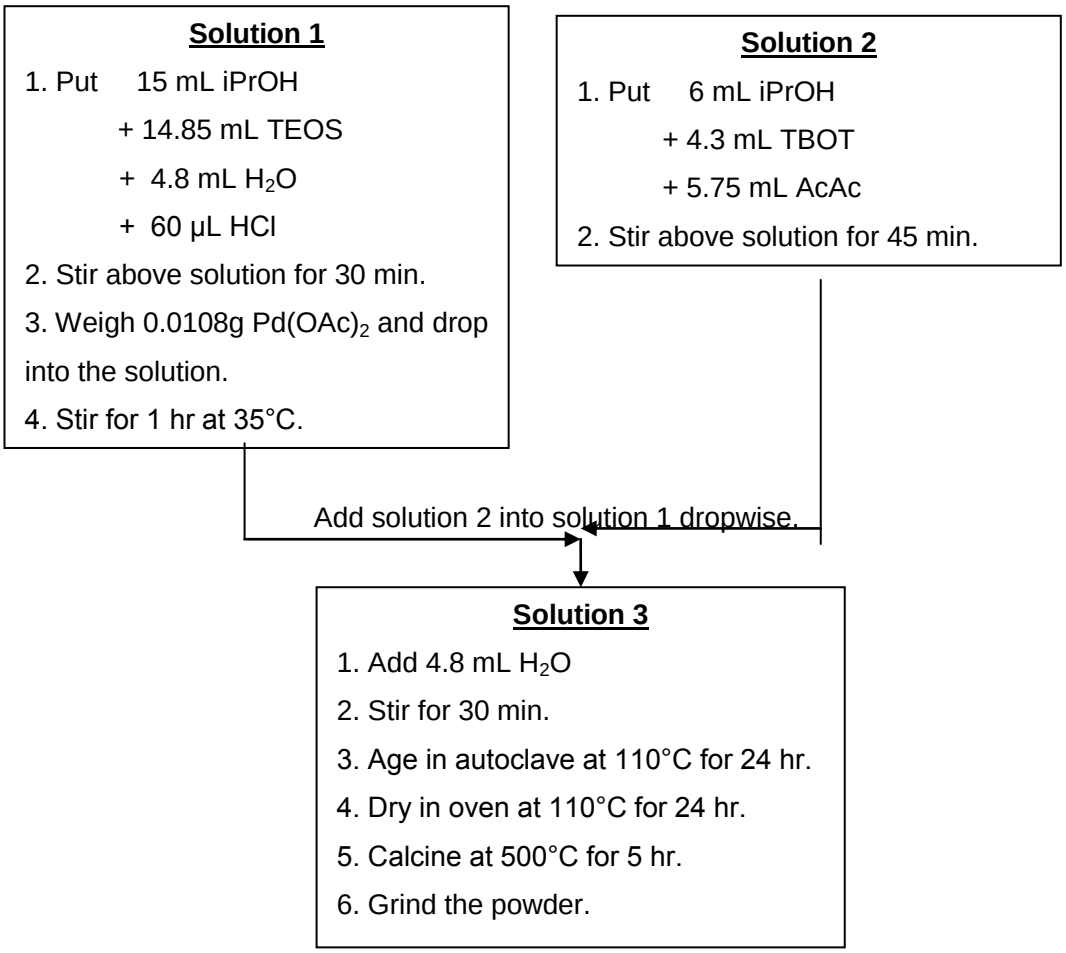

APPENDIX E

BJH ISOTHERMS AND PORE SIZE DUSTRIBUTIONS

E.1. Nitrogen Adsorption/Desorption Isotherms

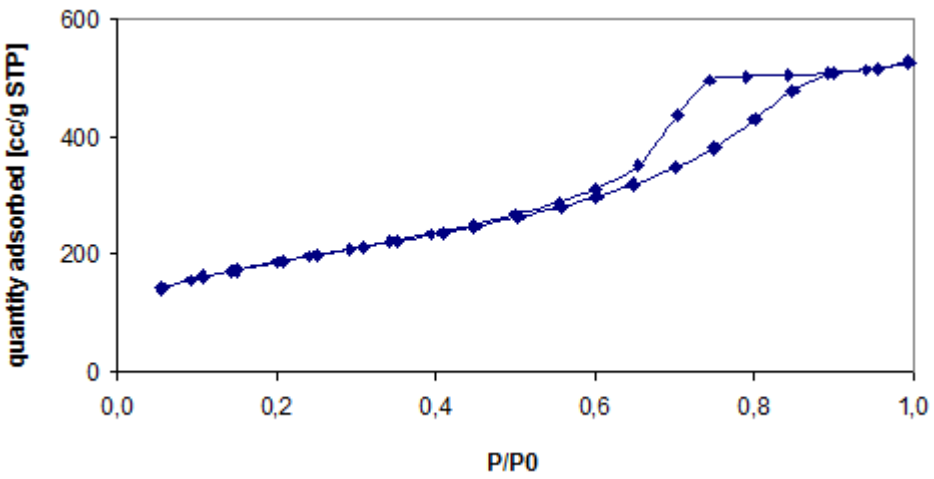

Figure E.1.1. Nitrogen adsorption/desorption isotherms for P-BiB3 (0.1%Pd/66%SiO_2/34%TiO_2)

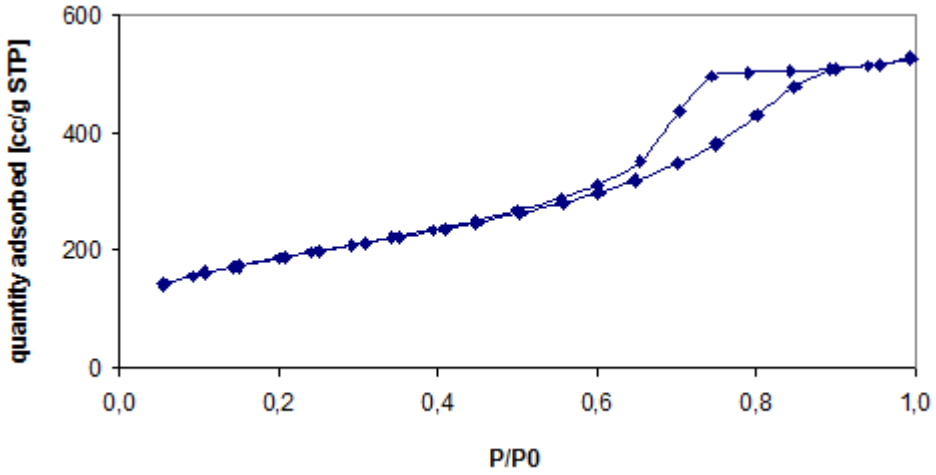

x

Figure E.1.2. Nitrogen adsorption/desorption isotherms for P-BiB5 (0.1%Pd/5%SiO_2/95%TiO_2)

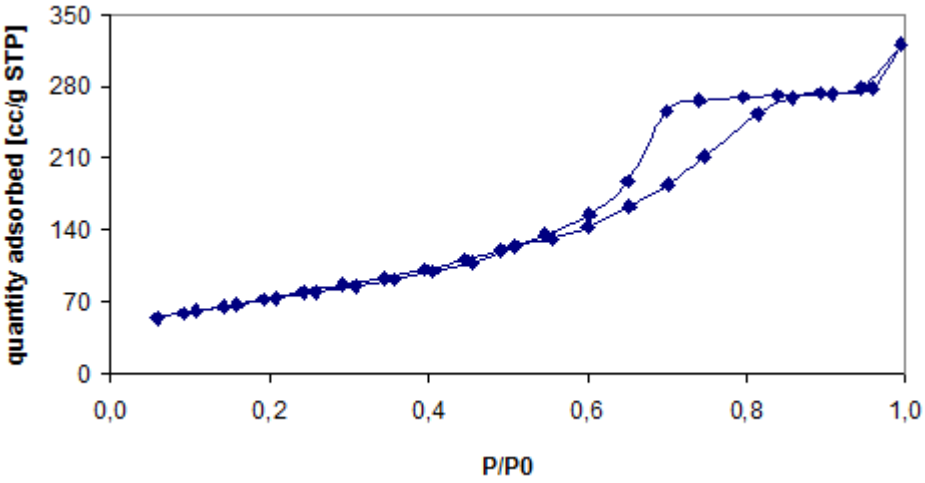

Figure E.1.3. Nitrogen adsorption/desorption isotherms for P-BiB10 (0.1%Pd/10%SiO_2/90%TiO_2)

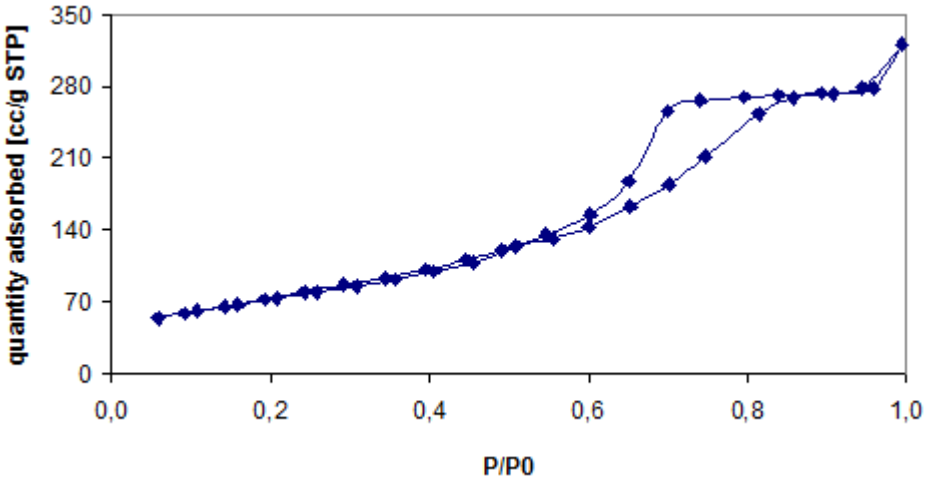

Figure E.1.4. Nitrogen adsorption/desorption isotherms for P-BiB12 (0.1%Pd/80%SiO_2/20%TiO_2)

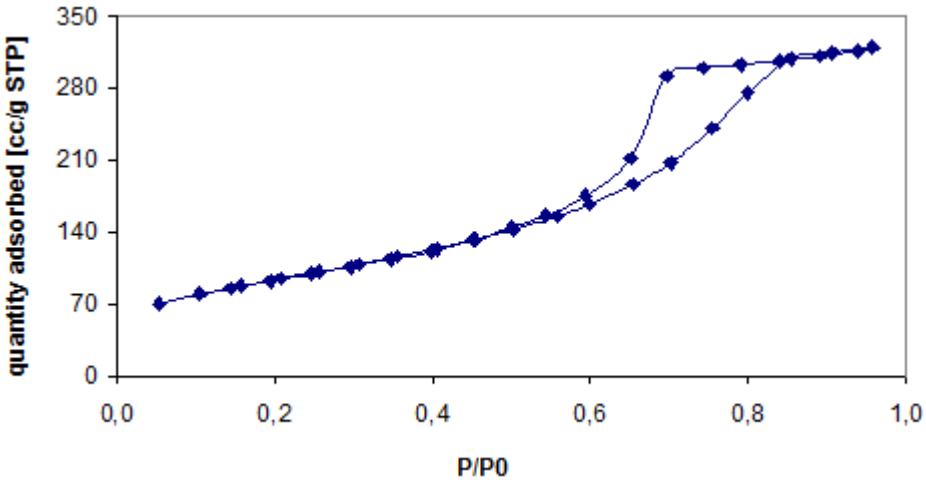

Figure E.1.5. Nitrogen adsorption/desorption isotherms for P-BiB14 (0.1%Pd/20%SiO_2/80%TiO_2)

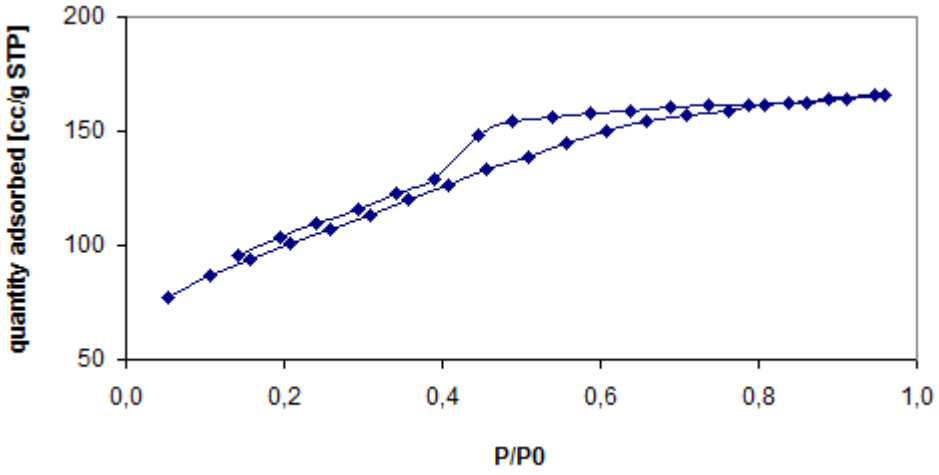

Figure E.1.6. Nitrogen adsorption/desorption isotherms for P-BiB22 (0.1%Pd/35%SiO_2/65%TiO_2)

E.2. Pore Size Distributions

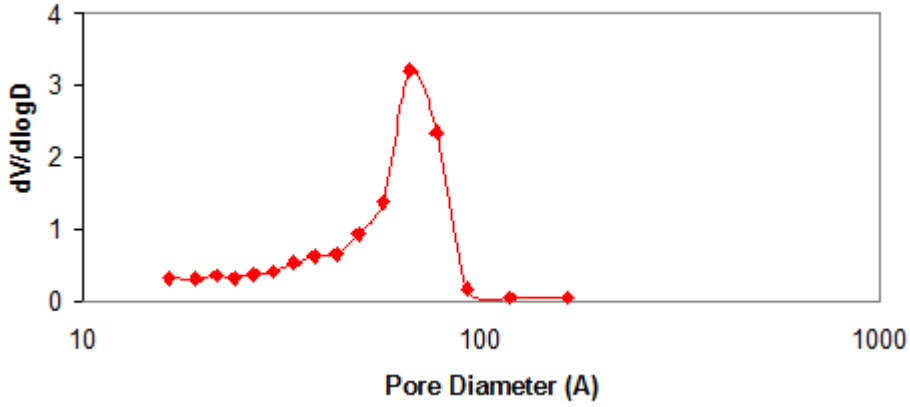

Figure E.2.1. Pore size distribution for P-BiB3 (0.1%Pd/66%SiO_2/34%TiO_2)

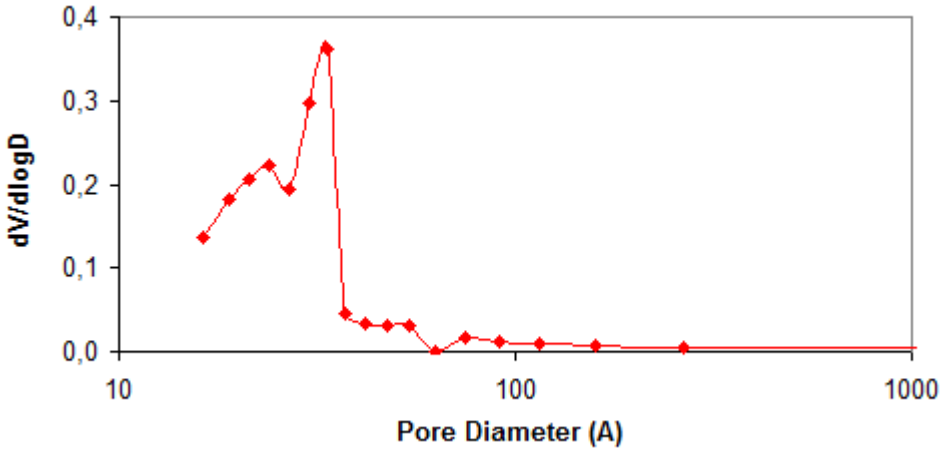

Figure E.2.2. Pore size distribution for P-BiB5 (0.1%Pd/5%SiO_2/95%TiO_2)

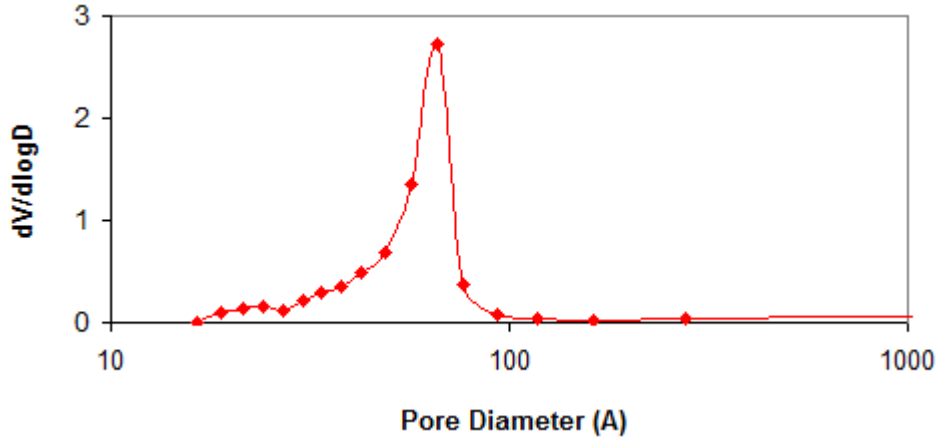

Figure E.2.3. Pore size distribution for P-BiB10 (0.1%Pd/10%SiO_2/90%TiO_2)

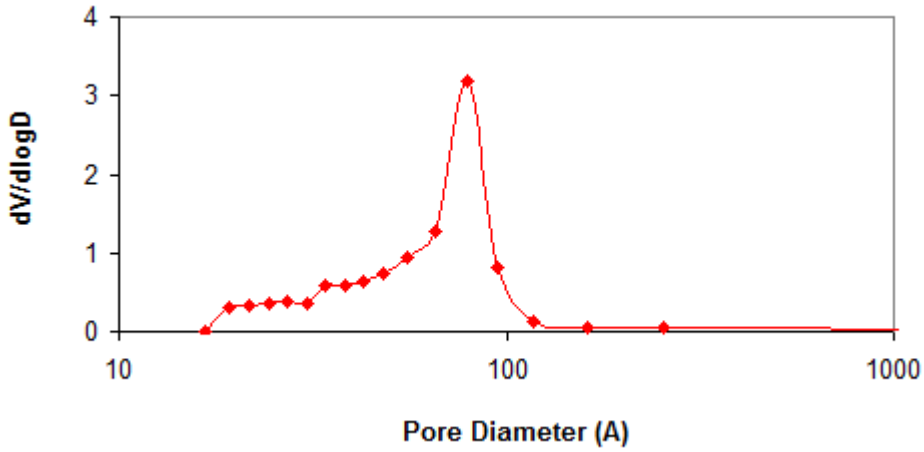

Figure E.2.4. Pore size distribution for P-BiB12 (0.1%Pd/80%SiO_2/20%TiO_2)

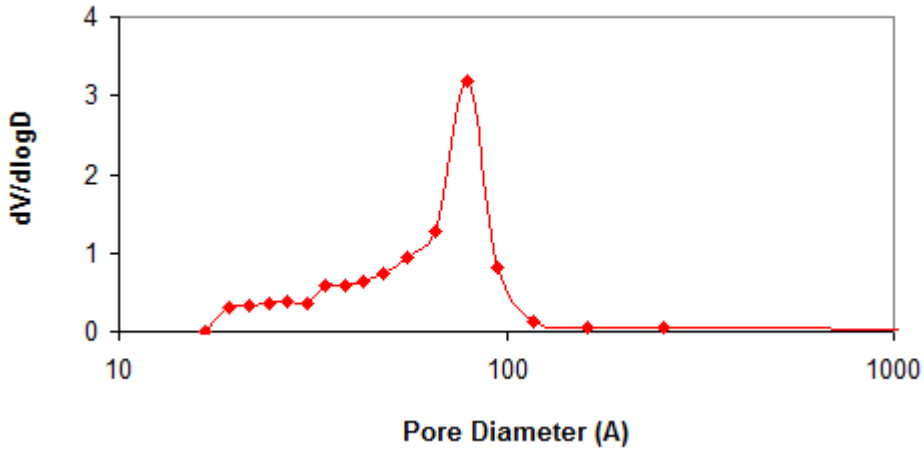

Figure E.2.5. Pore size distribution for P-BiB14 (0.1%Pd/20%SiO_2/80%TiO_2)

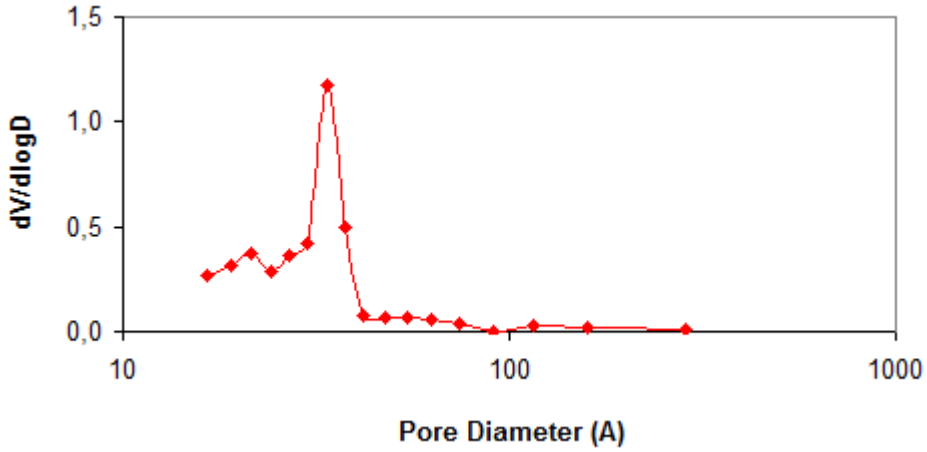

Figure E.2.6. Pore size distribution for P-BiB22 (0.1%Pd/35%SiO_2/65%TiO_2)